Electronic supplementary information (ESI)

Heavy-Metal Free Near Infrared Photoredox Catalysts in Cancer Phototherapy

Mst Nasima Khatun[a], Satyendu Nandy[b], Chakali Srinivas[a], Mrinalini Singh[a], Ramkrishna Das Adhikari[C], Sachin Kumar[b], and Parameswar Krishnan Iyer*[a,c]*

[a]Department of Chemistry, Indian Institute of Technology Guwahati, Guwahati-781039, India.

[b]Department of Bioscience and Bioengineering, Indian Institute of Technology Guwahati, Guwahati-781039, Assam, India

[c]Centre for Nanotechnology, Indian Institute of Technology Guwahati, Guwahati-781039, Assam, India.

FAX: +913612582349; E-mail: pki@iitg.ac.in

Contents

1. Experiment Section 2
1.1. Materials and Instrumentation 2
1.2. Preparation of the Test Solution 2
1.3. Preparation of FESEM samples 3
1.4. Theoretical Studies 3
1.5. Photoluminescence Quantum Yield Calculations 3
1.6. Synthesis of **RPI** 3
1.7. Computational Studies 6
1.8. $^1O_2$ generation quantum yield Estimation 6
1.9. Reactive oxygen species (ROS) Generation/Measurement 7
1.10. The Point of Zero Zeta Potential Evaluation 8
1.11. The Energy of the Valence Band and Conduction Band Calculations 8
1.12. Cell studies 9
1.12.1. Cell culture 9
1.12.2. Dark & Light Cytotoxicity Evaluated by MTT assay 9
1.12.3. Cellular Uptake 9
1.12.4. Live/dead cell dual-staining assay 9
1.13. Theoretical properties studies 26
1.14. Fenton reaction 57
2. Supporting figures 60
3. References 74

1. **Experimental Section**

1.1. Materials and instrumentations:

All the reagents and starting materials, such as Perylene-3,4,9,10-tetracarboxylic acid anhydride (**PDA**), zinc acetate [Zn $(OAc)_2$], imidazole, and various boronic acid including phenylboronic acid, 4-amino phenylboronic acid, 4-(dimethylamino) phenylboronic acid, triphenylamine-4-boronic acid, and (4-(di([1,1'-biphenyl]-4-yl)amino)phenyl) boronic acid (**BTPA**), along with reactive oxygen species detectors such as 2',7'-dichlorodihydrofluorescein diacetate (DCFDA), terephthalic acid (TA), dihydrorhodamine 123 (DHR 123), 2,3-bis-(2-methoxy-4-nitro-5-sulfophenyl)-2H-tetrazolium-5-carboxanilide (XTT), 2,2,6,6-tetramethylpiperidin (TEMP), 9,10-anthracenediyl-bis(methylene) dimalonic acid (ABDA), and 5,5-dimethyl-1-pyrroline-N-oxide (DMPO), were obtained from Sigma Aldrich (India). High-performance liquid chromatography (HPLC)-grade solvents were sourced from Fisher Scientific Ltd. and RANKEM. Nuclear magnetic resonance (NMR) spectra, including ^{1}H and ^{13}C, were recorded using a Bruker Avance 400 MHz spectrometer, with residual solvent signals serving as internal references for all NMR solutions. Mass spectra were acquired using matrix-assisted laser desorption/ionization-time of flight (MALDI-TOF) spectrometry. Ultraviolet-visible (UV/vis) and photoluminescence (PL) spectra were measured using a Perkin-Elmer Lambda-750 spectrophotometer and a Horiba Fluoromax-4 spectro fluorometer, respectively, with a 375 nm laser diode (DeltaDiode-375) as the excitation source. All measurements were conducted at 298 K using 4 mm quartz cuvettes. The compounds' hydrodynamic diameter and zeta potential were determined using a Malvern Zetasizer instrument. Electron spin resonance (ESR) spectra were recorded using a Bruker EMXplus-10/12. Time resolved photoluminescence (TRPL) study has been performed using Edinburg FLS 1000. Ultra-high performance liquid chromatograph-quadrupole time of flight-high resolution mass spectrometer (UHPLC-QTF-HRMS) has been performed using the agilent, G6546A mode. For phototherapy studies, a white light source with an intensity of 50 mW cm^{-2}, specifically the "Pick Ur Needs 120W Plastic Lithium Battery Search Light Long 1 Km Range with Multi-Functional + Blinker Rechargeable Handheld Torch" in black, was used. DMEM, propidium iodide (PI), and calcein-AM (AM) were sourced from Hi Media.

1.2. Preparation of the Test Solution: Stock solutions of **PhPI**/**ANPI**/**DMPI**/**TPPI**/**BPPI** (20 mM) were prepared in DMSO. For aggregation studies, 100 μM test solutions were made by

varying the water fraction (f_w) in DMSO. Samples were thoroughly shaken at room temperature prior to spectral analysis.

1.3. Preparation of FESEM samples: FESEM images of the aggregate have been drop casted on the glass slide, followed by in the presence and absence of light.

1.4. Theoretical Studies: DFT calculations were performed using Gaussian 16 with the B3LYP functional and 6-31G (d, p) basis set to optimize ground-state geometries of **RPI** and determine their HOMO-LUMO energies and electron densities.[1, 2]

1.5. Photoluminescence quantum Yield Calculations: PL quantum yield (Φ_{PL}) of **RPI** were measured relative to rhodamine 6G ($\Phi_r = 0.95$ in ethanol) using the eqn:

$$\Phi_{PL} = \Phi_r (A_r F_s / A_s F_r) (\eta_s^2 / \eta_r^2) \quad \text{(S1)}$$

where subscripts "s" and "r" denote sample and reference, respectively; A is absorbance, F is integrated PL, and η is refractive index.

1.6. Synthesis of RPI

Synthetic procedures for perylenimide (PI): PI was synthesized via a hydrothermal condensation of PDA (2.54 mmol), Zn $(OAc)_2$ (1.72 mmol), amine (1.35 mmol), imidazole (5 g), and water (1 mL) in a Teflon-lined autoclave at 190 °C for 20 h under 15 bar pressure. The dark reddish product was extracted with $CHCl_3$ and water under acidic conditions, followed by washed, dried over Na_2SO_4, filtered, and concentrated. Final purification by column chromatography ($CHCl_3$) yielded 400 mg of **PI** (40%).

Characterization data for PI: ^{1}H NMR (400 MHz, $CDCl_3$) 0.84 (t, 3H),1.28-1.44 (m, 6H), 1.70 (dd, 2H), 4.09-4.14 (t, 2H), 7.52 (t, 2H), 7.80 (d, 2H), 8.24 (d, 2H), 8.29 (d, 2H), 8.44 (d, 2H)). ^{13}C NMR (101 MHz, CDCl3) δ 14.09, 22.58, 26.92, 28.19, 31.64, 40.49, 120.12, 120.83, 123.67, 126.73, 126.96, 127.75, 129.10, 130.90, 131.29, 134.35, 136.94, 163.86. MALDI-TOF: calculated for $C_{28}H_{23}NO_2$: 405.17 $[M]^+$, Found: 404.95 $[M-H]^+$.

Synthetic Route

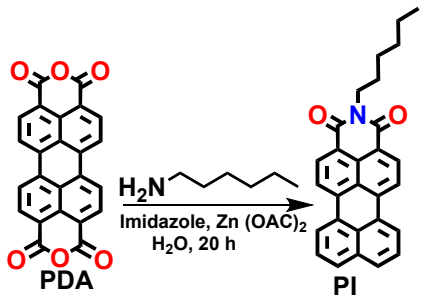

Scheme S1. The synthetic method used to prepare **PI.**

Synthetic procedures for BrPI: PI (1 mmol) was dissolved in 5 mL chlorobenzene with mild heating, followed by the addition of bromine (4.5 mmol). The mixture was stirred at 50 °C for 4.5 h. After completion, solvents and excess bromine were removed under vacuum, and the resulting red solid was crystallized from methanol to afford the desired compound in 95% yield.

Characterization data for 8-bromo-2-hexyl-1H-benzo[5,10] anthra[2,1,9-def]isoquinoline-1,3(2H)-dione (BrPI): ^{1}H NMR (400 MHz, $CDCl_3$) δ 0.93 (t, 3H), 1.3-1.6 (m, 6H), 1.88 (dd, 2H), 3.77 (t, 2H), 7.69 (t, 1H),7.86 (d, 1H), 8.13 (d, 1H), 8.27 (d, 2H), 8.33 (d, 1H). 8.38 (d, 1) 8.55 (dd, 2H). ^{13}C NMR (101 MHz, CDCl3) δ.14.09, 22.58, 26.92, 28.19, 31.64, 40.49, 120.12, 123.67, 126.96, 127.75, 129.15, 130.80, 131.32, 172.56 MALDI-TOF: calculated for $C_{28}H_{22}BrNO_2$: 483.08 $[M]^+$, Found: 483.397 $[M]^+$

Synthetic Route

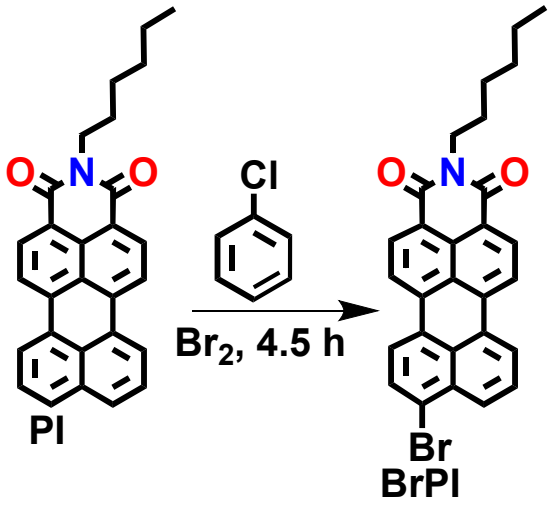

Scheme S2. The synthetic procedure employed to prepare **BrPI.**

Synthetic procedures for RPI: BrPI (0.5 mmol), boronic acid (1 mmol), and 5 mg Pd $(PPh_3)_4$ were added to a 50 mL round-bottom flask, purged with nitrogen for 30 min. THF (6 mL) and 2.0 M K_2CO_3 (2 mL) were added, and the mixture was stirred at 85 °C under nitrogen for 24 h. After cooling, the reaction was extracted with $CHCl_3$, dried over Na_2SO_4, and concentrated. Purification by column chromatography yielded **PhPI** (red solid) and **ANPI/DMPI/TPPI/BPPI** (brownish solids) in 60% yield.

Characterization data for 2-hexyl-8-phenyl-1H-benzo[5,10]anthra[2,1,9-def]isoquinoline-1,3(2H)-dione (PhPI): ^{1}H NMR (400 MHz, $CDCl_3$) δ 0.89 (t, 3H), 1.41 (m, 6H), 1.76 (dt, 2H), 4.14 (t, 2H), 7.53 (m, 7H),7.98 (d, 1H) 8.37 (d, 2H), 8.42 (t, 2H), 8.55 (m, 2H). ^{13}C NMR (101 MHz, CDCl3) δ 14.07, 22.62, 26.77, 28.07, 29.02, 31.56, 40.39, 114.10, 120.13, 119.69, 123.56, 126.05, 128.52, 129.20, 130.01, 131.99, 132.66, 136.66, 139.74, 143.11, 163.73. MALDI-TOF: calculated for $C_{34}H_{29}NO_2$: 481.20 $[M]^+$, Found: 482.666$[M+H]^+$

Characterization data for 8-(4-aminophenyl)-2-hexyl-1H-benzo[10,5]anthra[2,1,9-def]isoquinoline-1,3(2H)-dione (ANPI): ^{1}H NMR (400 MHz, $CDCl_3$) δ 0.90 (t, 3 H), 1.36 (m,4H), 1.72 (dt,3H), 4.19 (t,2H), 5.06 (s, 2H), 6.88 (t, 2H), 7.43 (m, 2H), 7.59 (m, 2H), 8.42 (t, 2H), 8.47 (m, 3H), 8.60 (m, 2H), ^{13}C NMR (101 MHz, $CDCl_3$) δ 14.30, 22.28, 25.29, 28.29, 32.67, 40.34, 119.53, 121.88, 127.60, 122.50, 126.83, 127.54, 129.25, 130.59, 134.97, 135.28, 136.92, 138.58, 139.64, 141.59, 141.59, 143.33, 149.28, 159.66. MALDI-TOF: calculated for $C_{34}H_{28}N_2O_2$: 496.22 $[M]^+$, Found:497.403 $[M+H]^+$

Characterization data for 8-(4-(dimethylamino)phenyl)-2-hexyl-1H-benzo[10,5]anthra[2,1,9-def]isoquinoline-1,3(2H)-dione (DMPI): ^{1}H NMR (400 MHz, $CDCl_3$) δ 0.88 (t, 3H), 1.35 (m, 5H), 1.78 (m, 3H), 3.07 (s, 6H), 4.20 (t, 2H), 6.88 (t, 3H), 7.43 (m, 2H), 7.57 (m, 2H), 8.13 (m, 1H), 8.39 (m, 3H). 8.60 (t, 2H). ^{13}C NMR (101 MHz, $CDCl_3$) δ 13.24, 21.30, 24.98, 26.94, 39.36, 42.38, 115.53, 120.60,124.19, 127.60, 129.25, 130.24, 131.27, 132.25, 132.93, 134.28, 135.56, 140.61, 140.61, 148.68, 156.35, 160.64. MALDI-TOF: calculated for $C_{36}H_{32}N_2O_2$: 524.25 $[M]^+$, Found: 525.375 $[M]^+$

Characterization data for 8-(4-(diphenylamino)phenyl)-2-hexyl-1H-benzo[10,5]anthra[2,1,9-def]isoquinoline-1,3(2H)-dione (TPPI): ^{1}H NMR (400 MHz, $CDCl_3$) δ 0.88 (t, 3H), 1.35 (m, 5H), 1.76 (m, 3H), 4.18 (t, 2H), 6.90 (t, 3H), 7.43 (t, 2H), 7.59 (t, 2H), 7.86 (m, 5H), 7.90 (t, 1H), 8.13 (m, 6H), 8.39 (m, 3H), 8.47 (t, 2H). ^{13}C NMR (101 MHz, $CDCl_3$) δ 13.92, 17.61, 23.64, 28.29,

31.68, 38.01, 117.58, 119.24, 120.24, 127.89, 129.25, 130.24, 131.94, 132.57, 133.60, 133.92, 134.97, 135.56, 136.24, 137.39, 138.27, 140.61, 141.59, 143.33, 144.59, 146.63, 160.64. MALDI-TOF: calculated for $C_{46}H_{36}N_2O_2$: 646.28 $[M]^+$, Found: 648.632 $[M]^+$

Characterization data for 8-(4-(di([1,1'-biphenyl]-4-yl)amino)phenyl)-2-hexyl-1H-benzo[10,5]anthra[2,1,9-def]isoquinoline-1,3(2H)-dione (BPPI): ^{1}H NMR (400 MHz, $CDCl_3$) δ 0.86 (t, 3H), 1.25 (m, 6H), 1.74 (m, 2H), 4.22 (t, 2H), 6.80 (t, 2H), 7.42 (t, 2H), 7.56 (t, 2H), 7.74 (m, 6H), 7.780(m, 6H), 7.79 (m, 1H), 8.13 (m, 6H), 8.45 (d, 3H), 8.58 (t, 3H). ^{13}C NMR (101 MHz, $CDCl_3$) δ 13.24, 21.01, 24, 61, 29.65, 34.69, 40.34, 117.58, 120.89, 123.23, 124.58, 125.94, 126.24, 127.89, 128.26, 130.24, 131.27, 131.94, 132.57, 135.28, 136.98, 136.27, 139.25, 140.61, 149.65, 161.67. MALDI-TOF: calculated for $C_{58}H_{44}N_2O_2$: 800.34 $[M]^+$, Found: 800.327 $[M]^+$

Synthetic Route

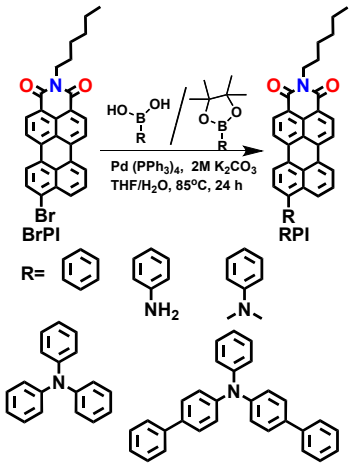

Scheme S3. The synthetic method is employed to prepare **RPI.**

1.7. Computational studies: This study employed TD-B3LYP/6-31G (d, p) within the Tamm-Dancoff approximation (TDA) to compute the optimized geometries, vibrational frequencies, excitation energies, and transition properties of **RPI**. Calculations were performed using Gaussian 16, while additional computations and spin-orbit coupling (SOC) constants for **PhPI**/**ANPI**/**DMPI**/**TPPI**/**BPPI** were obtained using ORCA 5.0 at the B3LYP/DEF2-SVP level.[3, 4]

1.8. $^1O_2$ generation quantum yield estimation: Rose bengal (singlet oxygen quantum yield, $\Phi_\Delta = 0.76$ in ethanol) was used as a reference in dilute solutions, maintaining absorbance maxima at 0.2 to minimize inner filter effects. **RPI** (100 μM) were mixed with ABDA (100 μM), and

ABDA absorbance at 378 nm was monitored under white light (400-700 nm, 50 *m*W cm^{-2}) over time. Φ_Δ of **RPI** in 99% PBS/DMSO was then calculated using the following eqn:

$$\Phi_{AIEgen} = \Phi_{RB} (K_{AIEgen} A_{RB}/K_{RB} A_{AIEgen}) \quad \text{(S2)}$$

Φ_{AIEgen} is the Φ_Δ of AIEgen in 99% PBS/DMSO. A_{RB} and A_{AIEgen} represent light absorbed by Rose Bengal and AIEgen, respectively, at absorbance 0.2, calculated by integrating the 400-700 nm absorption spectra. K_{RB} and K_{AIEgen} are the ABDA decomposition rate constants for Rose Bengal and AIEgen, respectively, obtained from linear plots of ln (A_0/A) vs. time, where A_0 and A are ABDA absorbances at 378 nm under white light irradiation.[5, 6]

1.9. Reactive oxygen species (ROS) generation/measurement

Singlet oxygen ($^1O_2$) Test: $^1O_2$ generation was quantified by ESR spectroscopy using TEMP as a spin trap. Upon white light irradiation (50 *m*W cm^{-2}, 30 min) of PSs (100 μM) in 99% PBS/DMSO containing 100 μM TEMP, $^1O_2$ reacted with TEMP to form TEMPO. ESR Samples were loaded into quartz capillaries and spectra (3000-3600G) were recorded with background correction using pre-irradiation samples.[7, 8]

A solution of 100 μM ABDA and **RPI** in 99% PBS/DMSO was irradiated with white light (50 *m*W cm^{-2}) for 0, 2, 4, 6, 8, 10, and 20 min. ABDA absorbance at 378 nm was measured after each interval to monitor degradation.

Total ROS Test: A solution of 10 μM DCFDA and 100 μM **RPI** in 99% PBS/DMSO was irradiated with white light (50 *m*W cm^{-2}) for 0, 5, 10, 15, 20, 25, and 30 min. PL were recorded after each interval to evaluate ROS generation using DCFDA as the indicator.

Type-I ROS:

Superoxide anion radical ($O_2^{\bullet-}$) Test:

1) The feasibility of $O_2^{\bullet-}$ generation was evaluated through theoretical calculations using ORCA 5.0 software.

2) ESR analysis confirmed $O_2^{\bullet-}$ production using DMPO as the spin-trapping agent. Samples containing 100 μM DMPO in 99% PBS/DMSO and 100 μM of **PhPI**, **ANPI**, **DMPI**, **TPPI**, or

BPPI were loaded into quartz capillaries. Spin spectra were recorded after 10 min of white light irradiation (50 *m*W cm^{-2}).

3) XTT was used as an indicator for $O_2^{\bullet-}$, converting to XTT formazan in its presence. A solution containing 100 μM XTT and 100 μM **PhPI**, **ANPI**, **DMPI**, **TPPI**, or **BPPI** was irradiated with white light for 0, 5, 10, 20, and 30 min, and UV-vis spectra were measured. UV-vis spectra of XTT under white light irradiation were also recorded as a control.

DHR123 was used to detect $O_2^{\bullet-}$, converting to rhodamine 123 in the presence of $O_2^{\bullet-}$. Solutions containing 100 μM **PhPI**, **ANPI**, **DMPI**, **TPPI**, or **BPPI** in 99% PBS/DMSO were exposed to white light (400-700 nm, 50 *m*W cm^{-2}) for 5-30 min, and PL were recorded after each irradiation. A control group with DHR123 alone was irradiated (λ_{ex} = 500 nm, λ_{em} = 527 nm).

Hydroxyl Radical (HO$^{\bullet}$) Test: This test assessed HO$^{\bullet}$ generation. A solution containing 100 μM TA and 100 μM of various **RPI** in 99% PBS/DMSO was prepared. The procedure followed the method for total ROS determination using DCFDA. Upon HO$^{\bullet}$ trapping, TA was converted to hydroxyl terephthalic acid, resulting in increased PL (λ_{ex} = 315 nm).

1.10. The Point of Zero Zeta Potential (PZZP) evaluation

As reported in the literature, PZZP for **RPI** was determined. Initially, the aqueous solutions of these **PI** were neutral (pH 7). Adjusting the pH with dilute sodium hydroxide or hydrochloric acid shifted the solutions to either alkaline or acidic conditions. Zeta potential measurements revealed a transition from negative to positive as the pH decreased from alkaline (pH 9) to acidic (pH 1).

1.11. The energy of the valence band and conduction band calculations: The valence band energy (E_V) was determined using Ultraviolet Photoelectron Spectroscopy (UPS) data. The conduction band energy (E_C) was estimated from the energy gap obtained from the onset absorption data in UV-visible spectroscopy. E_C was then calculated relative to the normal hydrogen electrode (NHE) using eqn (S3) and (S4).

$$E_V = -E_{HOMO} - 4.5 \quad \text{(S3)}$$

$$E_C = -E_{LUMO} - 4.5 \quad \text{(S4)}$$

The E_V and E_C calculated for **RPI** were documented in Table S17. Additionally, E_C and E_V at a pH of 5.6, corresponding to the PZZP, were determined using eqn (S5) and (S6) from the literature data.

$$E_{C,pH} = E_C + 0.059 \times (PZZP - pH) \quad (S5)$$

$$E_{V,pH} = E_V + 0.059 \times (PZZP - pH) \quad (S6)$$

PZZP refers to the points of zero zeta potential for **RPI** at pH 5.6. The estimated E_C and E_V at pH 5.6 for **PhPI**/**ANPI**/**DMPI**/**TPPI**/**BPPI** were provided in Table S17.

1.12. Cell studies

1.12.1. Cell culture: HeLa (cervical cancer) and MCF-7 (breast cancer) cells were obtained from the National Centre for Cell Sciences (NCCS) in Pune, India. The cells were cultured in Dulbecco's Modified Eagle Medium (DMEM), supplemented with 10% fetal bovine serum and 100 U/ml of penicillin and streptomycin. Cultures were maintained in a controlled environment with 5% CO_2 at 37°C.

1.12.2. Dark & Light cytotoxicity evaluated by MTT assay

In the cell viability assay on HeLa and MCF7 cancer cell lines, the MTT method was used. Initially, 5000 cells were seeded into individual wells of a 96-well plate and cultured in DMEM media at 37°C with 5% CO_2 for 24 hrs. The cells were treated with varying concentrations of **DMPI**/**TPPI**/**BPPI** for 4 hrs. After treatment, specific cell samples were exposed to white light (50 mW cm^{-2}) for 30 min using a handheld torch. Following irradiation, cells were incubated with other treatment groups for 24 hrs at 37°C in a CO_2 humidified incubator. After incubation, the MTT assay was performed to assess cell viability by measuring the conversion of MTT to formazan by mitochondrial enzymes in viable cells. The formazan product was quantified spectrophotometrically at 570 nm, with a reference wavelength of 655 nm. The absorbance of the formazan product directly correlated with the number of viable cells in the samples.

1.12.4. Live/dead cell dual staining assay

In the study, HeLa cells were seeded in 35-mm glass-bottomed dishes at a density of 3×10^5 cells per dish and incubated overnight in standard culture media. They were treated separately with **DMPI**/**TPPI**/**BPPI** at concentrations of 20 to 25 μM for 4 hrs. After treatment, the cells were irradiated with white light (50 mW cm^{-2}) for 30 min using a handheld torch. One set of cells was stained with 2 μM calcein AM and 4 μM propidium iodide (PI) for 1 hr, washed with Dulbecco's Phosphate-Buffered Saline (DPBS), and fluorescence images were acquired using a fluorescence microscope. Another set of cells, after 4 hrs of treatment with **RPI**, was treated with 10 μM DCFDA for 1 hr, washed with DPBS, irradiated with the handheld torch (50 mW cm^{-2}) for 20 min, and their fluorescence images were acquired. Additionally, HeLa cells were cultured in a normoxic environment (21% O_2) for 24 hrs.

Table S1. Comparison table of the presented materials with their distinct structure-property relationships and applications.

MATERIALS	STRUCTURE_PROPERTY RELATIONSHIPS			APPLICATIONS	$\Delta E_{S0\text{-}T1}$ (eV)
	AQUEOUS MEDIA (WATER)	SOLID STATE	THEORETICAL		
PhPI	ACQ (λ_{max} = 646 nm), Type-I PS ($O_2^{\bullet-}$) (Φ_Δ): 0.0054	Faint emissive (λ_{max}= 646 nm) Stokes shift: 146 nm	ΔG ($O_2^{\bullet-}$): -10.29 kcal mol^{-1}	**ACQ Photoredox catalyst**	1.165
ANPI	ACQ (λ_{max} = 620 nm Type-I PS ($O_2^{\bullet-}$ OH^-) (Φ_Δ): 0.0045	Faint emissive (λ_{max}= 620 nm) Stokes shift: 117 nm	ΔG ($O_2^{\bullet-}$): -10.31 kcal mol^{-1} ΔG (OH^-): -413 kcal mol^{-1}	**ACQ Photoredoxg catalyst**	1.079
DMPI	NIR AIEE λ_{max} = 720 nm Type-I PS ($O_2^{\bullet-}$) (Φ_Δ): 0.000	NIR emissive (λ_{max}= 770 nm) Stokes shift: 270 nm	ΔG ($O_2^{\bullet-}$): -9.06 kcal mol^{-1}	**NIR AIEE/ NIR Photoredox catalyst**	1.002
TPPI	Far-red AIE (λ_{max}= 686 nm), **(Φ_Δ): 0.60** Type-I,Type-II PS ($^1O_2$, $O_2^{\bullet-}$)	NIR emission (λ_{max}= 713 nm) Stokes shift: 213 nm	ΔG ($O_2^{\bullet-}$) :-9.92 kcal mol^{-1}	**NIR/Far-red AIE dual type-I/type-II photosensitizer (IC_{50} = 20.5 μM)**	2.532
BPPI	Far-red AIEE (λ_{max}= 675 nm), Type-I PS ($O_2^{\bullet-}$) (Φ_Δ): 0.025	NIR emission (λ_{max}= 716 nm) Stokes shift: 216 nm	ΔG ($O_2^{\bullet-}$): -11.69 kcal mol^{-1}	**NIR/Far-red AIEE photoredox catalyst in cancer cell**	0.871

Table S2. Below is a comparison table of recently published NIR emissive materials with **RPI**, highlighting their design strategies, structure-property relationships, and photosensitizing behaviors for phototherapy application.

References	Present work			*ACS Nano* 2020, *14*, 854-866
Materials	DMPI	TPPI	BPPI	TTB
AIE	NIR-AIEE (a)	NIR emissive (a)	NIR-emissive (a)	NIR AIE (a)

Stokes- shift (nm)		270,213	213,186	216,175	g
Φ_{PL}		0.196	0.0534	0.033 (a)	g
Φ_{Δ}		-(c)	0.592(c)	0.025	g(d)
Light used		50*m*Wcm^{-2} (e)	50 *m*Wcm^{-2} (e)	50 *m*Wcm^{-2} (e)	(e)
ROS	Types	Type-I, ($O_2^{\cdot-}$)	Type-I, Type-II ($^1O_2$, $O_2^{\cdot-}$)	Type-I ($O_2^{\cdot-}$)	Type-I, Type-II
	Specificity	Specific	Specific	Specific	Not very specific
Total ROS	DCFDA (μM)	10	10	10	1
	T (min)	5	5	5	5
	I	1.8x10^5	2.5x10^5	2x10^5	3x10^6
ROS (mechanism)		DCFDA, ABDA,TA, ESR, Theoretical (ΔG, SOC), Band energy/NHE)	DCFDA, ABDA ,TA, ESR, Theoretical (ΔG, SOC), Band energy/NHE)	DCFDA, ABDA ,TA, ESR, Theoretical (ΔG, SOC), Band energy/NHE)	ABDA,DCFH,DHR,EPR
Phototherapy (Cancer cell)	In vitro	Normoxia (Hela)	Normoxia (Hela)	Normoxia (Hela)	Normoxia (Hela)
Liposome		x	x	x	yes
Design strategy		Structure-property relationship and application			Application-based

a, b, c, and d, are the different solvent systems (a= 99% f_w, b = toluene, c = 99% PBS, and d = ethanol, respectively), whereas, e is the white light used for the PS [g = not observed, x = not used].

Table S3: CIE coordinates for the **RPI** in solution, aggregated and solid state.

Materials	**Solution**		**Aggregated**		**Solid**	
	X	**Y**	**X**	**Y**	**X**	**Y**
PhPI	0.4591	0.5346	0.4409	0.5468	0.668	**0.3318**
ANPI	0.5288	0.4667	0.5574	0.441	0.7343	0.2657
DMPI	0.5161	0.4801	0.6487	**0.3509**	0.7266	0.2733
TPPI	0.4638	0.5304	0.6696	**0.3302**	0.6651	**0.3346**
BPPI	0.4773	0.5178	0.5644	0.43	0.7195	0.2805

A represents not observed due to non-emissive characteristics.

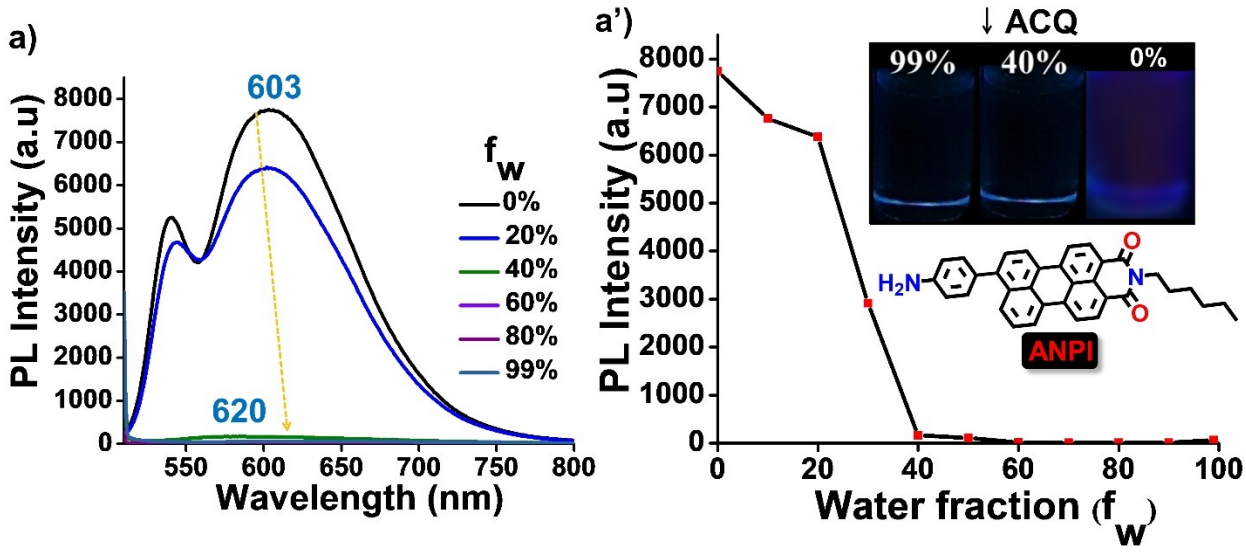

Fig. S1. PL spectra of (a) **ANPI** at different f_w in DMSO (100 μM, λ_{ex} = 500 nm). (a') plots of $\lambda_{em,max}$ at various f_w along with Insets: digital photographs under 365 nm UV excitation at 0%, 40%, and 99% f_w, with the chemical structure.

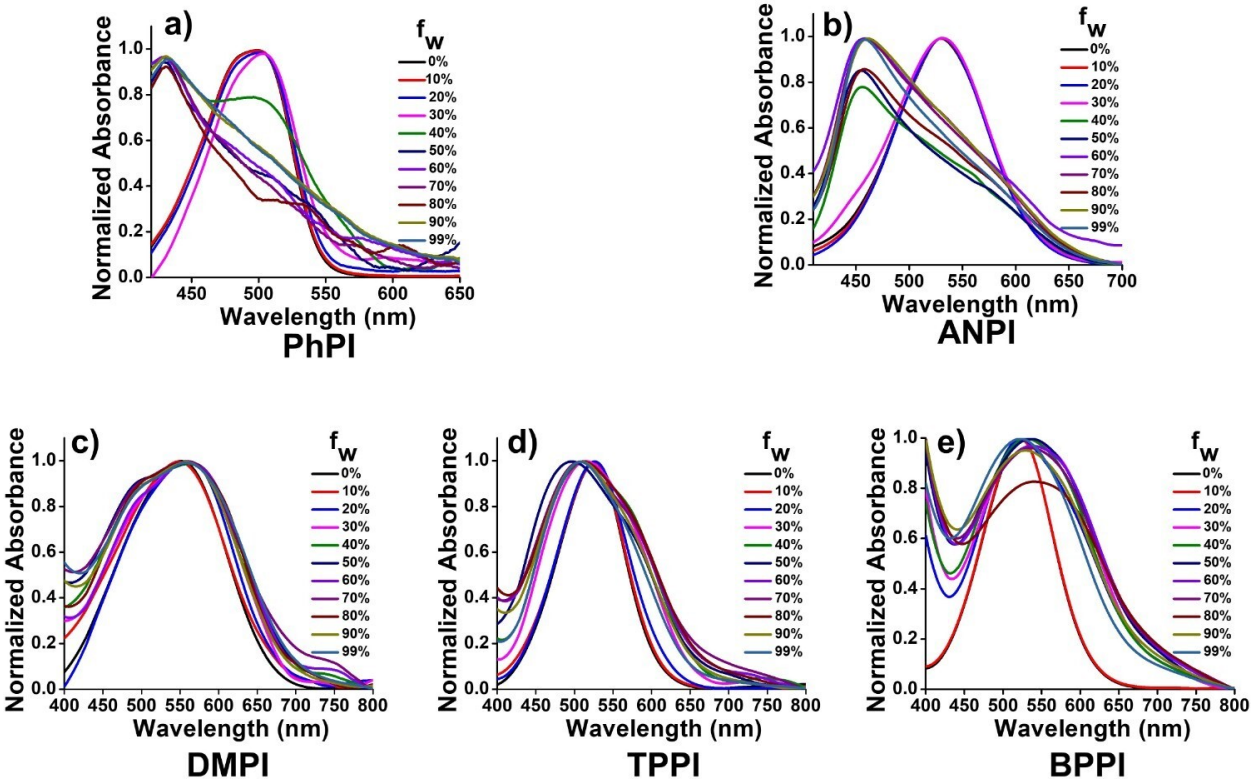

Fig. S2. (a-e) Normalized UV-vis spectra of **RPI** at different f_w in DMSO.

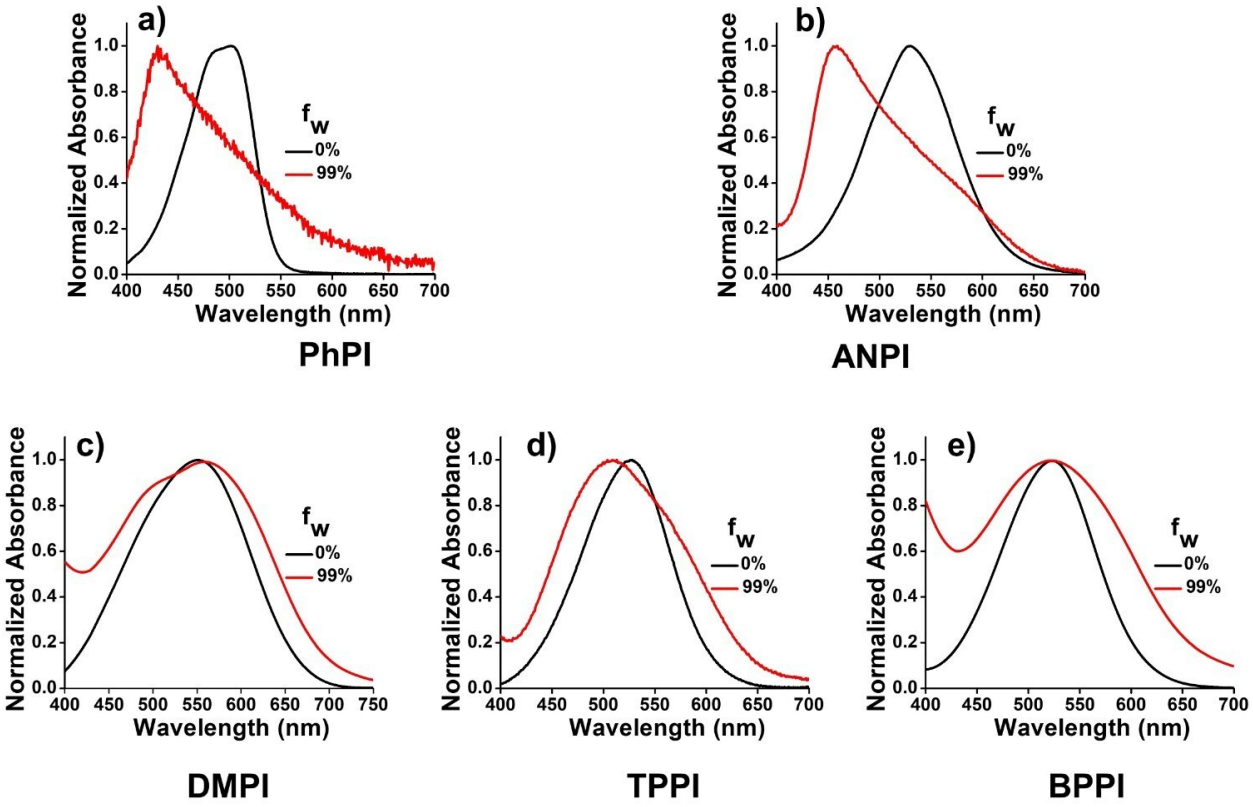

Fig. S3. (a-e) Normalized UV-vis spectra of **RPI** at 0% and 99% f_w in DMSO.

Table S4. UV-vis absorption data for the **RPI** in DMSO.

Materials	Water fraction (f_w)	$\lambda_{abs.max}$	A	Δλ
PhPI	0%	483,500	0.509675, 0.492852	70,53
	99%	430	0.005114	
ANPI	0%	530	0.506787	73
	99%	457	0.081402	
DMPI	**0%**	550	0.109475	10
	99%	560	0.054649	
TPPI	**0%**	527	0.481864	27/33
	99%	500,560	0.124295	
BPPI	**0%**	525	0.260888	g
	99%	525	0.155969	

A, Δλ, are the absorbance and wavelength maxima shift in their absorption.

Table S5: Comparison of the blue shifted $\lambda_{abs.max}$ with the reported data which has demonstrated enhanced H-aggregation that is crucial for phototherapy efficacy by boosting SOC.

References	Materials	Blue shifted $\lambda_{abs.max}$ (nm)	H-aggregation

Present work		**PhPI**	70/53	Highly pronounced
		ANPI	73	Highly pronounced
a	*Adv. Mater.* **2022**, *34*, 210814	PTTe	74	Pronounced
		PTSe	71	Pronounced
		PTS	30	Moderate
b	*Nature Materials* **2015**, *14*, 685-690	DPhCzT	14	Moderate
b	*Nanoscale* **2016**, *8*, 17422-17426	$(OB4)_4$	10	Moderate

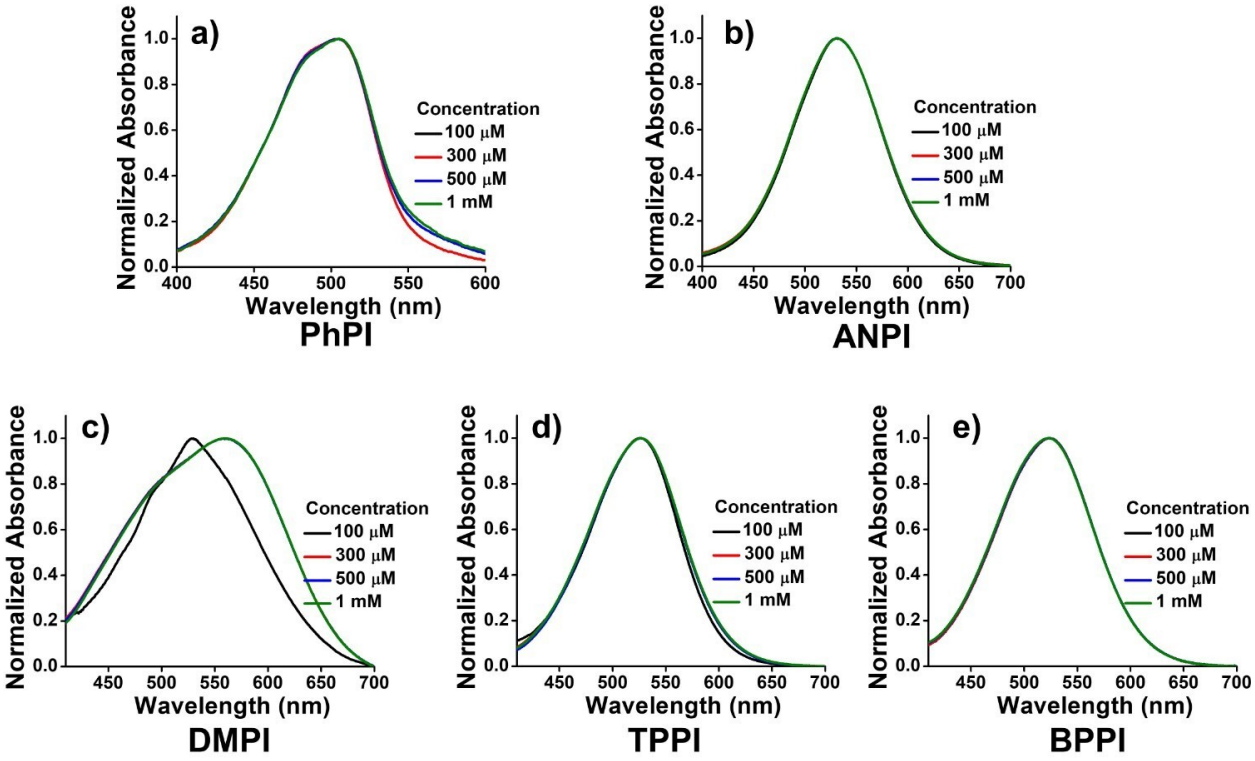

Fig. S4. (a-e) Normalized UV-vis spectra of **RPI** at different concentrations in DMSO.

Table S6. UV-vis absorption data for the **RPI** at different concentrations in DMSO.

Materials	Concentration (μM)	$\lambda_{abs.max}$	A	$\Delta\lambda$
PhPI	100	483,500	0.108465	g
	300	483,500	0.352256	
	500	483,500	0.411161	
	1	483,500	0.688183	
ANPI	100	530	0.736023	g
	300	530	0.843427	
	500	530	1.273721	
	1	530	2.151821	

DMPI	100	530	0.109475	12
	300	562	0.362236	
	500	562	0.411071	
	1	562	0.698194	
TPPI	100	527	0.481864	1
	300	527	0.747022	
	500	528	0.844528	
	1	528	1.383712	
BPPI	100	522	0.260921	3
	300	525	1.676819	
	500	525	1.642449	
	1	525	2.347619	

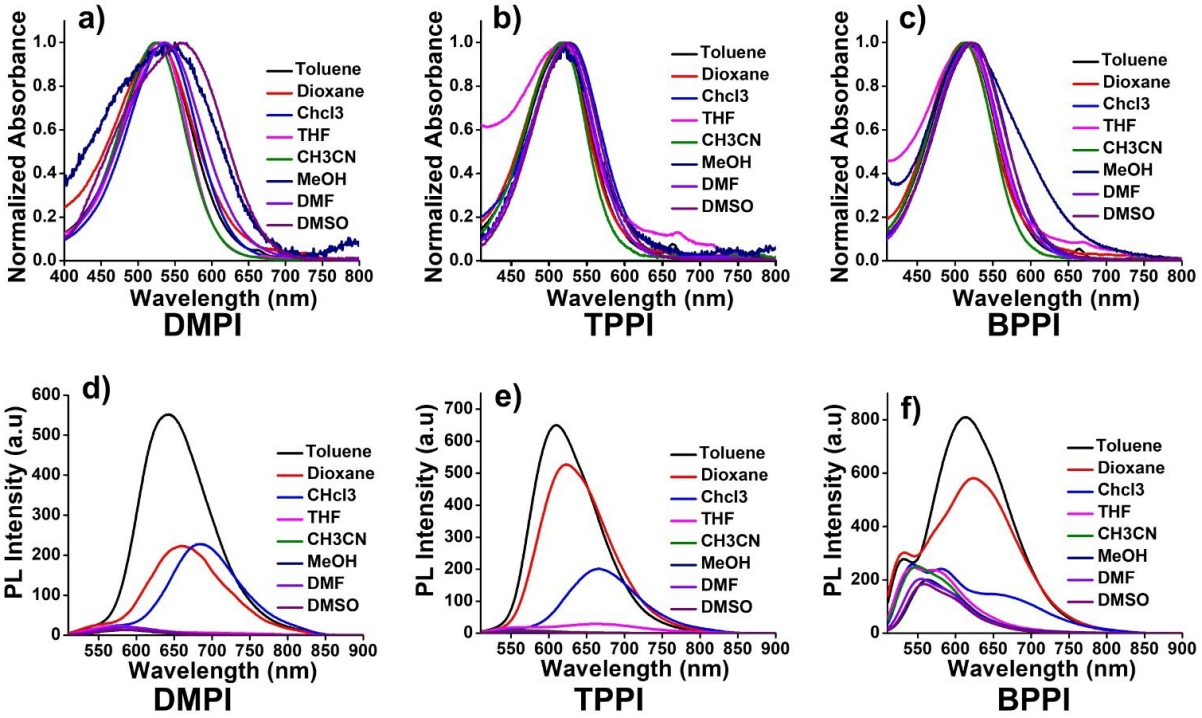

Fig. S5. Solvatochromic spectra of the **DMPI/TPPI/BPPI**. (a-c) Normalized absorbance, (d-f) PL of **DMPI/TPPI/BPPI** in various solvents from nonpolar to polar (100 μM, λ_{ex} = 370 nm).

Table S7. The solvatochromic UV-vis data for the **DMPI/TPPI/BPPI** in various solvents from nonpolar to polar (100 μM, λ_{ex} = 500 nm).

Materials	Solvents	$\lambda_{abs.max}$	A	Δλ
DMPI	Toluene	523	0.11558	38
	Dioxane	523	0.361995	
	$CHCl_3$	527	0.461564	
	THF	527	0.391699	
	CH_3CN	531	0.177949	

	MeOH	536	0.33932	
	DMF	536	0.024984	
	DMSO	561	0.054814	
TPPI	Toluene	515	0.119248	12
	Dioxane	516	0.108587	
	$CHCl_3$	516	0.020489	
	THF	517	0.166852	
	CH_3CN	520	0.142639	
	MeOH	523	0.083359	
	DMF	526	0.095205	
	DMSO	527	0.138597	
BPPI	Toluene	512	0.143156	10
	Dioxane	514	0.239489	
	$CHCl_3$	514	0.160268	
	THF	515	0.195539	
	CH_3CN	516	0.083211	
	MeOH	518	0.148083	
	DMF	520	0.091218	
	DMSO	522	0.169722	

$\Delta\lambda$ is the wavelength maxima shift in their absorption.

Table S8. The solvatochromic PL data of **DMPI/TPPI/BPPI** in various solvents from nonpolar to polar (100 μM, λ_{ex} = 500 nm).

Materials	**Solvents**	$\lambda_{em.max}$	**Δλ**
DMPI	Toluene	644	56
	Dioxane	665	
	$CHCl_3$	687	
	THF	700	
	CH_3CN	700	
	MeOH	700	
	DMF	700	
	DMSO	700	
TPPI	Toluene	611	49
	Dioxane	623	
	$CHCl_3$	657	
	THF	658	
	CH_3CN	660	
	MeOH	660	
	DMF	660	
	DMSO	660	
BPPI	Toluene	612	38
	Dioxane	626	
	$CHCl_3$	650	
	THF	650	

	CH_3CN	650	
	MeOH	650	
	DMF	650	
	DMSO	650	

$\Delta\lambda$ is the absorbance and wavelength maxima shift in their emission.

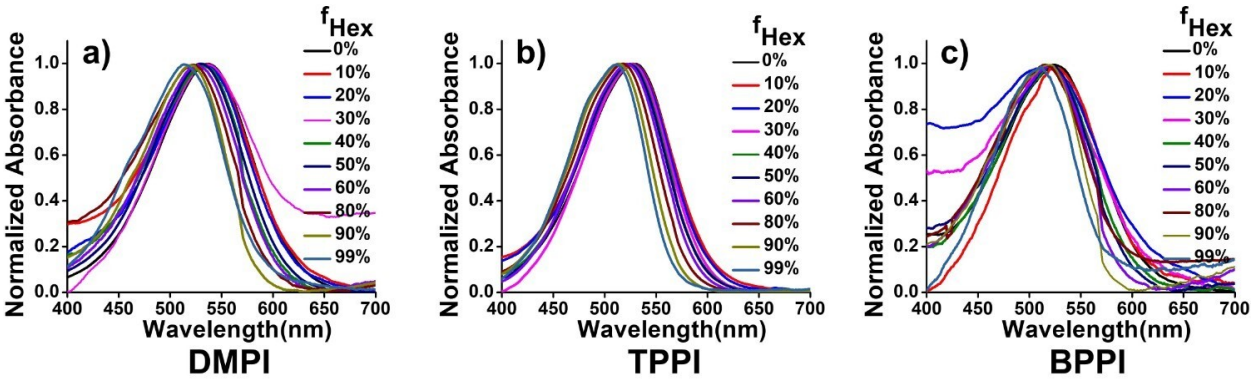

Fig. S6. (a-c) Normalized UV-vis spectra of **RPI** at various f_{Hex} in $CHCl_3$.

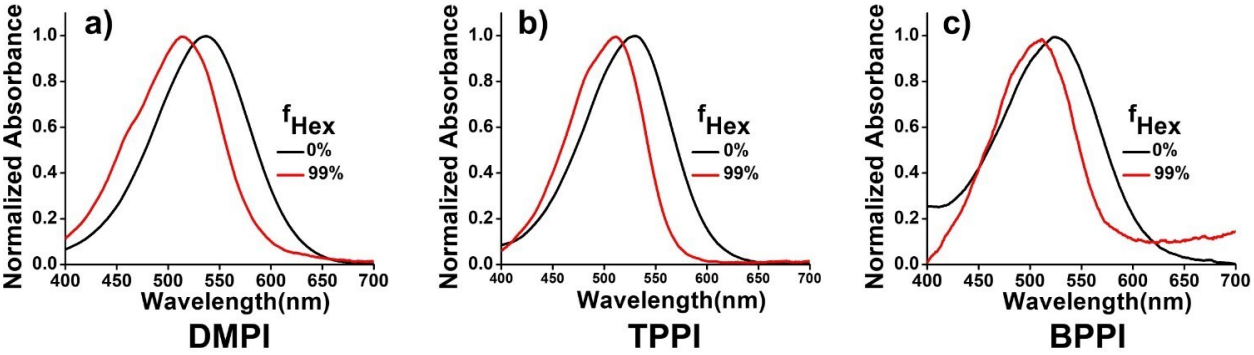

Fig. S7. (a-e) Normalized UV-vis spectra of **RPI** at 0% and 99% f_{Hex} in $CHCl_3$.

Table S9. UV-vis absorption data for **RPI**.

Materials	Hexane fraction (f_{Hex})	$\lambda_{abs.max}$	$\lambda_{em.max}$	A	$\Delta\lambda$
DMPI	0%	536	676	0.146474	22
	99%	514	570	0.04589	
TPPI	0%	530	657	0.128937	11
	99%	511	570	0.049999	
BPPI	0%	523	657	0.034017	10
	99%	513	570	0.016903	

A, $\Delta\lambda$, are the absorbance and wavelength maxima shift in their absorption.

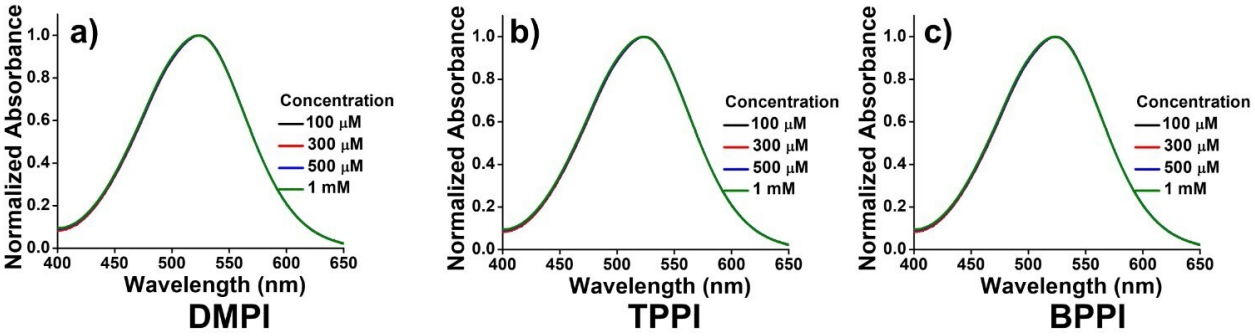

Fig. S8. (a-c) Normalized UV-vis spectra of **RPI** at different concentrations in $CHCl_3$.

Table S10. UV-vis absorption data for the **RPI** at different concentrations in $CHCl_3$.

Materials	Concentration (μM)	$\lambda_{abs.max}$	A	$\Delta\lambda$
DMPI	100	536	0.381863	3
	300	537	0.447021	
	500	538	0.944528	
	1	539	1.483712	
TPPI	100	530	0.491864	2
	300	531	0.767022	
	500	531	0.944528	
	1	532	1.683712	
BPPI	100	523	0.461864	1
	300	523	0.777022	
	500	524	0.844528	
	1	524	1.393712	

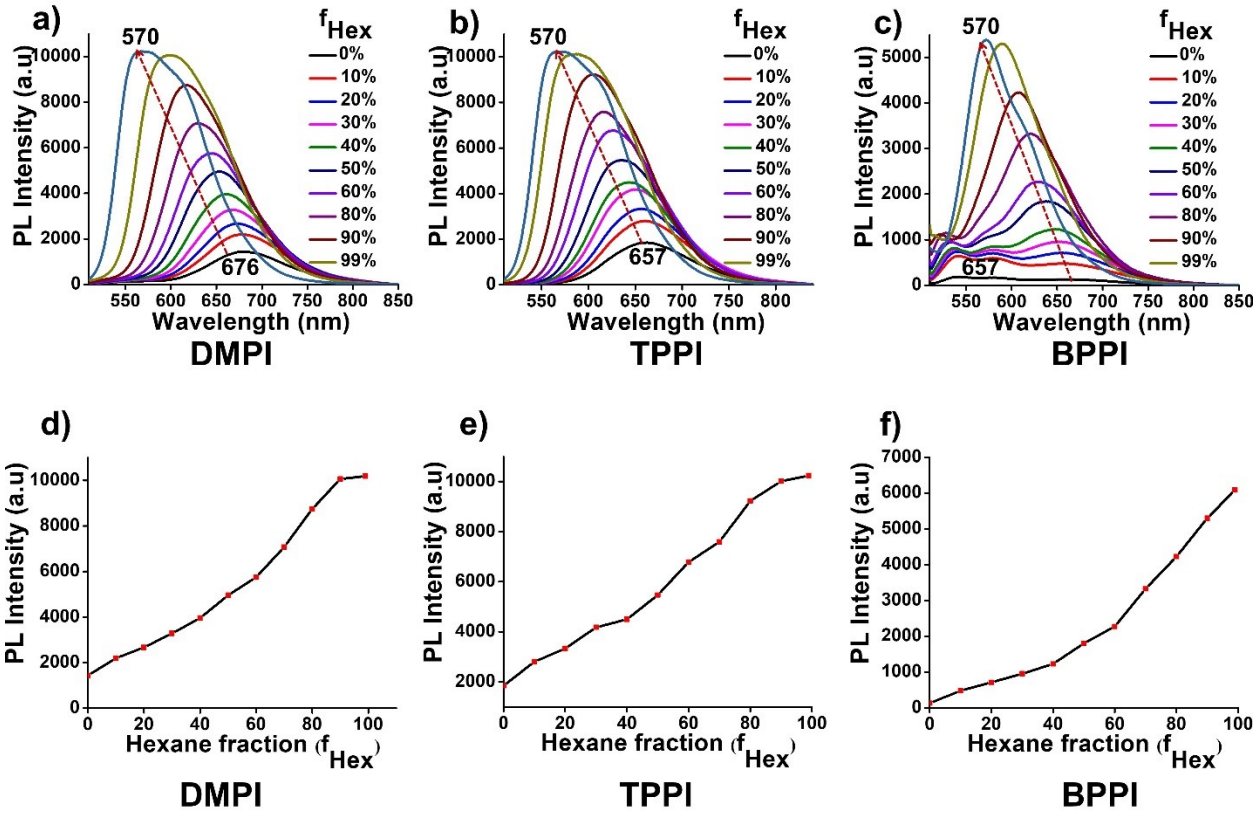

Fig. S9. PL spectra of (a) **DMPI**, (b) **TPPI**, and (c) **BPPI,** respectively, at various f_{Hex} in $CHCl_3$ (100 μM, λ_{ex} = 500). (d-f) plots of $\lambda_{em,max}$ at different f_{Hex} in $CHCl_3$.

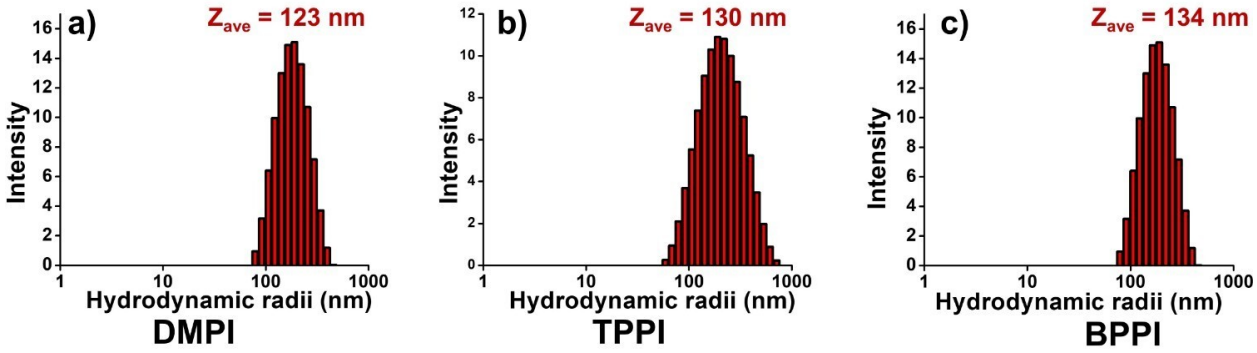

Fig. S10. (a-c) Hydrodynamic radius vs intensity plot of the **DMPI/TPPI/BPPI** at 99.9% f_w in DMSO (100 μM).

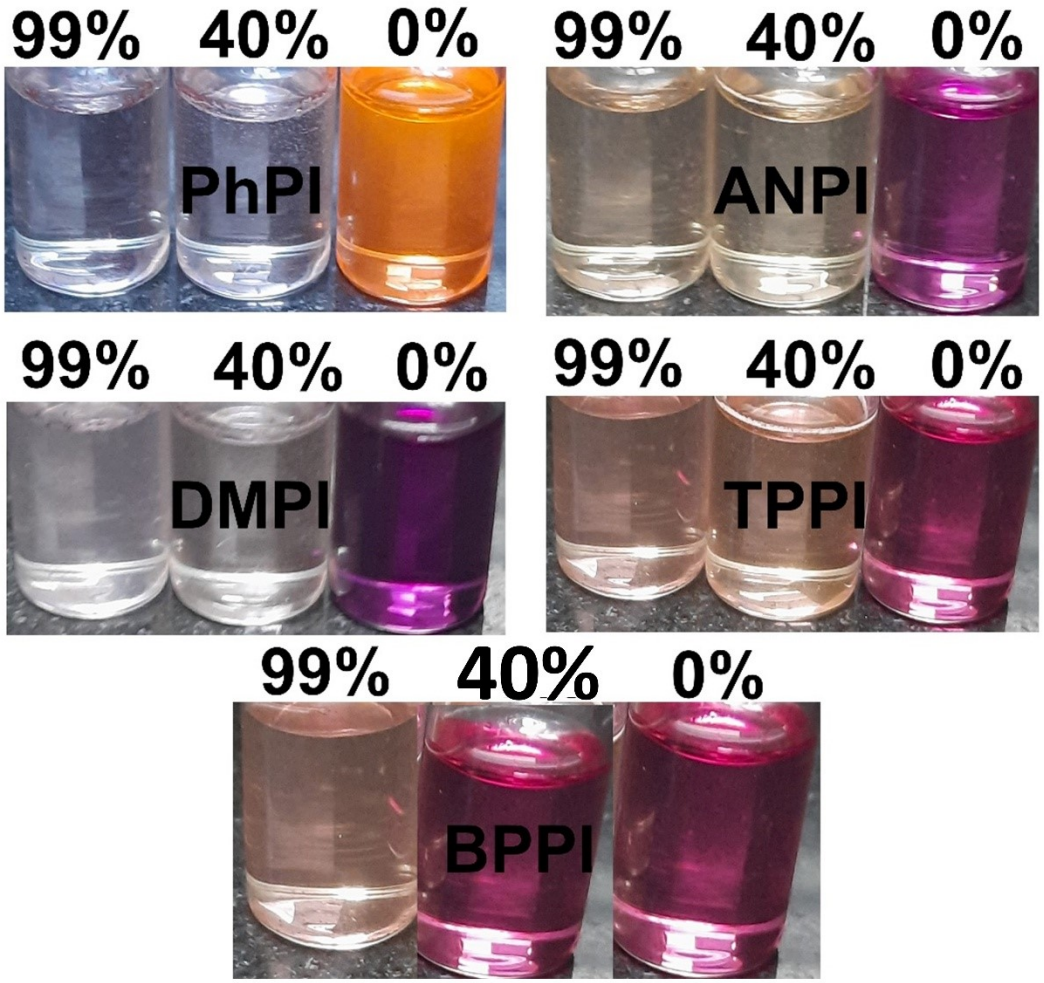

Fig. S11. Capturing daylight photographs of **PhPI/ANPI/DMPI/TPPI/BPPI** at 0%, 40%, and 99% f_w in DMSO.

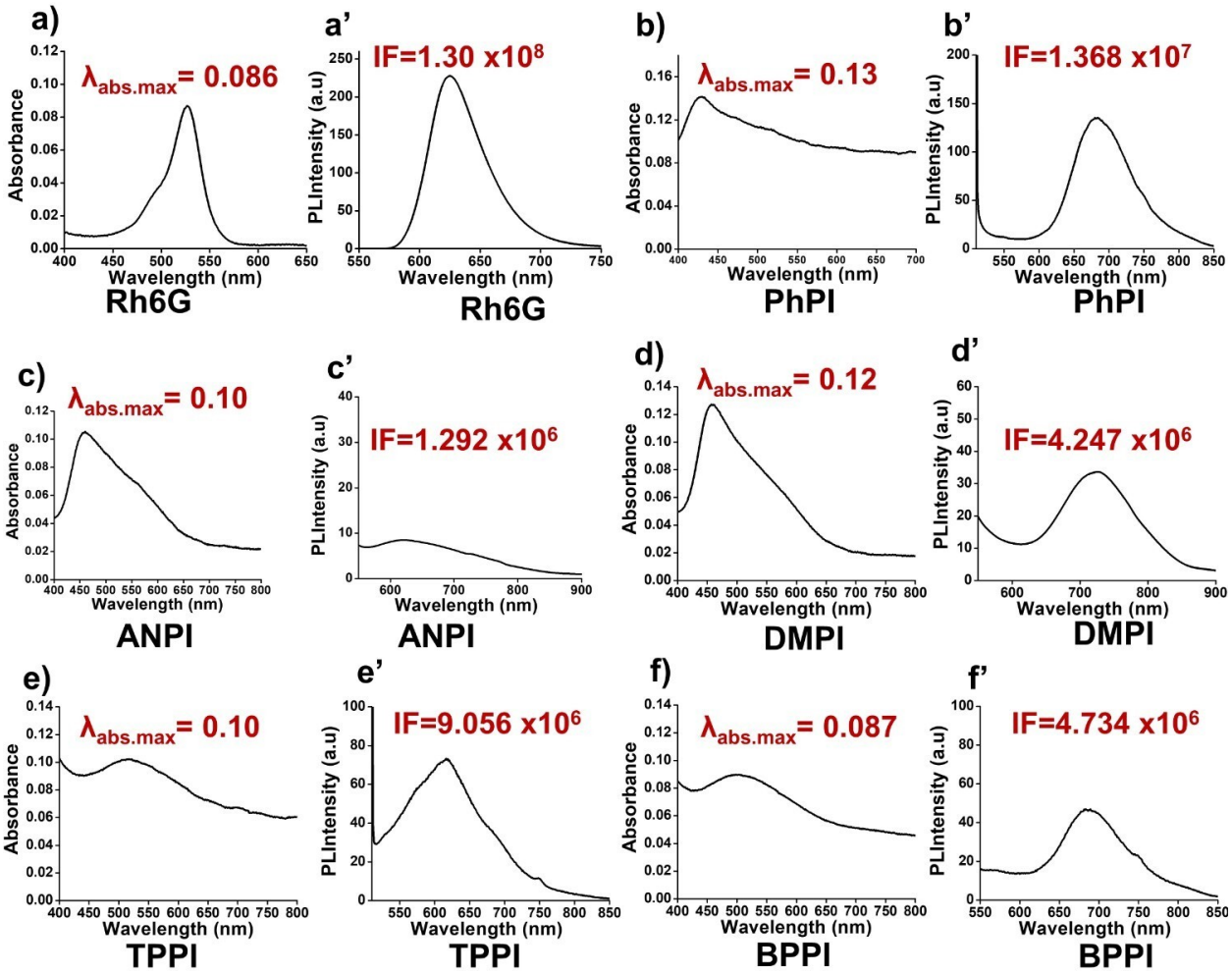

Fig. S12. (a and a'), (b and b'), (c and c'), (d and d'), (e and e'), and (f and f') are the absorbance and emission peak area of rhodamine 6G/**PhPI/ANPI/DMPI/TPPI/BPPI** at 99% f_w in DMSO, at their corresponding slit.

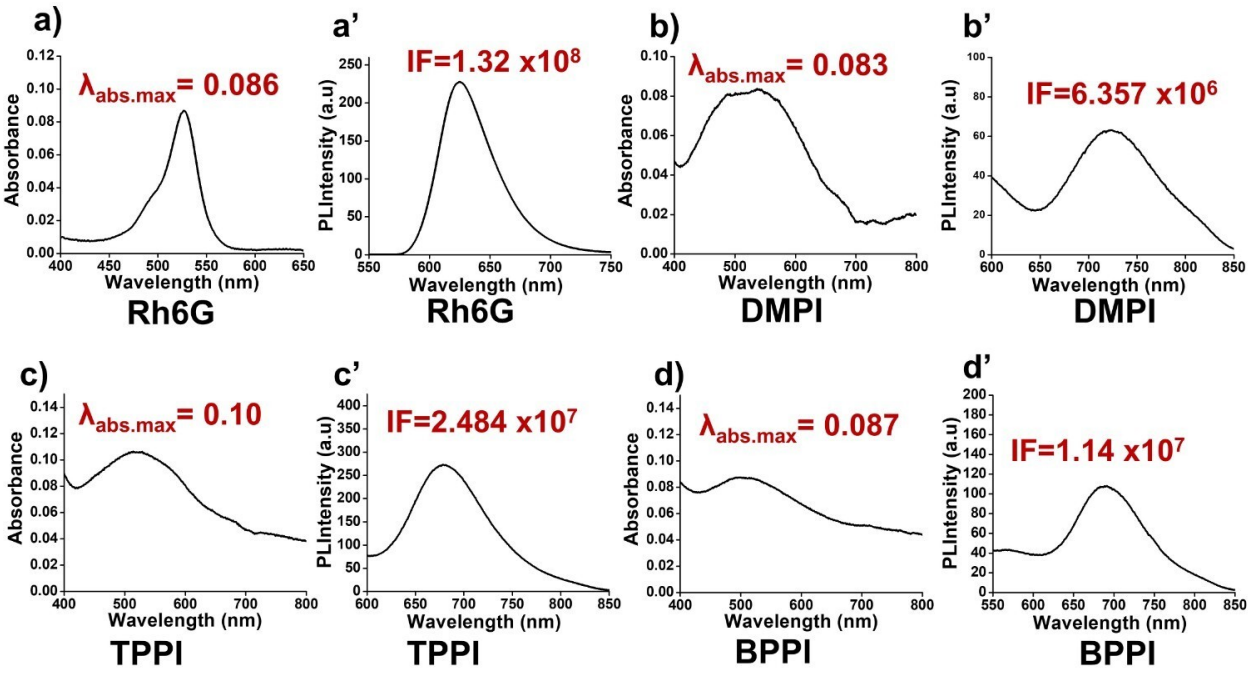

Fig. S13. (a and a'), (b and b'), (c and c'), and, (d and d') are the absorbance and emission peak area of rhodamine 6G/**PhPI/ANPI/DMPI/TPPI/BPPI**, at 40% f_w in DMSO, at their corresponding slit.

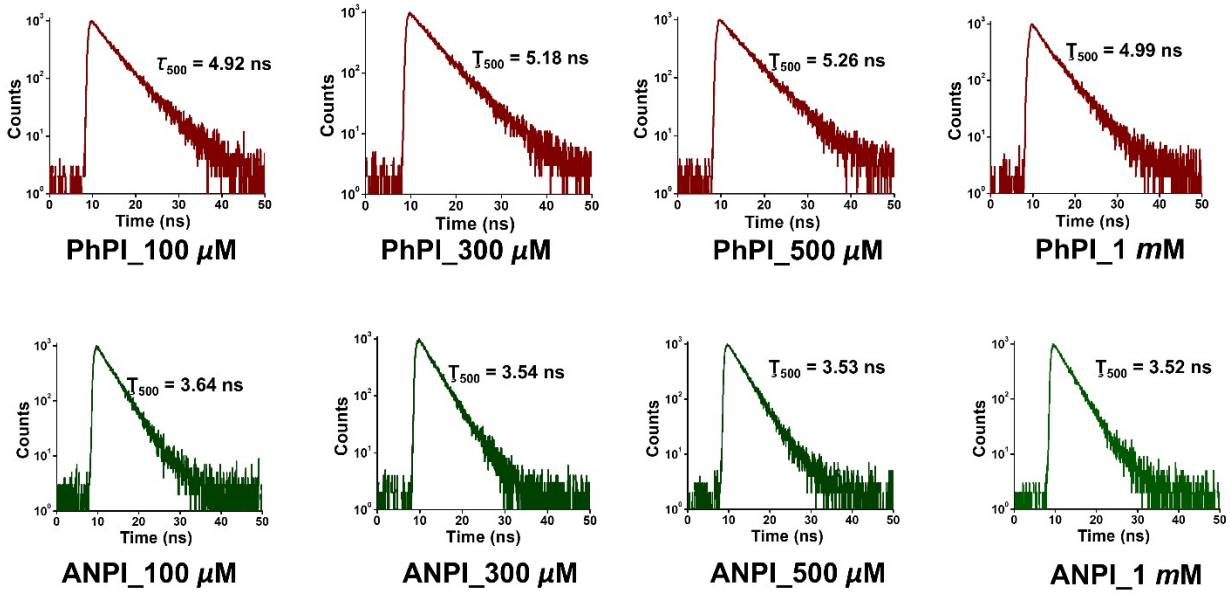

Fig. S14. Life time studies using time resolved photoluminescence (TRPL) spectroscopy of **PhPI** and **ANPI** at their lower to higher concentrations.

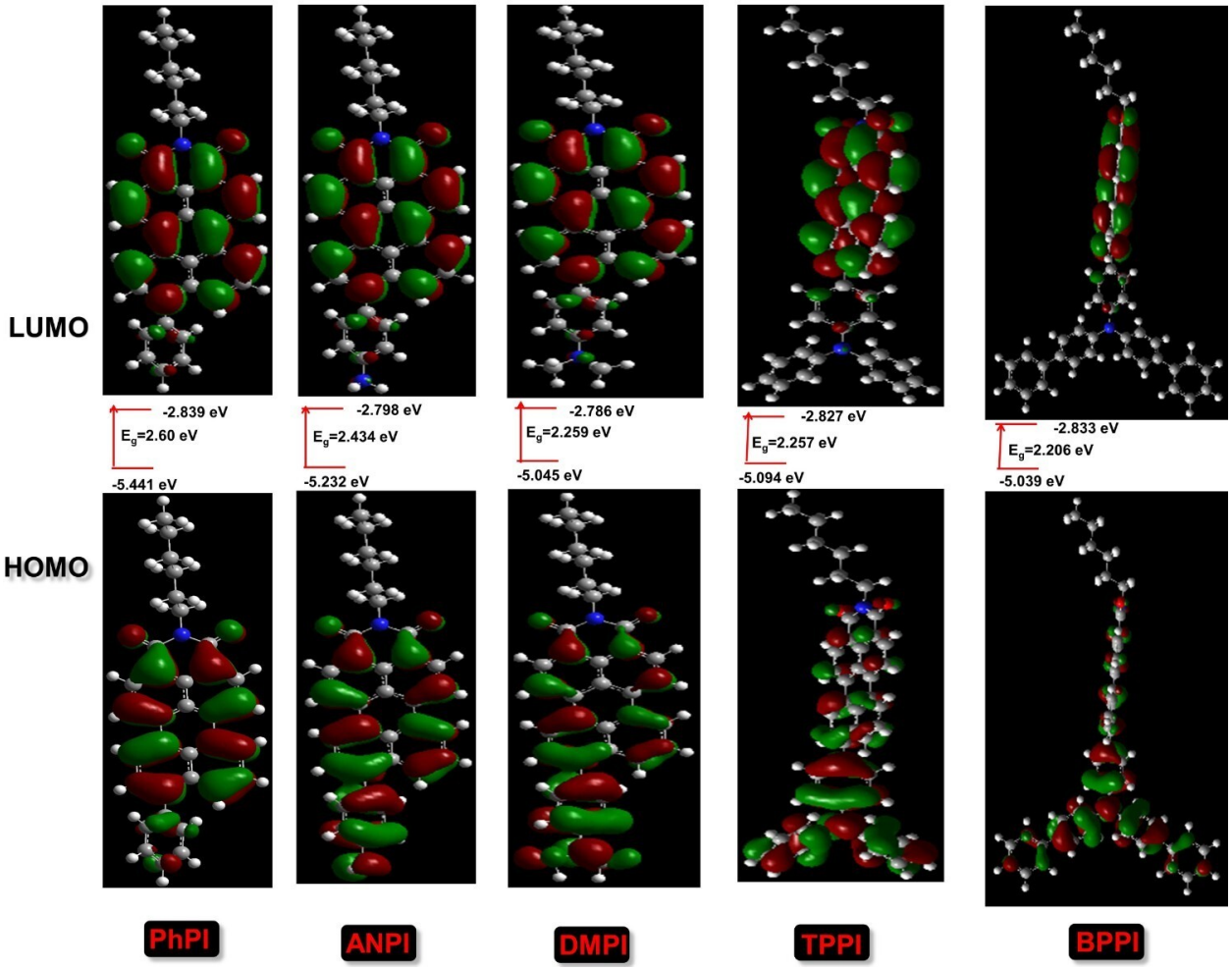

Fig. S15. Optimized ground state band energies (eV) of **RPI** in DMSO, calculated using DFT/B3LYP with the 6-31G (d, p) basis set (Gaussian 16).

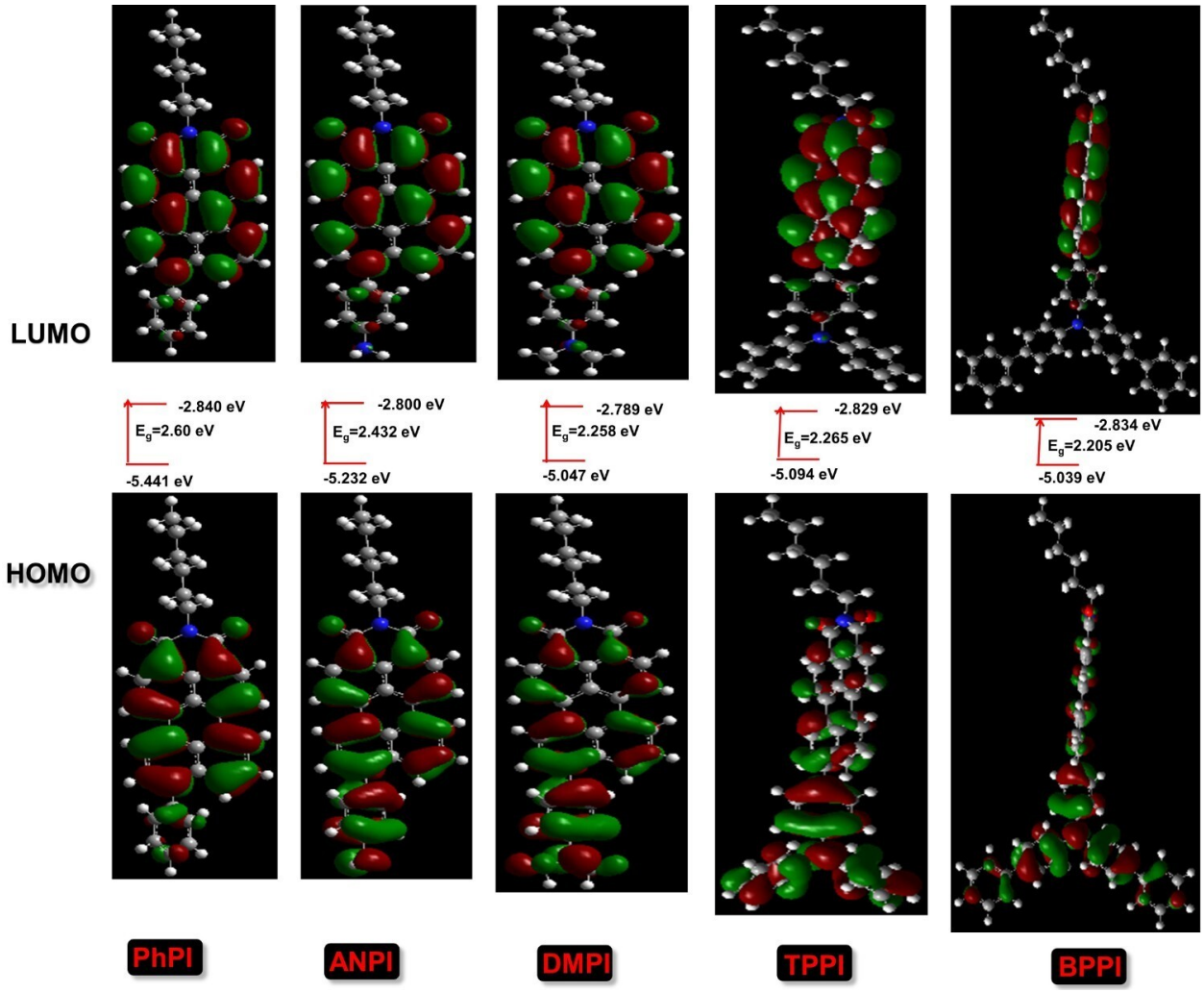

Fig. S16. Ground state band energies (eV) of **RPI** in water, calculated using DFT/B3LYP with the 6-31G (d, p) basis set (Gaussian 16).

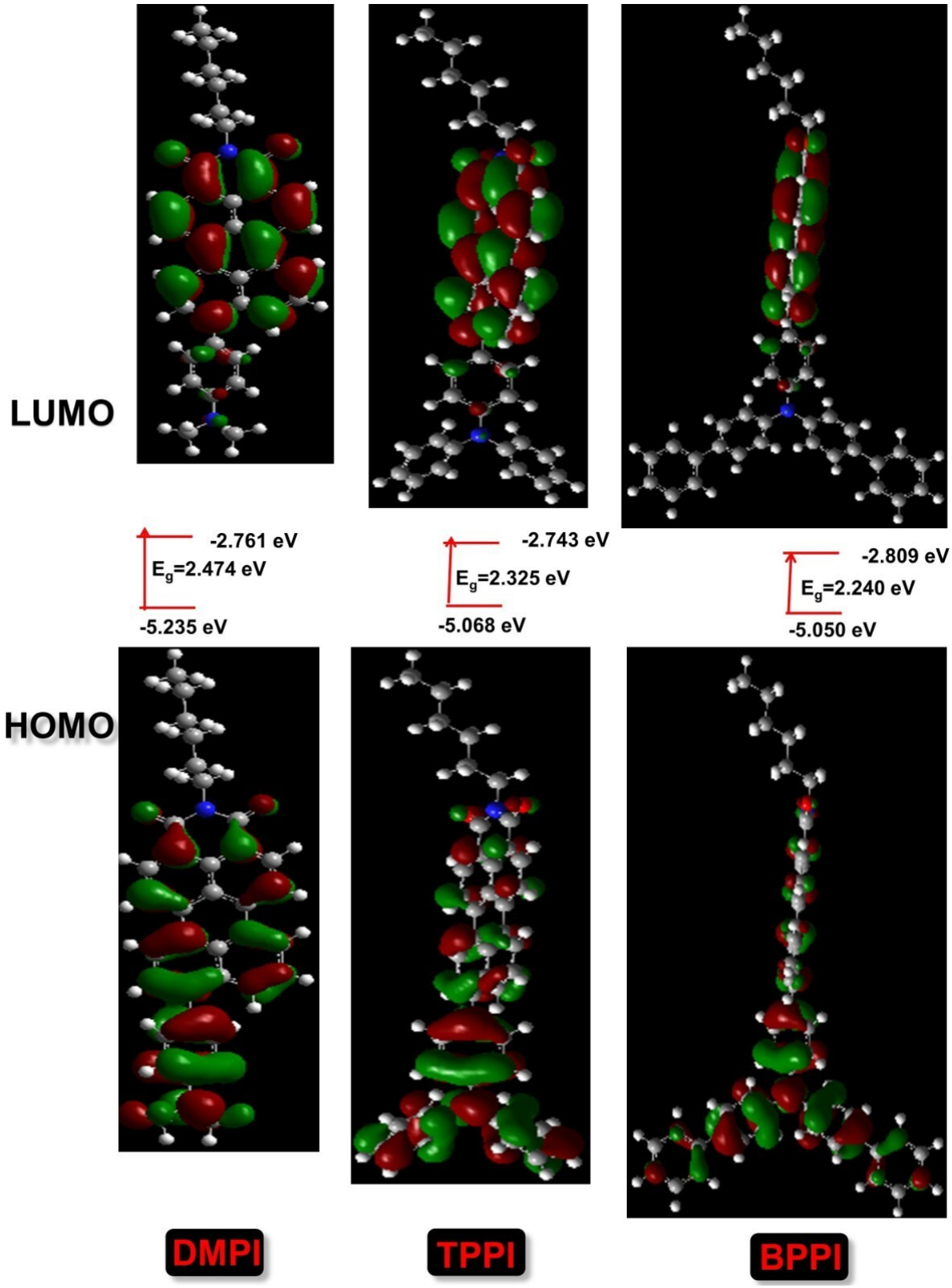

Fig. S17. Optimized ground state band energies (eV) of **DMPI**/**TPPI**/**BPPI** in chloroform, calculated using DFT/B3LYP with the 6-31G (d, p) basis set (Gaussian 16).

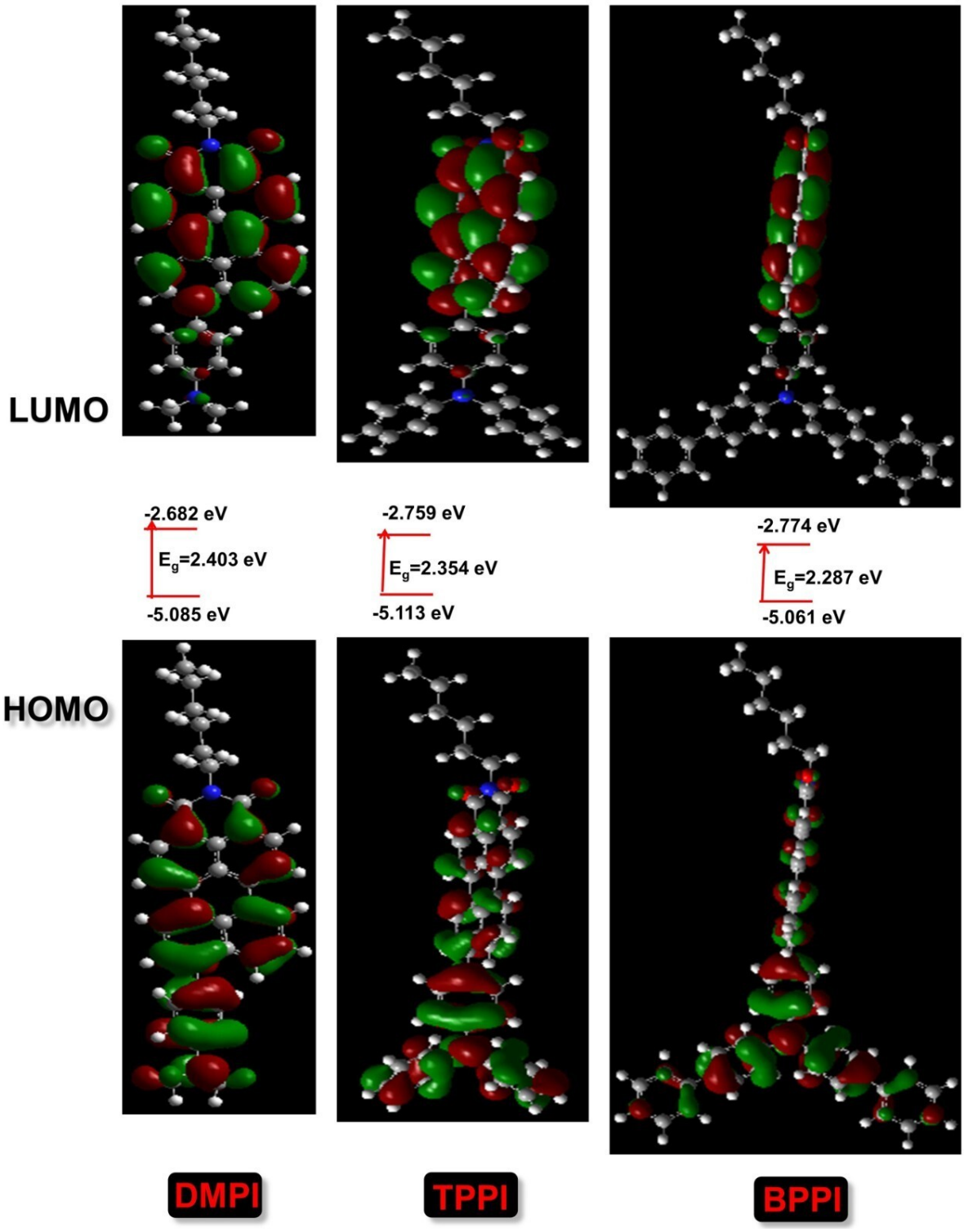

Fig. S18. Optimized band energies (eV) of **DMPI/TPPI/BPPI** in hexane, calculated using DFT/B3LYP with the 6-31G (d, p) basis set (Gaussian 16), in their ground state.

1.13. Theoretical properties studies

The S_1 singlet state, initially populated at the Franck-Condon point, involves an electron transition from HOMO to LUMO and exhibits partial charge-transfer character (Fig. S19 and see reference 47 in manuscript). Both S_1 and T_1 states are $\pi\pi^*$ and involve HOMO to LUMO transitions, but differ in their electronic properties (See reference 47 in manuscript). Upon photo irradiation, ground state PSs are excited to the singlet excited state ($^1PS^*$), which then undergoes ISC to the triplet excited state ($^3PS^*$). For effective type-I PSs, the following design criteria must be met: 1) Efficient ISC from S_1 to T_1. 2) Long T_1 lifetime for ROS production. 3) T_1 energy lower than 0.98 eV to avoid $^1O_2$ production (type-II processes). 4) Appropriate redox potential for generating ROS. Due to these challenges, type-I metal-free PSs are rare.[9, 10] Effective ISC is crucial for both type-I electron transfer and type-II energy transfer processes. For a good system, the ISC rate constant (K_{ISC}) is expected to follow the eqn: $K_{ISC} \propto \langle T_1 | (H_{SO}) | S_1 \rangle^2 / (\Delta E_{S1\text{-}T1})^2$, where H_{SO} is the Hamiltonian for SOC (See reference 47 in manuscript).[11, 12] According to this eqn, ISC efficiency increases quadratically as the energy gap $\Delta E_{S1\text{-}T1}$ decreases.

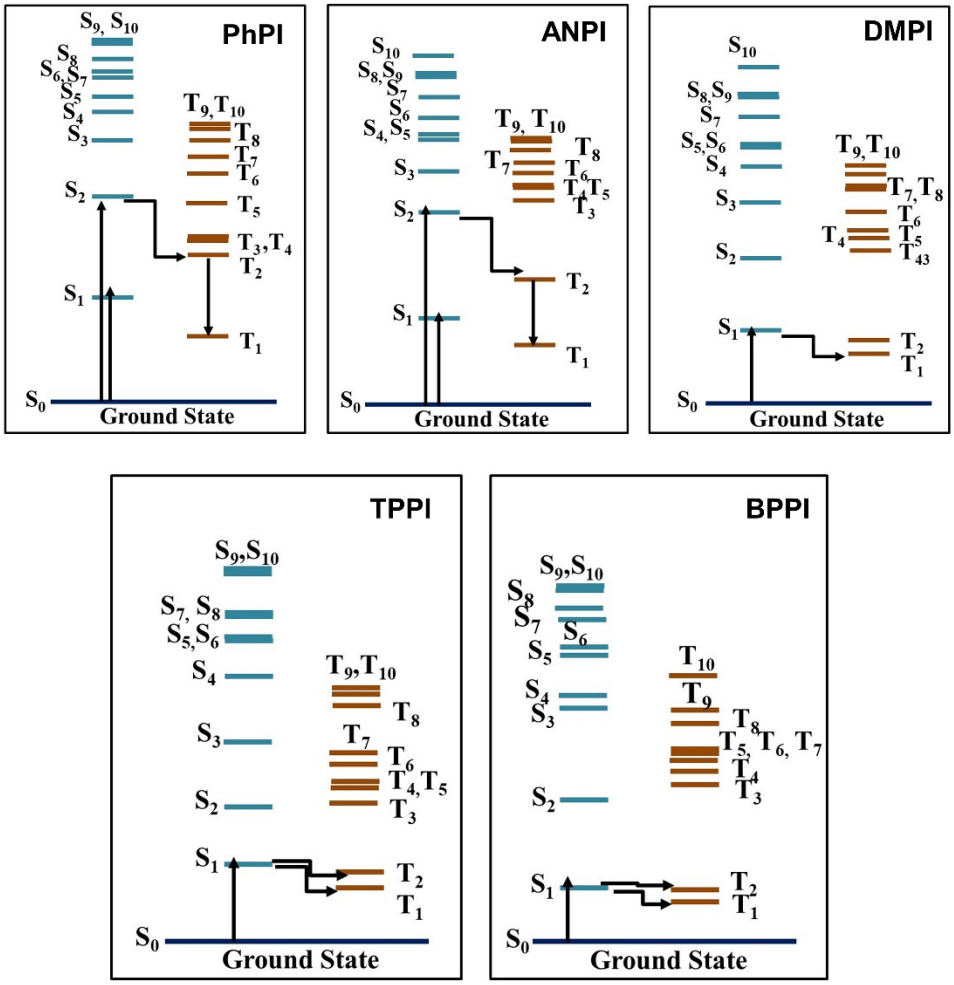

Fig. S19. (b) SOC is evaluated using the SOC-TDDFT method by ORCA 5.0 Software for all **RPI**: **PhPI/ ANPI/DMPI/TPPI/BPPI**. [**DMPI**: $\Delta E_{S1\text{-}T1}$ = 0.623, $\Delta E_{S2\text{-}T2}$ = 0.637, ζ (S_1, T_1) = 0. 447 cm^{-1}, ζ (S_2T_2) = 0.7 cm^{-1}, **TPPI**: $\Delta E_{S1\text{-}T1}$ = 0.639, $\Delta E_{S2\text{-}T2}$ = 0.628, ζ (S_1, T_1) = 0. 141 cm^{-1}, ζ (S_2, T_2) = 0.282 cm^{-1}, **BPPI**: $\Delta E_{S1\text{-}T1}$ = 0.592, $\Delta E_{S2\text{-}T2}$ = 0.702, ζ (S_1, T_1) = 0. 141 cm^{-1}, ζ (S_2, T_2) = .387 cm^{-1}].

Table S11. Spin-orbit coupling matrix elements (SOCME) <Sm|HSO|Tn>, in cm^{-1}, of **RPI** in optimized structures, calculated using ORCA 5.0 at B3LYP/6-31G (d, p) and B3LYP/DEF2SVP levels.

SOC	PhPI	ANPI	DMPI	TPPI	BPPI
$S_0 \leftrightarrow T_1$	0.264575	0.2	0.1	0.141421	0.34641
$S_1 \leftrightarrow T_1$	0	0	0.447214	0.141421	0.141421
$S_2 \leftrightarrow T_1$	4.2	0.173205	0.387298	0.1	0.264575
$S_3 \leftrightarrow T_1$	0.774597	4.1833	4.150904	4.136424	0.424264
$S_4 \leftrightarrow T_1$	1.252996	0.655744	0.648074	0.52915	3.756328

$S_5 \leftrightarrow T_1$	1.79722	1.860108	1.122497	0.316228	0.412311
$S_6 \leftrightarrow T_1$	1.791647	0.509902	1.496663	1.670329	0.43589
$S_7 \leftrightarrow T_1$	1.783255	2.085665	1.769181	1.68226	0.883176
$S_8 \leftrightarrow T_1$	0.768115	1.1	1.252996	1.621727	0.989949
$S_9 \leftrightarrow T_1$	0.894427	0.574456	1.870829	1.694107	1.967232
$S_{10} \leftrightarrow T_1$	0.616441	0.728011	0.7	0.173205	1.109054
$S_0 \leftrightarrow T_2$	1.153256	0.781025	0.787401	0.556776	0.52915
$S_1 \leftrightarrow T_2$	0.69282	0.424264	0.141421	0.282843	0.223607
$S_2 \leftrightarrow T_2$	3.714835	0.43589	0.7	0.282843	0.387298
$S_3 \leftrightarrow T_2$	0.866025	3.104835	2.26495	2.459675	0.883176
$S_4 \leftrightarrow T_2$	1.679286	0.728011	0.894427	0.412311	2.22486
$S_5 \leftrightarrow T_2$	2.435159	1.854724	0.424264	0.282843	0.52915
$S_6 \leftrightarrow T_2$	2.547548	0.69282	0.565685	0.969536	0.519615
$S_7 \leftrightarrow T_2$	2.328089	2.293469	1.555635	1.407125	0.678233
$S_8 \leftrightarrow T_2$	0.943398	0.969536	1.081665	1.345362	0.479583
$S_9 \leftrightarrow T_2$	0.7	0.728011	1.004988	0.943398	1.356466
$S_{10} \leftrightarrow T_2$	1.004988	0.556776	0.648074	0.67082	0.877496
$S_0 \leftrightarrow T_3$	3.274141	2.161018	1.228821	1.363818	0.994987
$S_1 \leftrightarrow T_3$	1.760682	0.921954	0.866025	0.648074	0.424264
$S_2 \leftrightarrow T_3$	2.491987	1.081665	0.678233	0.685565	0.331662
$S_3 \leftrightarrow T_3$	1.459452	2.343075	3.641428	3.509986	0.2
$S_4 \leftrightarrow T_3$	0.818535	0.173205	0.538516	0.648074	0.141421
$S_5 \leftrightarrow T_3$	1.053565	1.780449	1.431782	0.663325	0.3
$S_6 \leftrightarrow T_3$	1.509967	0.424264	1.972308	2.227106	0.632456
$S_7 \leftrightarrow T_3$	2.123676	2.213594	2.609598	2.45153	0.608276
$S_8 \leftrightarrow T_3$	0.866025	1.445683	1.708801	2.271563	0.2
$S_9 \leftrightarrow T_3$	1.224745	0.793725	2.541653	2.238303	0.223607
$S_{10} \leftrightarrow T_3$	1.24499	0.8	0.877496	0.360555	0
$S_0 \leftrightarrow T_4$	7.098591	5.889822	2.167948	2.293469	1.090871
$S_1 \leftrightarrow T_4$	3.931921	2.898275	0.387298	0.447214	0.678233

$S_2 \leftrightarrow T_4$	1.249	2.760435	1.135782	1.228821	0.43589
$S_3 \leftrightarrow T_4$	2.54951	2.776689	2.513961	2.565151	0.458258
$S_4 \leftrightarrow T_4$	2.116601	1.788854	0.959166	0.6245	2.856571
$S_5 \leftrightarrow T_4$	3.17175	3.083829	1.019804	0.360555	0.842615
$S_6 \leftrightarrow T_4$	2.557342	1.4	1.30767	1.486607	0.173205
$S_7 \leftrightarrow T_4$	2.186321	2.925748	1.581139	1.410674	0.806226
$S_8 \leftrightarrow T_4$	1.095445	1.862794	1.260952	1.577973	1.034408
$S_9 \leftrightarrow T_4$	1.979899	1.315295	2.044505	1.881489	2.088061
$S_{10} \leftrightarrow T_4$	2.167948	1.509967	0.509902	0.768115	1.334166
$S_0 \leftrightarrow T_5$	1.634013	6.170899	7.174956	7.165891	0.360555
$S_1 \leftrightarrow T_5$	0.959166	2.984962	1.780449	2.042058	0.1
$S_2 \leftrightarrow T_5$	3.508561	2.922328	3.956008	3.954744	0.52915
$S_3 \leftrightarrow T_5$	1.752142	2.769476	0.911043	0.948683	0.173205
$S_4 \leftrightarrow T_5$	2.372762	1.646208	2.435159	2.123676	2.946184
$S_5 \leftrightarrow T_5$	3.718871	1.493318	1.208305	0.979796	0.812404
$S_6 \leftrightarrow T_5$	4.257934	1.473092	1.957039	2.063977	0.6
$S_7 \leftrightarrow T_5$	4.236744	1.161895	3.433657	3.229551	0.316228
$S_8 \leftrightarrow T_5$	2.158703	2.543619	1.473092	1.907878	1.034408
$S_9 \leftrightarrow T_5$	2.085665	1.92873	2.080865	2.428992	2.204541
$S_{10} \leftrightarrow T_5$	2.315167	1.574802	0.282843	1.75784	1.28841
$S_0 \leftrightarrow T_6$	2.206808	1.603122	1.574802	1.558846	2.837252
$S_1 \leftrightarrow T_6$	1.224745	0.793725	0.34641	0.43589	0.547723
$S_2 \leftrightarrow T_6$	2.984962	0.905539	#NUM!	0.948683	1.523155
$S_3 \leftrightarrow T_6$	1.618641	3.482815	3.443835	3.417601	0.2
$S_4 \leftrightarrow T_6$	1.452584	0.774597	1.367479	0.565685	1.949359
$S_5 \leftrightarrow T_6$	2.807134	3.832754	2.029778	0.768115	0.141421
$S_6 \leftrightarrow T_6$	3.634556	0.282843	2.880972	3.358571	0.927362
$S_7 \leftrightarrow T_6$	3.869108	4.90306	4.05216	3.831449	1.024695
$S_8 \leftrightarrow T_6$	2.3	2.58457	2.863564	3.772267	0.547723
$S_9 \leftrightarrow T_6$	2.321637	1.813836	4.453089	4.106093	0.640312

$S_{10}\leftrightarrow T_6$	2.48998	1.581139	1.8	0.5	0.583095
$S_0\leftrightarrow T_7$	1.549193	2.247221	1.195826	1.431782	6.465292
$S_1\leftrightarrow T_7$	0.866025	1.063015	0.223607	0.655744	1.637071
$S_2\leftrightarrow T_7$	0.9	1.131371	0.43589	0.387298	3.548239
$S_3\leftrightarrow T_7$	0.8	2.946184	2.085665	2.649528	0.565685
$S_4\leftrightarrow T_7$	0.74162	0.989949	0.331662	0.5	0.905539
$S_5\leftrightarrow T_7$	0.7	2.847806	0.860233	0.616441	0.244949
$S_6\leftrightarrow T_7$	1.67332	0.583095	0.969536	1.802776	1.89473
$S_7\leftrightarrow T_7$	2.007486	4.33705	1.417745	1.992486	1.905256
$S_8\leftrightarrow T_7$	1.421267	2.455606	1.122497	2.004994	2.19089
$S_9\leftrightarrow T_7$	1.459452	2.012461	0.6	1.876166	3.556684
$S_{10}\leftrightarrow T_7$	1.552417	1.946792	0.141421	0.6245	1.997498
$S_0\leftrightarrow T_8$	3.198437	2.114237	2.238303	2.253886	1.772005
$S_1\leftrightarrow T_8$	1.606238	1.014889	0.72111	0.591608	0.489898
$S_2\leftrightarrow T_8$	2.505993	0.984886	1.208305	1.236932	1.004988
$S_3\leftrightarrow T_8$	1.264911	1.630951	3.054505	2.93087	0.331662
$S_4\leftrightarrow T_8$	2.280351	1.236932	1.479865	1.144552	3.762978
$S_5\leftrightarrow T_8$	1.967232	0.974679	1.363818	0.43589	0.141421
$S_6\leftrightarrow T_8$	1.9	0.685565	2.213594	2.515949	0.927362
$S_7\leftrightarrow T_8$	3.08707	2.903446	3.340659	3.127299	1.228821
$S_8\leftrightarrow T_8$	2.56125	1.830301	2.473863	3.248076	1.513275
$S_9\leftrightarrow T_8$	2.712932	1.75784	4.204759	3.948417	3.722902
$S_{10}\leftrightarrow T_8$	2.908608	1.74069	1.941649	0.34641	2.345208
$S_0\leftrightarrow T_9$	3.910243	2.632489	2.211334	0.883176	0.591608
$S_1\leftrightarrow T_9$	2	1.118034	0.74162	0.632456	0.848528
$S_2\leftrightarrow T_9$	1.852026	1.144552	1.081665	0.1	0.223607
$S_3\leftrightarrow T_9$	0.2	1.838478	2.295648	0.8544	0.1
$S_4\leftrightarrow T_9$	3.793415	1.615549	1.2	0.574456	1.034408
$S_5\leftrightarrow T_9$	4.485532	2.163331	0.360555	0.754983	0.173205
$S_6\leftrightarrow T_9$	3.283291	0.824621	1.014889	0.6	0.714143

$S_7 \leftrightarrow T_9$	0.3	1.542725	1.997498	0.632456	0.812404
$S_8 \leftrightarrow T_9$	2.75318	1.431782	1.67332	0.244949	0.5
$S_9 \leftrightarrow T_9$	3.029851	1.876166	3.054505	1.204159	0.781025
$S_{10} \leftrightarrow T_9$	3.122499	1.774824	1.618641	0.141421	0.519615
$S_0 \leftrightarrow T_{10}$	1.019804	4.08534	2.267157	2.059126	2.291288
$S_1 \leftrightarrow T_{10}$	0.509902	1.763519	0.223607	0.685565	0.728011
$S_2 \leftrightarrow T_{10}$	0.6	1.873499	1.122497	1.081665	1.228821
$S_3 \leftrightarrow T_{10}$	0.3	0.591608	1.264911	1.954482	0.3
$S_4 \leftrightarrow T_{10}$	0.877496	2.782086	0.974679	1.157584	3.167018
$S_5 \leftrightarrow T_{10}$	0.959166	4.644351	1.424781	0.616441	0.2
$S_6 \leftrightarrow T_{10}$	0.678233	1.456022	1.442221	0.979796	0.964365
$S_7 \leftrightarrow T_{10}$	0.34641	2.497999	1.462874	1.752142	1.048809
$S_8 \leftrightarrow T_{10}$	0.774597	1.603122	0.583095	2.073644	0.663325
$S_9 \leftrightarrow T_{10}$	0.774597	2.840775	1.967232	2.803569	2.754995
$S_{10} \leftrightarrow T_{10}$	0.774597	2.858321	1.43527	0.4	1.824829

Table S12. Excited state singlet-triplet energy difference (ΔE_{ST}) in eV for **RPI**, calculated using ORCA 5.0 at B3LYP/6-31G (d, p) and B3LYP/DEF2SVP levels.

ΔE_{ST}	PhPI	ANPI	DMPI	TPPI	BPPI
$S_1 \leftrightarrow T_1$	1.182	1.083	0.623	0.639	0.522
$S_1 \leftrightarrow T_2$	-0.163	-0.065	0.026	0.007	0
$S_1 \leftrightarrow T_3$	-0.294	-0.399	-0.773	-0.774	-0.741
$S_1 \leftrightarrow T_4$	-0.312	-0.432	-0.867	-0.855	-0.84
$S_1 \leftrightarrow T_5$	-0.435	-0.439	-0.905	-0.891	-0.921
$S_1 \leftrightarrow T_6$	-0.574	-0.556	-1.025	-1.012	-0.971
$S_1 \leftrightarrow T_7$	-0.673	-0.703	-1.161	-1.042	-0.985
$S_1 \leftrightarrow T_8$	-0.732	-0.79	-1.164	-1.155	-1.118
$S_1 \leftrightarrow T_9$	-0.777	-0.882	-1.269	-1.234	-1.155
$S_1 \leftrightarrow T_{10}$	-0.8	-0.894	-1.339	-1.25	-1.259
$S_2 \leftrightarrow T_1$	1.692	1.46	1.234	1.26	1.225

$S_2 \leftrightarrow T_2$	0.347	0.312	0.637	0.628	0.703
$S_2 \leftrightarrow T_3$	0.216	-0.022	-0.162	-0.153	-0.038
$S_2 \leftrightarrow T_4$	0.198	-0.055	-0.256	-0.234	-0.137
$S_2 \leftrightarrow T_5$	0.075	-0.062	-0.294	-0.27	-0.218
$S_2 \leftrightarrow T_6$	-0.064	-0.179	-0.414	-0.391	-0.268
$S_2 \leftrightarrow T_7$	-0.163	-0.326	-0.55	-0.421	-0.282
$S_2 \leftrightarrow T_8$	-0.222	-0.413	-0.553	-0.534	-0.415
$S_2 \leftrightarrow T_9$	-0.267	-0.505	-0.658	-0.613	-0.452
$S_2 \leftrightarrow T_{10}$	-0.29	-0.517	-0.728	-0.629	-0.556
$S_3 \leftrightarrow T_1$	1.948	1.718	1.728	1.729	1.678
$S_3 \leftrightarrow T_2$	0.603	0.57	1.131	1.097	1.156
$S_3 \leftrightarrow T_3$	0.472	0.236	0.332	0.316	0.415
$S_3 \leftrightarrow T_4$	0.454	0.203	0.238	0.235	0.316
$S_3 \leftrightarrow T_5$	0.331	0.196	0.2	0.199	0.235
$S_3 \leftrightarrow T_6$	0.192	0.079	0.08	0.078	0.185
$S_3 \leftrightarrow T_7$	0.093	-0.068	-0.056	0.048	0.171
$S_3 \leftrightarrow T_8$	0.034	-0.155	-0.059	-0.065	0.038
$S_3 \leftrightarrow T_9$	-0.011	-0.247	-0.164	-0.144	0.001
$S_3 \leftrightarrow T_{10}$	-0.034	-0.259	-0.234	-0.16	-0.103
$S_4 \leftrightarrow T_1$	2.026	2.022	1.991	2.005	1.707
$S_4 \leftrightarrow T_2$	0.681	0.874	1.394	1.373	1.185
$S_4 \leftrightarrow T_3$	0.55	0.54	0.595	0.592	0.444
$S_4 \leftrightarrow T_4$	0.532	0.507	0.501	0.511	0.345
$S_4 \leftrightarrow T_5$	0.409	0.5	0.463	0.475	0.264
$S_4 \leftrightarrow T_6$	0.27	0.383	0.343	0.354	0.214
$S_4 \leftrightarrow T_7$	0.171	0.236	0.207	0.324	0.2
$S_4 \leftrightarrow T_8$	0.112	0.149	0.204	0.211	0.067
$S_4 \leftrightarrow T_9$	0.067	0.057	0.099	0.132	0.03
$S_4 \leftrightarrow T_{10}$	0.044	0.045	0.029	0.116	-0.074
$S_5 \leftrightarrow T_1$	2.08	1.487	2.045	2.049	1.876

$S_5 \leftrightarrow T_2$	0.735	2.635	1.448	1.417	1.354
$S_5 \leftrightarrow T_3$	0.604	2.969	0.649	0.636	0.613
$S_5 \leftrightarrow T_4$	0.586	3.002	0.555	0.555	0.514
$S_5 \leftrightarrow T_5$	0.463	3.009	0.517	0.519	0.433
$S_5 \leftrightarrow T_6$	0.324	3.126	0.397	0.398	0.383
$S_5 \leftrightarrow T_7$	0.225	3.273	0.261	0.368	0.369
$S_5 \leftrightarrow T_8$	0.166	3.36	0.258	0.255	0.236
$S_5 \leftrightarrow T_9$	0.121	3.452	0.153	0.176	0.199
$S_5 \leftrightarrow T_{10}$	0.098	3.464	0.083	0.16	0.095
$S_6 \leftrightarrow T_1$	2.16	0.965	2.072	2.076	1.907
$S_6 \leftrightarrow T_2$	0.815	0.631	1.475	1.444	1.385
$S_6 \leftrightarrow T_3$	0.684	0.598	0.676	0.663	0.644
$S_6 \leftrightarrow T_4$	0.666	0.591	0.582	0.582	0.545
$S_6 \leftrightarrow T_5$	0.543	0.474	0.544	0.546	0.464
$S_6 \leftrightarrow T_6$	0.404	0.327	0.424	0.425	0.414
$S_6 \leftrightarrow T_7$	0.305	0.24	0.288	0.395	0.4
$S_6 \leftrightarrow T_8$	0.246	0.148	0.285	0.282	0.267
$S_6 \leftrightarrow T_9$	0.201	0.136	0.18	0.203	0.23
$S_6 \leftrightarrow T_{10}$	0.178	3.6	0.11	0.187	0.126
$S_7 \leftrightarrow T_1$	2.2	2.203	2.154	2.168	1.935
$S_7 \leftrightarrow T_2$	0.855	1.055	1.557	1.536	1.413
$S_7 \leftrightarrow T_3$	0.724	0.721	0.758	0.755	0.672
$S_7 \leftrightarrow T_4$	0.706	0.688	0.664	0.674	0.573
$S_7 \leftrightarrow T_5$	0.583	0.681	0.626	0.638	0.492
$S_7 \leftrightarrow T_6$	0.444	0.564	0.506	0.517	0.442
$S_7 \leftrightarrow T_7$	0.345	0.417	0.37	0.487	0.428
$S_7 \leftrightarrow T_8$	0.286	0.33	0.367	0.374	0.295
$S_7 \leftrightarrow T_9$	0.241	0.238	0.262	0.295	0.258
$S_7 \leftrightarrow T_{10}$	0.218	0.226	0.192	0.279	0.154
$S_8 \leftrightarrow T_1$	2.275	2.228	2.193	2.2	2.029

$S_8 \leftrightarrow T_2$	0.93	1.08	1.596	1.568	1.507
$S_8 \leftrightarrow T_3$	0.799	0.746	0.797	0.787	0.766
$S_8 \leftrightarrow T_4$	0.781	0.713	0.703	0.706	0.667
$S_8 \leftrightarrow T_5$	0.658	0.706	0.665	0.67	0.586
$S_8 \leftrightarrow T_6$	0.519	0.589	0.545	0.549	0.536
$S_8 \leftrightarrow T_7$	0.42	0.442	0.409	0.519	0.522
$S_8 \leftrightarrow T_8$	0.361	0.355	0.406	0.406	0.389
$S_8 \leftrightarrow T_9$	0.316	0.263	0.301	0.327	0.352
$S_8 \leftrightarrow T_{10}$	0.293	0.251	0.231	0.311	0.248
$S_9 \leftrightarrow T_1$	2.358	2.292	2.232	2.243	2.098
$S_9 \leftrightarrow T_2$	1.013	1.144	1.635	1.611	1.576
$S_9 \leftrightarrow T_3$	0.882	0.81	0.836	0.83	0.835
$S_9 \leftrightarrow T_4$	0.864	0.777	0.742	0.749	0.736
$S_9 \leftrightarrow T_5$	0.741	0.77	0.704	0.713	0.655
$S_9 \leftrightarrow T_6$	0.602	0.653	0.584	0.592	0.605
$S_9 \leftrightarrow T_7$	0.503	0.506	0.448	0.562	0.591
$S_9 \leftrightarrow T_8$	0.444	0.419	0.445	0.449	0.458
$S_9 \leftrightarrow T_9$	0.399	0.327	0.34	0.37	0.421
$S_9 \leftrightarrow T_{10}$	0.376	0.315	0.27	0.354	0.317
$S_{10} \leftrightarrow T_1$	2.378	2.341	2.289	2.288	2.13
$S_{10} \leftrightarrow T_2$	1.033	1.193	1.692	1.656	1.608
$S_{10} \leftrightarrow T_3$	0.902	0.859	0.893	0.875	0.867
$S_{10} \leftrightarrow T_4$	0.884	0.826	0.799	0.794	0.768
$S_{10} \leftrightarrow T_5$	0.761	0.819	0.761	0.758	0.687
$S_{10} \leftrightarrow T_6$	0.622	0.702	0.641	0.637	0.637
$S_{10} \leftrightarrow T_7$	0.523	0.555	0.505	0.607	0.623
$S_{10} \leftrightarrow T_8$	0.464	0.468	0.502	0.494	0.49
$S_{10} \leftrightarrow T_9$	0.419	0.376	0.397	0.415	0.453
$S_{10} \leftrightarrow T_{10}$	0.396	0.364	0.327	0.399	0.349

Table S13. Excited state singlet (S) and triplet (T) energies of **RPI**, calculated using ORCA 5.0 at B3LYP/6-31G (d, p) and B3LYP/DEF2SVP levels.

Materials	S (eV)										T (eV)									
	S_1	S_2	S_3	S_4	S_5	S_6	S_7	S_8	S_9	S_{10}	T_1	T_2	T_3	T_4	T_5	T_6	T_7	T_8	T_9	T_{10}
PhPI	2.677	3.187	3.443	3.521	3.575	3.655	3.695	3.77	3.853	3.873	1.495	2.84	2.971	2.989	3.112	3.251	3.35	3.409	3.454	3.477
ANPI	2.57	2.947	3.205	3.509	3.572	3.6	3.69	3.715	3.779	3.828	1.487	2.635	2.969	3.002	3.009	3.126	3.273	3.36	3.452	3.464
DMPI	2.101	2.712	3.206	3.469	3.523	3.55	3.632	3.671	3.71	3.767	1.478	2.075	2.874	2.968	3.006	3.126	3.262	3.265	3.37	3.44
TPPI	2.112	2.733	3.202	3.478	3.522	3.549	3.641	3.673	3.716	3.761	1.473	2.105	2.886	2.967	3.003	3.124	3.154	3.267	3.346	3.362
BPPI	1.991	2.694	3.147	3.176	3.345	3.376	3.404	3.498	3.567	3.599	1.469	1.991	2.732	2.831	2.912	2.962	2.976	3.109	3.146	3.25

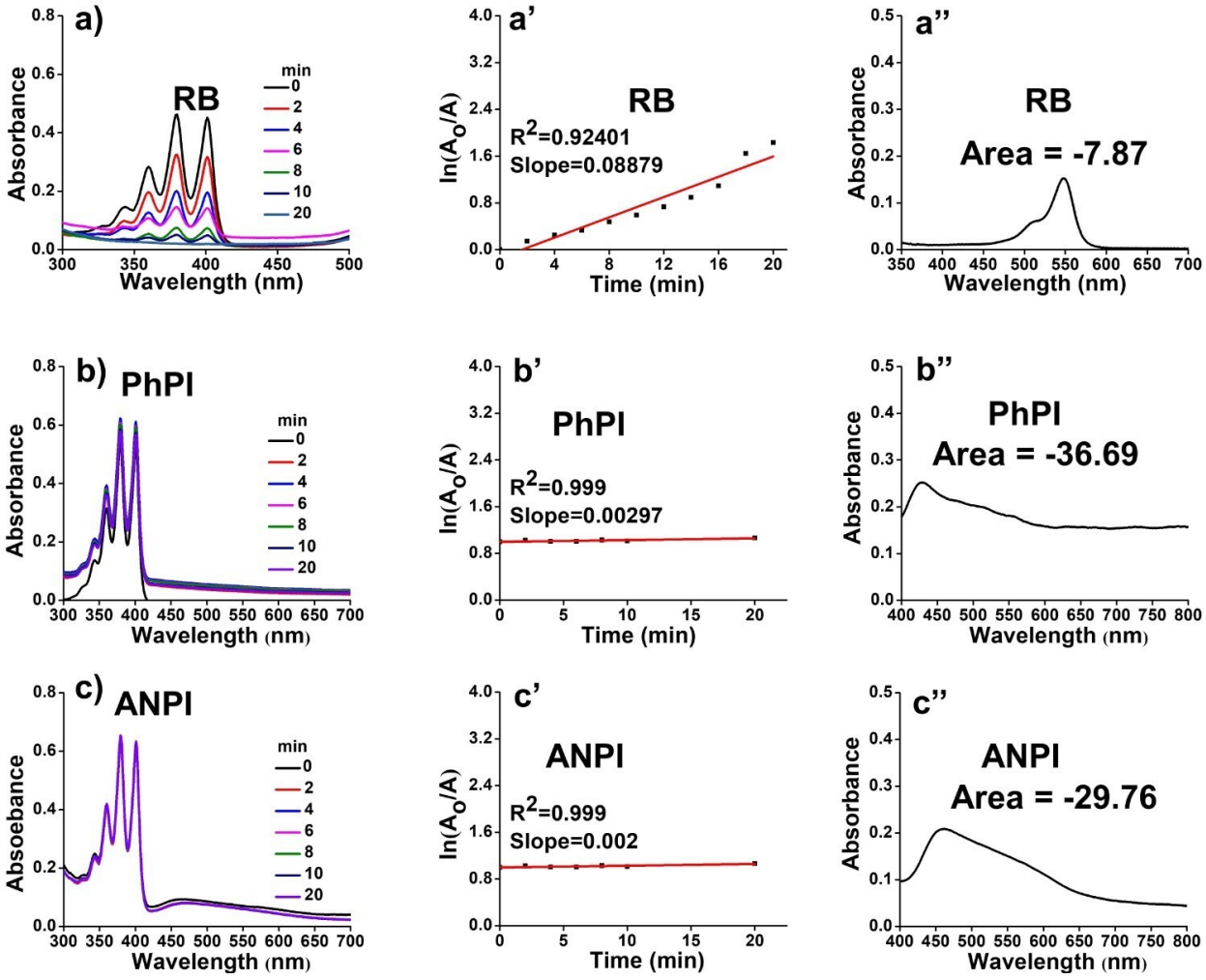

Fig. S20. The ROS quantum yield of **RPI** was determined via chemical trapping measurements, where ABDA photodegrades with (a) Rose Bengal, (b) **PhPI**, and (c) **ANPI** under white light at various time intervals. Rate constants for ABDA decomposition were measured in the presence of (a') Rose Bengal, (b') **PhPI,** and (c') **ANPI** under 20 min

of white light irradiation. The integrated absorption peak area was recorded for (a'') Rose Bengal, (b'') **PhPI**, and (c'') **ANPI**.

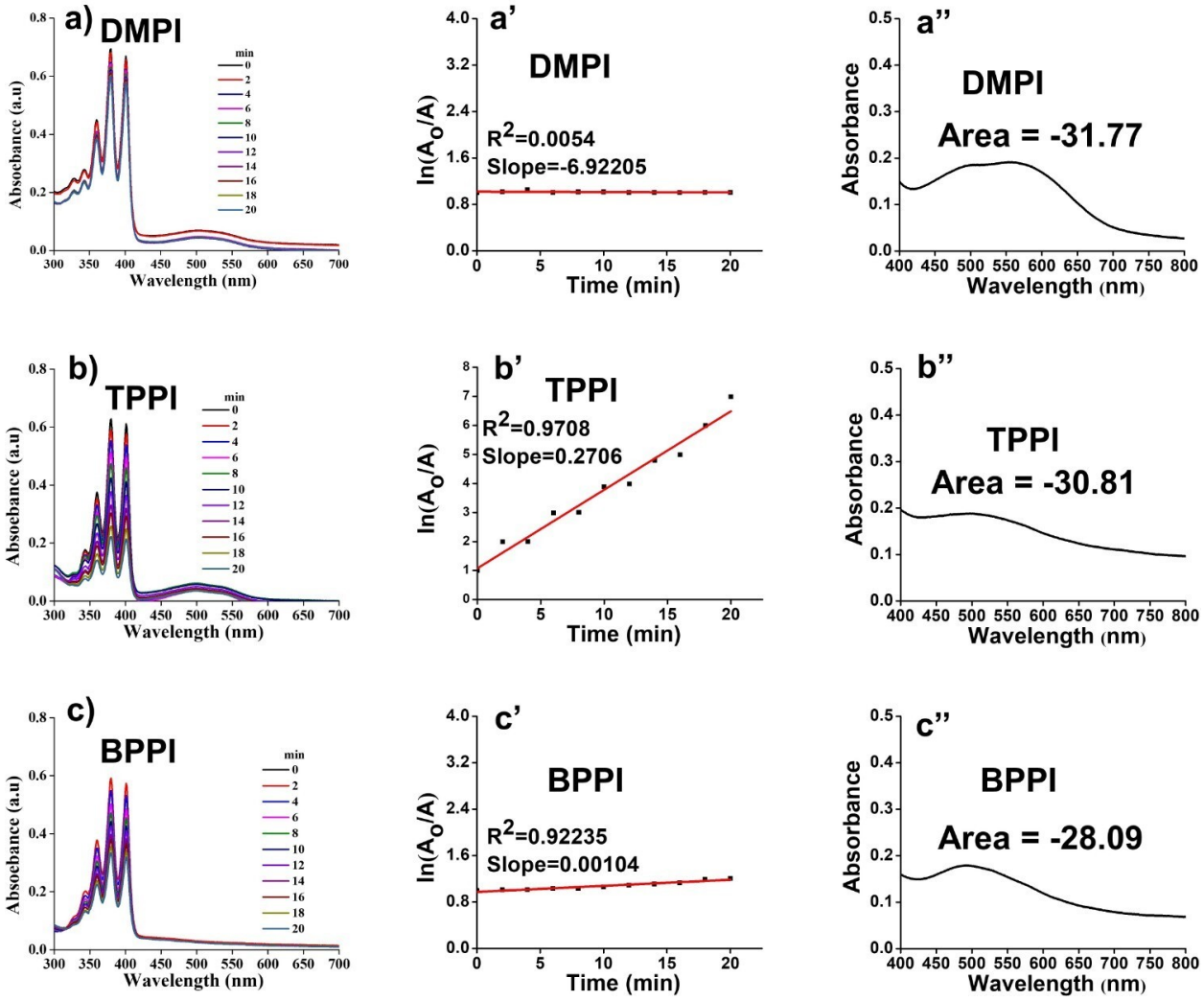

Fig. S21. The ROS quantum yield of **RPI** was determined using chemical trapping measurements. ABDA underwent photodegradation with (a) **DMPI**, (b) **TPPI**, and (c) **BPPI** under white light irradiation at various times. Rate constants for ABDA decomposition were measured in the presence of (a') **DMPI**, (b') **TPPI**, and (c') **BPPI** under 20 min of white light excitation. The integrated absorption peak areas were recorded for (a'') **DMPI**, (b'') **TPPI,** and (c'') **BPPI**.

Table S14. Comparison table of Φ_Δ of the recently published materials.

References	Materials	Φ_Δ	Solvent systems
Present work	**TPPI (Far-Red)**	0.592	99% f_w (aqueous media)
J. Am. Chem. Soc. **2019**, *141*, 16243.	Non-fluorescent	1.0	Toluene
Chem. Sci. **2022**, *13*, 9373.	LOCK (Red AIE)	1.1	THF
Adv. Mater. **2018**, *30*, 1802105.	TPA (Red AIE)	0.91	THF

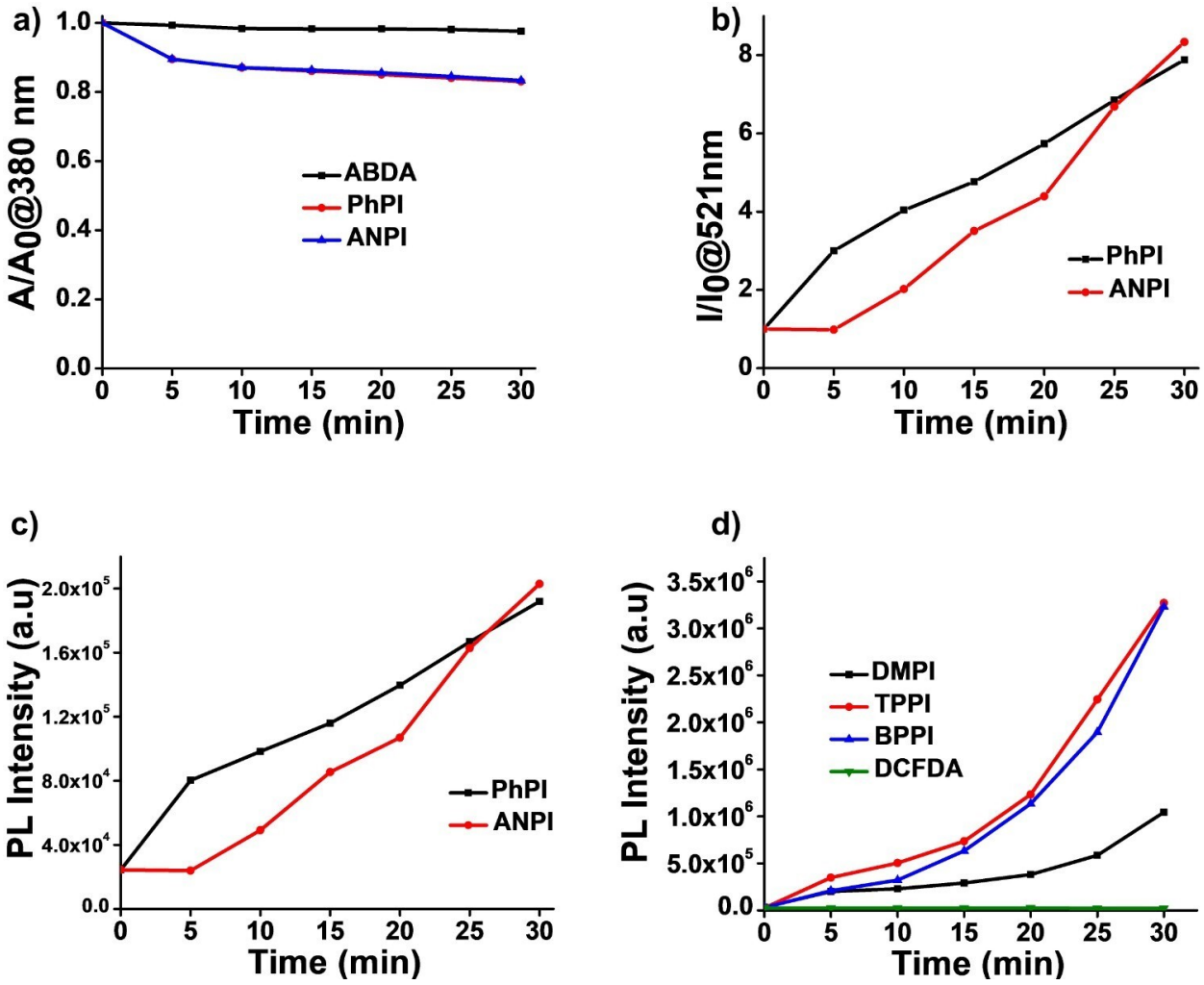

Fig. S22. (a) Decomposition rates of ABDA (100 μM) at $\lambda_{abs.max}$ of 380 nm by **PhPI**/**ANPI** PSs (100 μM) and (b, c, d) PL of the DCFDA indicator in the presence of **RPI** PSs at different time intervals. A_0 and A denote the absorbance of ABDA at $\lambda_{abs.max}$ of 380 nm before and after irradiation with white light. I_0 and I represent the PL of the indicator at $\lambda_{em,max}$ of 521 nm before and after irradiation with white light.

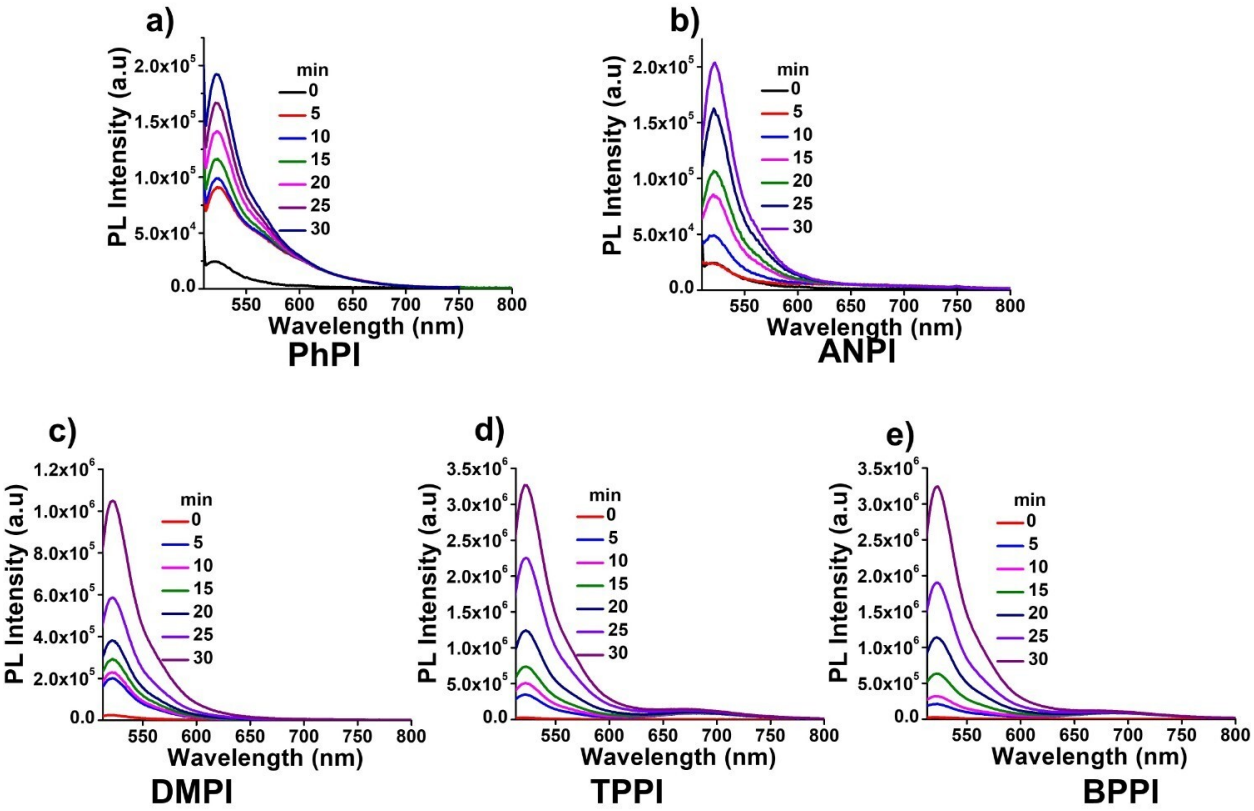

Fig. S23. ROS generation by **RPI**. (a-e) Assessment of ROS generation using DCFDA (10 μM) indicator by **RPI** PSs (100 μM) under white light excitation for various durations with 99% PBS fraction in DMSO (λ_{ex}=500 nm).

Table S15. Zeta potential measurements of **RPI** at various pH.

Materials	**pH**				
	1	**3**	**5.6**	**7.4**	**9**
PhPI$_\zeta$	1.49	-5.39	-15.9	-30.4	-33.4
ANPI$_\zeta$	0.103	-4.5	-14.1	-39.3	-45.2
DMPI$_\zeta$	17.3	-5.06	-13.4	-38.1	-44.3
TPPI$_\zeta$	1.126	-5.55	-15.9	-17.4	-20.8
BPPI$_\zeta$	1.23	-4.9	-12.3	-23.1	-35.3

ζ is the zeta potential of the respective **RPI**.

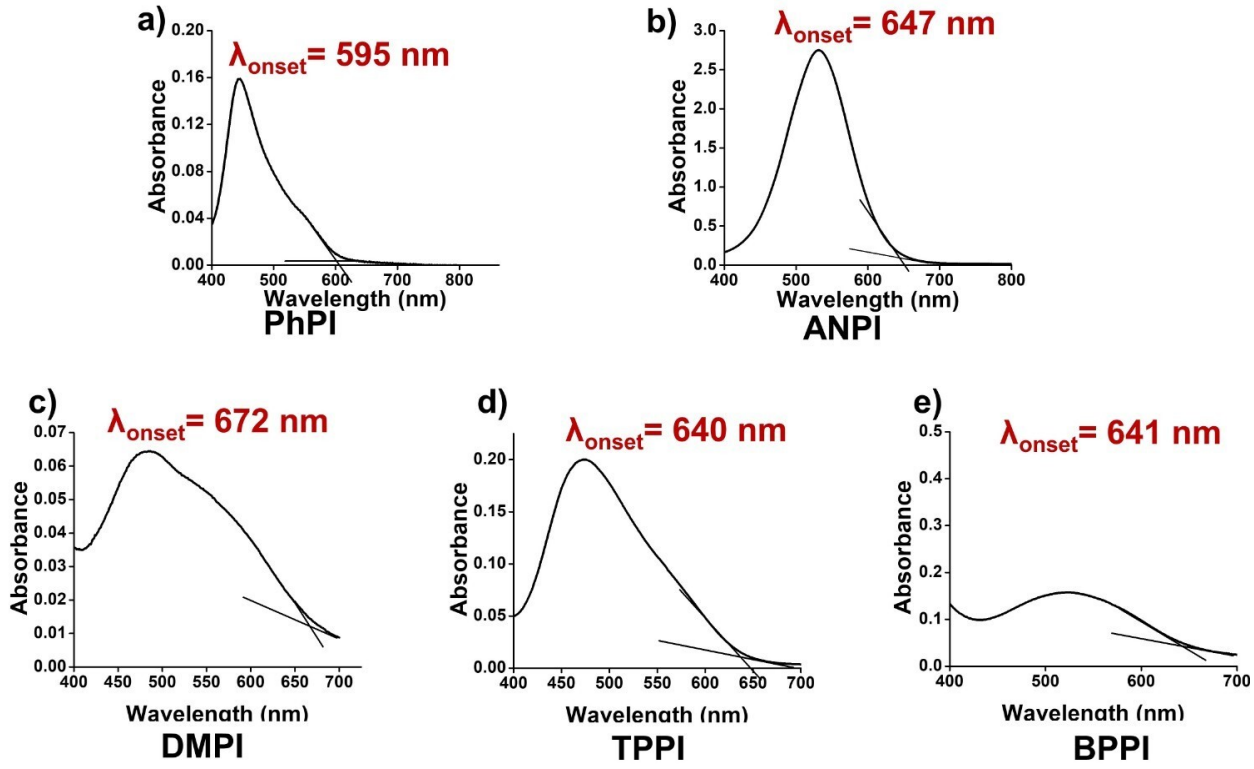

Fig. S24. (a-e) UV-vis spectra showing the onset absorption of **PhPI/ANPI/DMPI/TPPI/BPPI**.

Table S16. Optical band gap data of **RPI** derived from onset absorption of UV-vis spectra.

Materials	λ_{onset}	E_g (eV)
PhPI	595	2.08
ANPI	647	1.93
DMPI	672	1.85
TPPI	640	1.94
BPPI	641	1.92

λ_{onset} is the onset UV-vis absorption

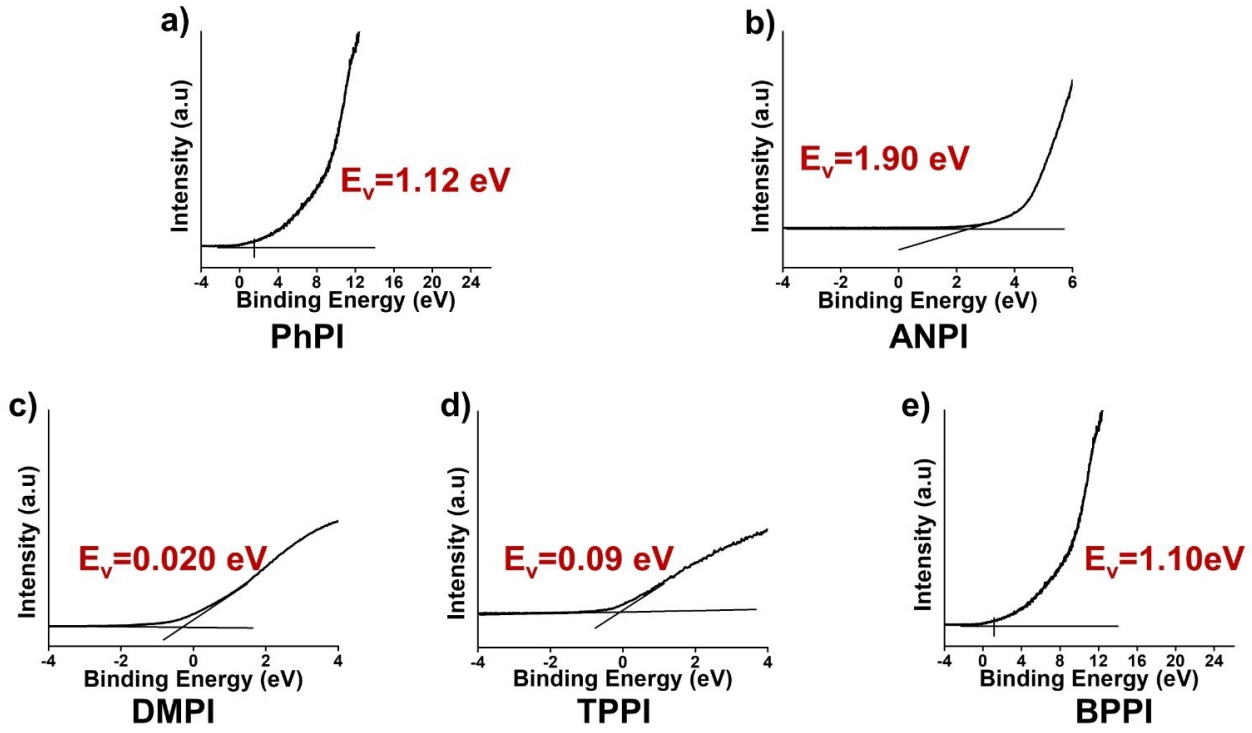

Fig. S25. XPS spectra showing E_v of **PhPI/ANPI/DMPI/TPPI/BPPI**.

Table S17. E_C and E_V of **RPI** at pH 5.6.

Materials	E_g	E_{HOMO}	E_{LUMO}	E_v	E_c	PZZP	$E_{V,5.6}$	$E_{C,5.6}$
PhPI	2.08	-5.62	-3.54	1.12	-0.96	1.49	0.87751	-1.20249
ANPI	1.93	-6.40	-4.47	1.90	-0.03	0.103	1.575677	-0.354323
DMPI	1.85	4.52	-2.67	0.02	-1.83	17.3	0.7103	-1.1397
TPPI	1.94	4.59	-2.65	0.09	-1.85	1.126	0.0862034	-2.113966
BPPI	1.92	-5.6	-3.68	1.10	-0.82	1.23	0.90707	-1.07783

PZZP, the point of zero zeta potential.

Table S18. The Gibbs free energy of **RPI** was calculated using ORCA 5.0 with the B3LYP/6-31G (d, p) and B3LYP/DEF2SVP levels.

Materials	G (E_h)		ΔG (Kcal/mol)
PhPI	PhPI+O_2	-1434.11849087	**-10.29**
	PhPI	-1284.04143802	
	O_2	-150.09346315	
ANPI	ANPI+O_2	-1720.04431030	**-10.31**
	ANPI	-1569.96727273	
	O_2	-150.09346315	
	ANPI+OH	-1646.26856485	**-413.93**
	OH	-75.64164459	
DMPI	DMPI+O_2	-2181.37520409	**-9.06**
	DMPI	-1648.39929796	
	O_2	-150.09346315	
TPPI	O_2	-150.09346315	**-9.92**
	TPPI+O_2	-2181.37520409	
	TPPI	-2031.29755415	
BPPI	O_2	-150.09346315	**-11.69**
	BPPI+O_2	-2642.70384384	
	BPPI	-2492.62900645	

Table S19. The Gibbs free energy of O_2 was calculated using ORCA 5.0 at the B3LYP/6-31G (d, p) and B3LYP/DEF2SVP levels with a quantum mechanics package.

O_2

----------GIBBS FREE ENERGY----------
The Gibbs free energy is G = H - T*S
Total enthalpy ... -150.07131287 Eh
Total entropy correction ... -0.02215028 Eh -13.90 kcal/mol
Final Gibbs free energy ... -150.09346315 Eh
For completeness - the Gibbs free energy minus the electronic energy
G-E(el) ... -0.01441918 Eh -9.05 kcal/mol
Timings for individual modules:
Sum of individual times ... 12.524 sec (= 0.209 min)
GTO integral calculation ... 2.186 sec (= 0.036 min) 17.5 %
SCF iterations ... 4.342 sec (= 0.072 min) 34.7 %
Analytical frequency calculation... 5.995 sec (= 0.100 min) 47.9 %

Table S20. The Gibbs free energy of OH was calculated using ORCA 5.0 at the B3LYP/6-31G (d, p) and B3LYP/DEF2SVP levels with a quantum mechanics package.

OH

----------GIBBS FREE ENERGY----------
The Gibbs free energy is G = H - T*S
Total enthalpy ... -75.62145382 Eh
Total entropy correction ... -0.02019077 Eh -12.67 kcal/mol
Final Gibbs free energy ... -75.64164459 Eh
For completeness - the Gibbs free energy minus the electronic energy
G-E(el) ... -0.00790092 Eh -4.96 kcal/mol
Timings for individual modules:
Sum of individual times ... 51.754 sec (= 0.863 min)
GTO integral calculation ... 3.889 sec (= 0.065 min) 7.5 %
SCF iterations ... 30.836 sec (= 0.514 min) 59.6 %
Analytical frequency calculation... 17.028 sec (= 0.284 min) 32.9 %

Table S21. The Gibbs free energy of **PhPI** was calculated using ORCA 5.0 at the B3LYP/6-31G (d, p) and B3LYP/DEF2SVP levels with a quantum mechanics package.

PhPI

----------GIBBS FREE ENERGY----------
The Gibbs free energy is G = H - T*S
Total enthalpy ... -1283.96760045 Eh
Total entropy correction ... -0.07383756 Eh -46.33 kcal/mol
Final Gibbs free energy ... -1284.04143802 Eh
For completeness - the Gibbs free energy minus the electronic energy
G-E(el) ... 0.39079777 Eh 245.23 kcal/mol
Timings for individual modules:
Sum of individual times ... 1678.820 sec (= 27.980 min)
GTO integral calculation ... 3.309 sec (= 0.055 min) 0.2 %
SCF iterations ... 153.473 sec (= 2.558 min) 9.1 %
Analytical frequency calculation... 1522.038 sec (= 25.367 min) 90.7 %

Table S22. The Gibbs free energy of **PhPI+O_2** was calculated using ORCA 5.0 at the B3LYP/6-31G (d, p) and B3LYP/DEF2SVP levels with a quantum mechanics package.

PhPI+0_2

----------GIBBS FREE ENERGY----------
The Gibbs free energy is G = H - T*S
Total enthalpy ... -1434.04127352 Eh
Total entropy correction ... -0.07721735 Eh -48.45 kcal/mol
Final Gibbs free energy ... -1434.11849087 Eh
For completeness - the Gibbs free energy minus the electronic energy
G-E(el) ... 0.39279138 Eh 246.48 kcal/mol
Timings for individual modules:
Sum of individual times ... 2134.643 sec (= 35.577 min)
GTO integral calculation ... 3.301 sec (= 0.055 min) 0.2 %
SCF iterations ... 696.217 sec (= 11.604 min) 32.6 %
Analytical frequency calculation... 1435.125 sec (= 23.919 min) 67.2 %

Table S23. The Gibbs free energy of **ANPI** was calculated using ORCA 5.0 at the B3LYP/6-31G (d, p) and B3LYP/DEF2SVP levels with a quantum mechanics package.

ANPI

----------GIBBS FREE ENERGY----------
The Gibbs free energy is G = H - T*S
Total enthalpy ... -1569.88421122 Eh
Total entropy correction ... -0.08306151 Eh -52.12 kcal/mol
Final Gibbs free energy ... -1569.96727273 Eh
For completeness - the Gibbs free energy minus the electronic energy
G-E(el) ... 0.48208487 Eh 302.51 kcal/mol
Timings for individual modules:Sum of individual times ... 2940.788 sec (= 49.013 min)
GTO integral calculation ... 3.530 sec (= 0.059 min) 0.1 %
SCF iterations ... 205.260 sec (= 3.421 min) 7.0 %
Analytical frequency calculation... 2731.998 sec (= 45.533 min) 92.9 %

Table S24. The Gibbs free energy of **ANPI+O_2** was calculated using ORCA 5.0 at the B3LYP/6-31G (d, p) and B3LYP/DEF2SVP levels with a quantum mechanics package.

ANPI+0_2

----------GIBBS FREE ENERGY----------
The Gibbs free energy is G = H - T*S
Total enthalpy ... -1719.95788448 Eh
Total entropy correction ... -0.08642582 Eh -54.23 kcal/mol-
Final Gibbs free energy ... -1720.04431030 Eh
For completeness - the Gibbs free energy minus the electronic energy
G-E(el) ... 0.48409358 Eh 303.77 kcal/mol

Timings for individual modules:
Sum of individual times ... 3881.758 sec (= 64.696 min)
GTO integral calculation ... 3.757 sec (= 0.063 min) 0.1 %
SCF iterations ... 1332.868 sec (= 22.214 min) 34.3 %
Analytical frequency calculation... 2545.134 sec (= 42.419 min) 65.6 %

Table S25. The Gibbs free energy of **ANPI+OH** was calculated using ORCA 5.0 at the B3LYP/6-31G (d, p) and B3LYP/DEF2SVP levels with a quantum mechanics package.

ANPI+OH

----------GIBBS FREE ENERGY----------
The Gibbs free energy is G = H - T*S
Total enthalpy ... -1646.18137635 Eh
Total entropy correction ... -0.08718850 Eh -54.71 kcal/mol
Final Gibbs free energy ... -1646.26856485 Eh
For completeness - the Gibbs free energy minus the electronic energy
G-E(el) ... 0.50127552 Eh 314.55 kcal/mol
Timings for individual modules:
Sum of individual times ... 2855.193 sec (= 47.587 min)
GTO integral calculation ... 3.567 sec (= 0.059 min) 0.1 %
SCF iterations ... 211.369 sec (= 3.523 min) 7.4 %
Analytical frequency calculation... 2640.258 sec (= 44.004 min) 92.5 %

Table S26. The Gibbs free energy of **DMPI** was calculated using ORCA 5.0 at the B3LYP/6-31G (d, p) and B3LYP/DEF2SVP levels with a quantum mechanics package.

DMPI

----------GIBBS FREE ENERGY----------
The Gibbs free energy is G = H - T*S
Total enthalpy ... -1648.31532427 Eh
Total entropy correction ... -0.08397369 Eh -52.69 kcal/mol
Final Gibbs free energy ... -1648.39929796 Eh
For completeness - the Gibbs free energy minus the electronic energy
G-E(el) ... 0.53905068 Eh 338.26 kcal/mol
Timings for individual modules:
Sum of individual times ... 3246.866 sec (= 54.114 min)
GTO integral calculation ... 2.352 sec (= 0.039 min) 0.1 %
SCF iterations ... 200.436 sec (= 3.341 min) 6.2 %
Analytical frequency calculation... 3044.078 sec (= 50.735 min) 93.8%

Table S27. The Gibbs free energy of **DMPI+O_2** was calculated using ORCA 5.0 at the B3LYP/6-31G (d, p) and B3LYP/DEF2SVP levels with a quantum mechanics package.

DMPI+0_2

----------GIBBS FREE ENERGY----------
The Gibbs free energy is G = H - T*S
Total enthalpy ... -2181.27013323 Eh
Total entropy correction ... -0.10507086 Eh -65.93 kcal/mol
Final Gibbs free energy ... -2181.37520409 Eh
For completeness - the Gibbs free energy minus the electronic energy
G-E(el) ... 0.63746245 Eh 400.01 kcal/mol
Timings for individual modules:
Sum of individual times ... 9513.404 sec (= 158.557 min)
GTO integral calculation ... 4.880 sec (= 0.081 min) 0.1 %
SCF iterations ... 3811.518 sec (= 63.525 min) 40.1 %
Analytical frequency calculation... 5697.006 sec (= 94.950 min)
59.9 %

Table S28. The Gibbs free energy of **TPPI** was calculated using ORCA 5.0 at the B3LYP/6-31G (d, p) and B3LYP/DEF2SVP levels with a quantum mechanics package.

TPPI

----------GIBBS FREE ENERGY----------
The Gibbs free energy is G = H - T*S
Total enthalpy ... -2031.19604293 Eh
Total entropy correction ... -0.10151123 Eh -63.70 kcal/mol
Final Gibbs free energy ... -2031.29755415 Eh
For completeness - the Gibbs free energy minus the electronic energy
G-E(el) ... 0.63565464 Eh 398.88 kcal/mol
Timings for individual modules:
Sum of individual times ... 6695.652 sec (= 111.594 min)
GTO integral calculation ... 6.866 sec (= 0.114 min) 0.1 %
SCF iterations ... 343.049 sec (= 5.717 min) 5.1 %
Analytical frequency calculation... 6345.738 sec (= 105.762 min)
94.8 %

Table S29. The Gibbs free energy of **TPPI+O_2** was calculated using ORCA 5.0 at the B3LYP/6-31G (d, p) and B3LYP/DEF2SVP levels with a quantum mechanics package.

TPPI+0_2

----------GIBBS FREE ENERGY----------
The Gibbs free energy is G = H - T*S
Total enthalpy ... -2181.27013323 Eh
Total entropy correction ... -0.10507086 Eh -65.93 kcal/mol
Final Gibbs free energy ... -2181.37520409 Eh
For completeness - the Gibbs free energy minus the electronic energy
G-E(el) ... 0.63746245 Eh 400.01 kcal/mol
Timings for individual modules:
Sum of individual times ... 9513.404 sec (= 158.557 min)
GTO integral calculation ... 4.880 sec (= 0.081 min) 0.1 %
SCF iterations ... 3811.518 sec (= 63.525 min) 40.1 %
Analytical frequency calculation... 5697.006 sec (= 94.950 min)
59.9 %

Table S30. The Gibbs free energy of **BPPI** was calculated using ORCA 5.0 at the B3LYP/6-31G (d, p) and B3LYP/DEF2SVP levels with a quantum mechanics package.

BPPI

----------GIBBS FREE ENERGY----------
The Gibbs free energy is G = H - T*S
Total enthalpy ... -2492.51448865 Eh
Total entropy correction ... -0.11451780 Eh -71.86 kcal/mol
Final Gibbs free energy ... -2492.62900645 Eh
For completeness - the Gibbs free energy minus the electronic energy
G-E(el) ... 0.79168414 Eh 496.79 kcal/mol
Timings for individual modules:Sum of individual times ...
10597.617 sec (= 176.627 min)
GTO integral calculation ... 5.688 sec (= 0.095 min) 0.1 %
SCF iterations ... 430.053 sec (= 7.168 min) 4.1 %
Analytical frequency calculation... 10161.876 sec (= 169.365 min)
95.9 %

Table S31. The Gibbs free energy of **BPPI+O_2** was calculated using ORCA 5.0 at the B3LYP/6-31G (d, p) and B3LYP/DEF2SVP levels with a quantum mechanics package.

BPPI+0_2

----------GIBBS FREE ENERGY----------

The Gibbs free energy is G = H - T*S

Total enthalpy ... -2642.58910206 Eh

Total entropy correction ... -0.11474178 Eh -72.00 kcal/mol

Final Gibbs free energy ... -2642.70384384 Eh

For completeness - the Gibbs free energy minus the electronic energy

G-E(el) ... 0.79588858 Eh 499.43 kcal/mol

Timings for individual modules:

Sum of individual times ... 16033.628 sec (= 267.227 min)

GTO integral calculation ... 10.121 sec (= 0.169 min) 0.1 %

SCF iterations ... 877.182 sec (= 14.620 min) 5.5 %

Analytical frequency calculation... 15146.326 sec (= 252.439 min) 94.5 %

Table S32. Calculated triplet (T_1) state energy of **RPI** via ORCA 5.0 at the B3LYP/6-31G (d, p) and B3LYP/DEF2SVP level, Gaussian (16) DFT-B3LYP/6-31G (d, p) level calculated energies (*E*, in eV) at the ground state optimized structures (S_0) of **RPI**, and main electronic configurations. Calculated vertical emission energies at T_1-min at the Gaussian (16) DFT-B3LYP/6-31G (d, p).

Materials	T_1 (eV)	S_0 (eV)	$\Delta E_{S0\text{-}T1}$ (eV)	Transition configuration	Vertical emission energy at T_1-minimum (eV)
PhPI	1.495	2.660	1.165	HOMO-to-LUMO	1.165
ANPI	1.487	2.566	1.079	HOMO-to-LUMO	1.079
DMPI	1.478	2.480	1.002	HOMO-to-LUMO	1.002
TPPI	1.473	2.410	0.937	HOMO-to-LUMO	2.532
		4.005	2.532	HOMO-to-LUMO+1	
BPPI	1.469	2.340	0.871	HOMO-to-LUMO	0.871

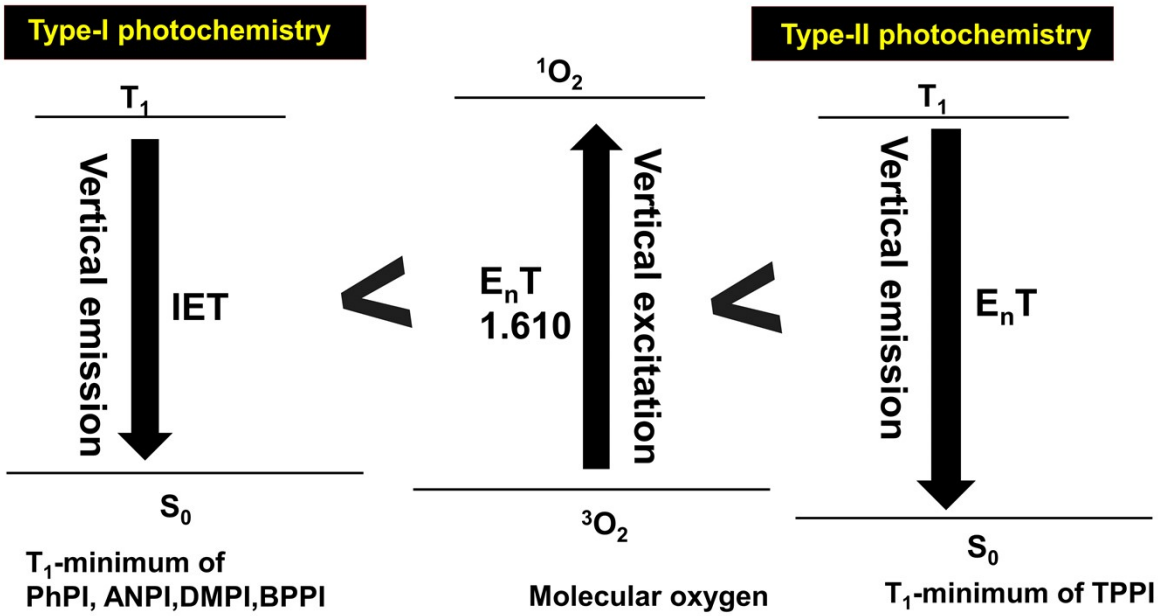

Fig. S26. Energy profile diagram for type-II energy transfer from the T_1 levels of **RPI** to $^3O_2$. Relevant energies (eV) were calculated using DFT/TD-DFT calculated at the B3LYP/6-31G (d, p) level using Gaussian 16 software.

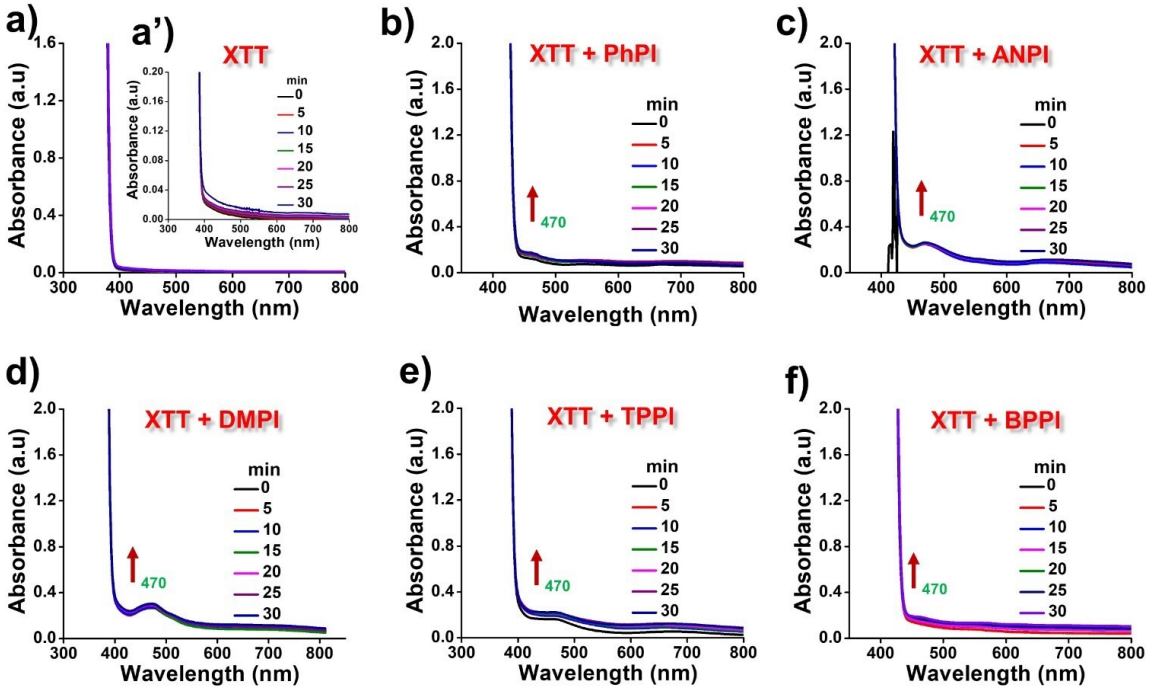

Fig. S27. (a-f) Changes in UV-vis absorption spectra of XTT at 470 nm after irradiation by white light at different times, in the presence and absence of **PhPI**, **ANPI**, **DMPI, TPPI**, or **BPPI,** respectively, in 99% $f_{PBS.}$ [**RPI**] = 100 μM.

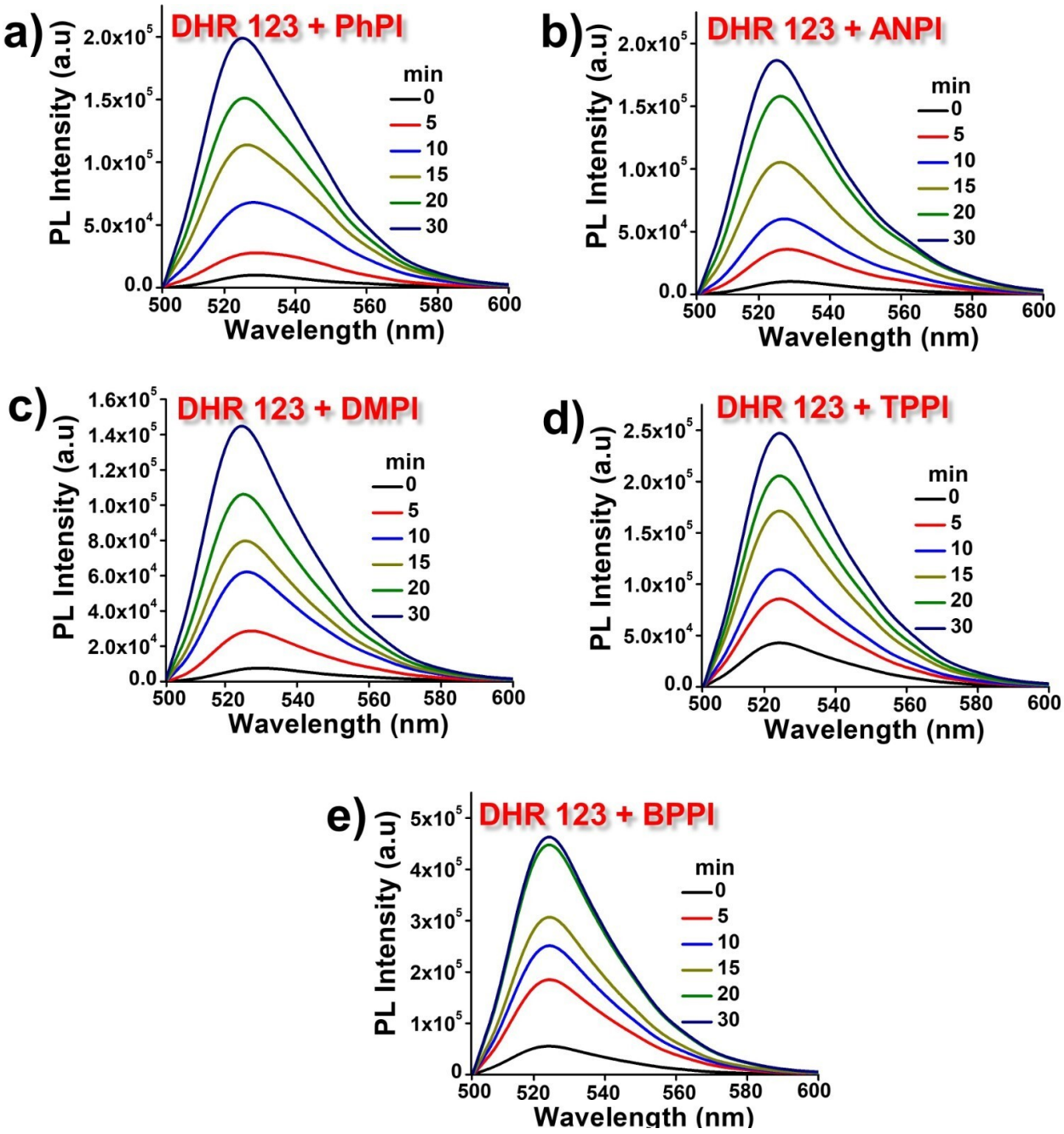

Fig. S28. (a-e) DHR 123 detection of $O_2^{\bullet-}$ in the presence of **PhPI**, **ANPI**, **DMPI, TPPI**, or **BPPI,** respectively, at various times after white light irradiation in in 99% $f_{PBS.}$ [**RPI**] = 100 μM.

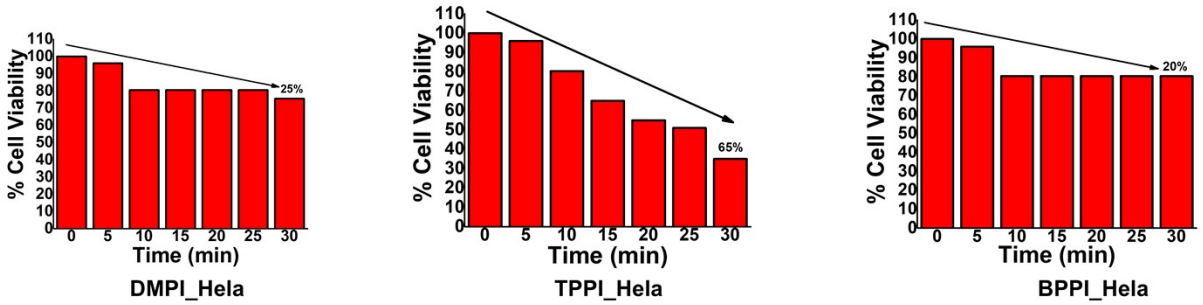

Fig. S29. MTT assay of **DMPI, TPPI**, or **BPPI,** respectively, at various irradiation. [**RPI**] =20 μM.

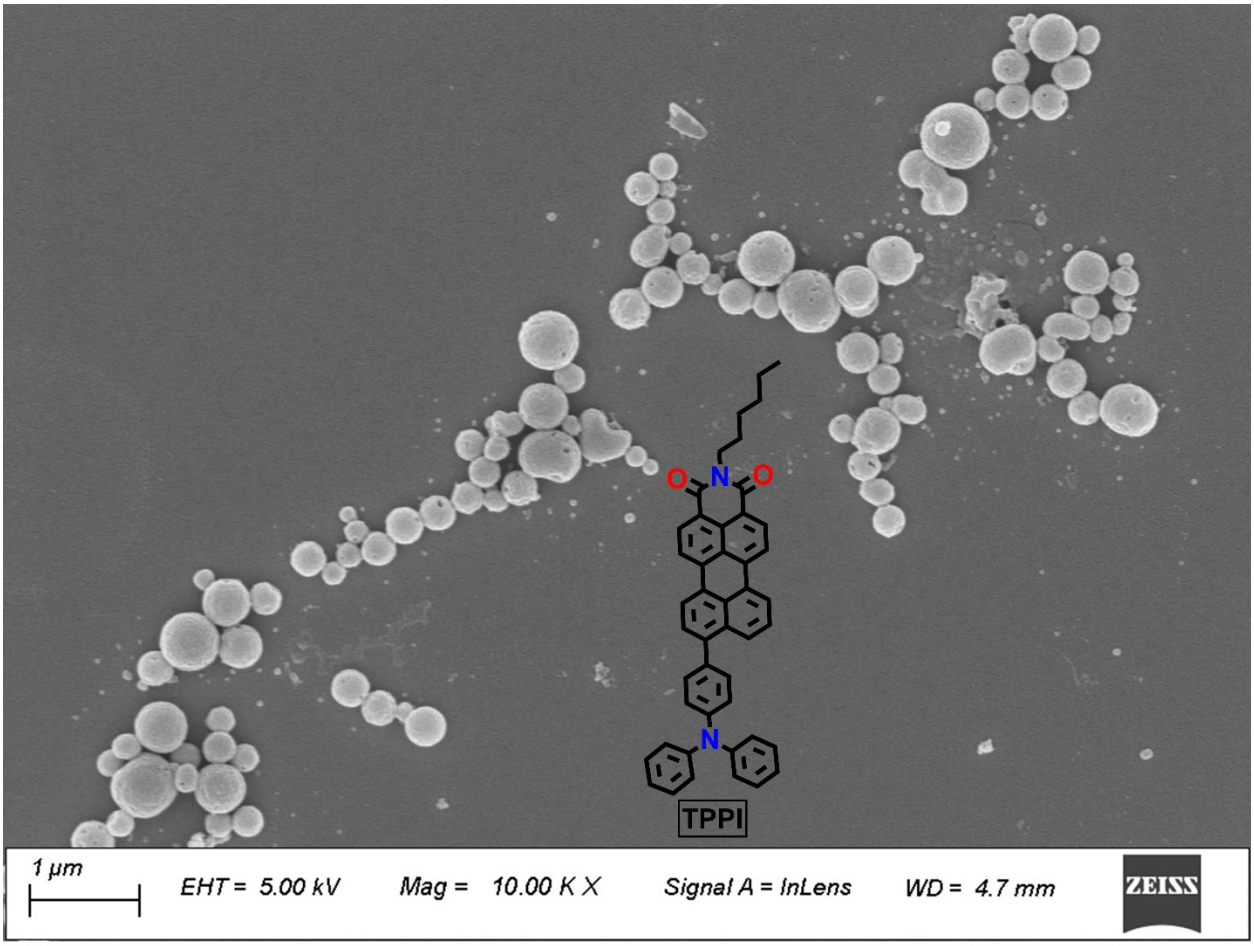

Fig. S30. FESEM images of **TPPI** aggregate before photoirradiation drop casted on the glass slide.

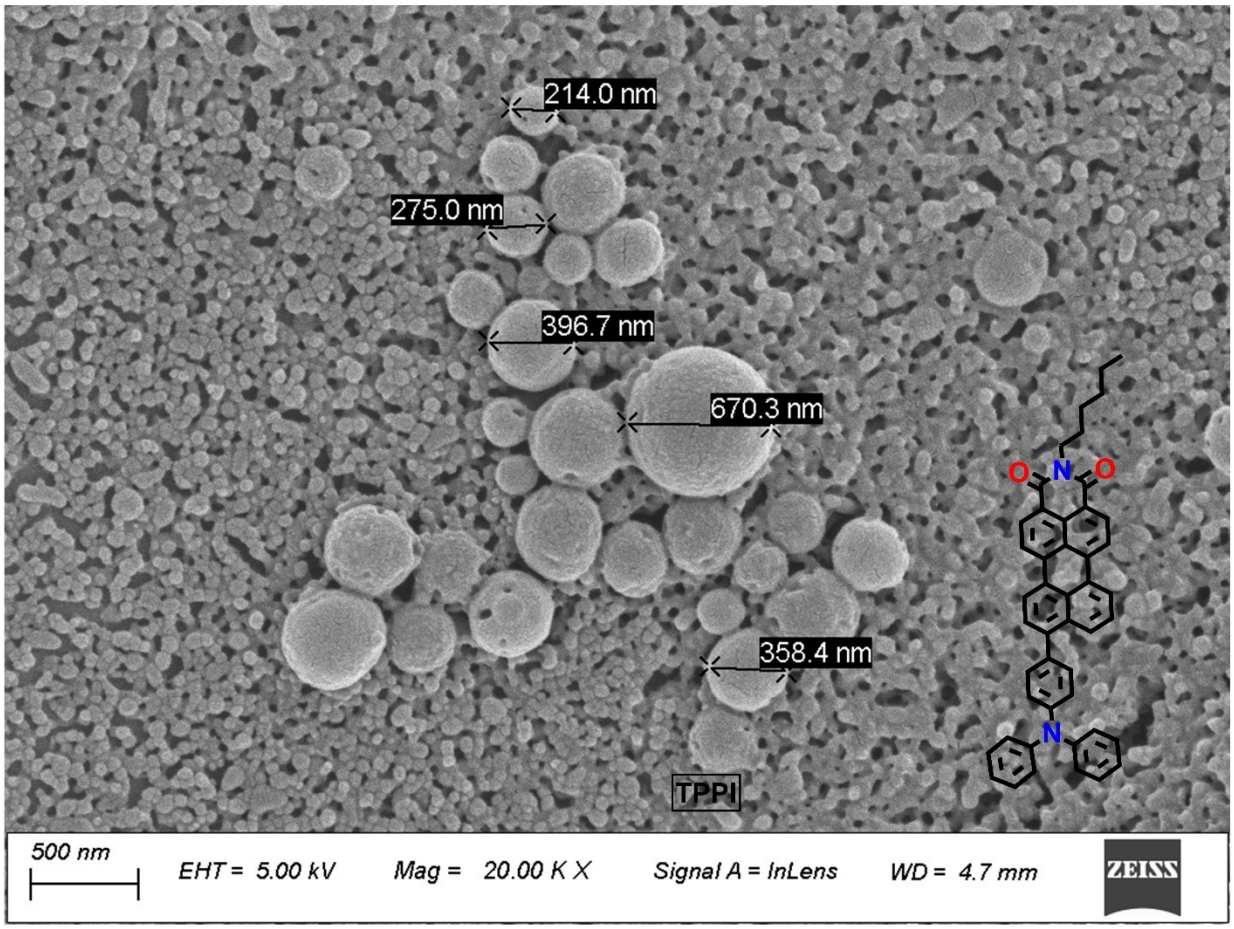

Fig.S31. FESEM images of **TPPI** aggregate before photoirradiation drop casted on the glass slide.

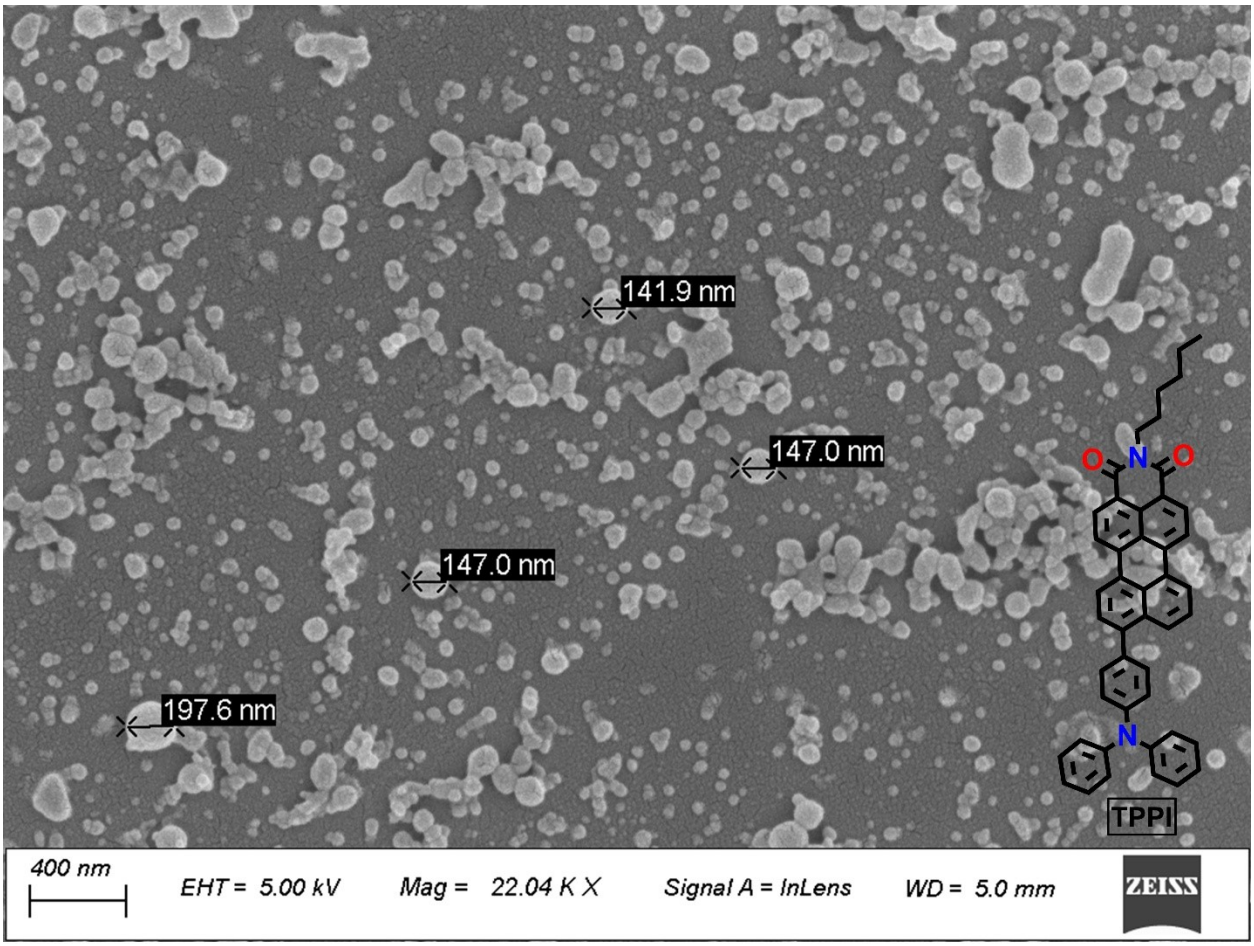

Fig. S32. FESEM images of **TPPI** aggregate after photoirradiation drop casted on the glass slide.

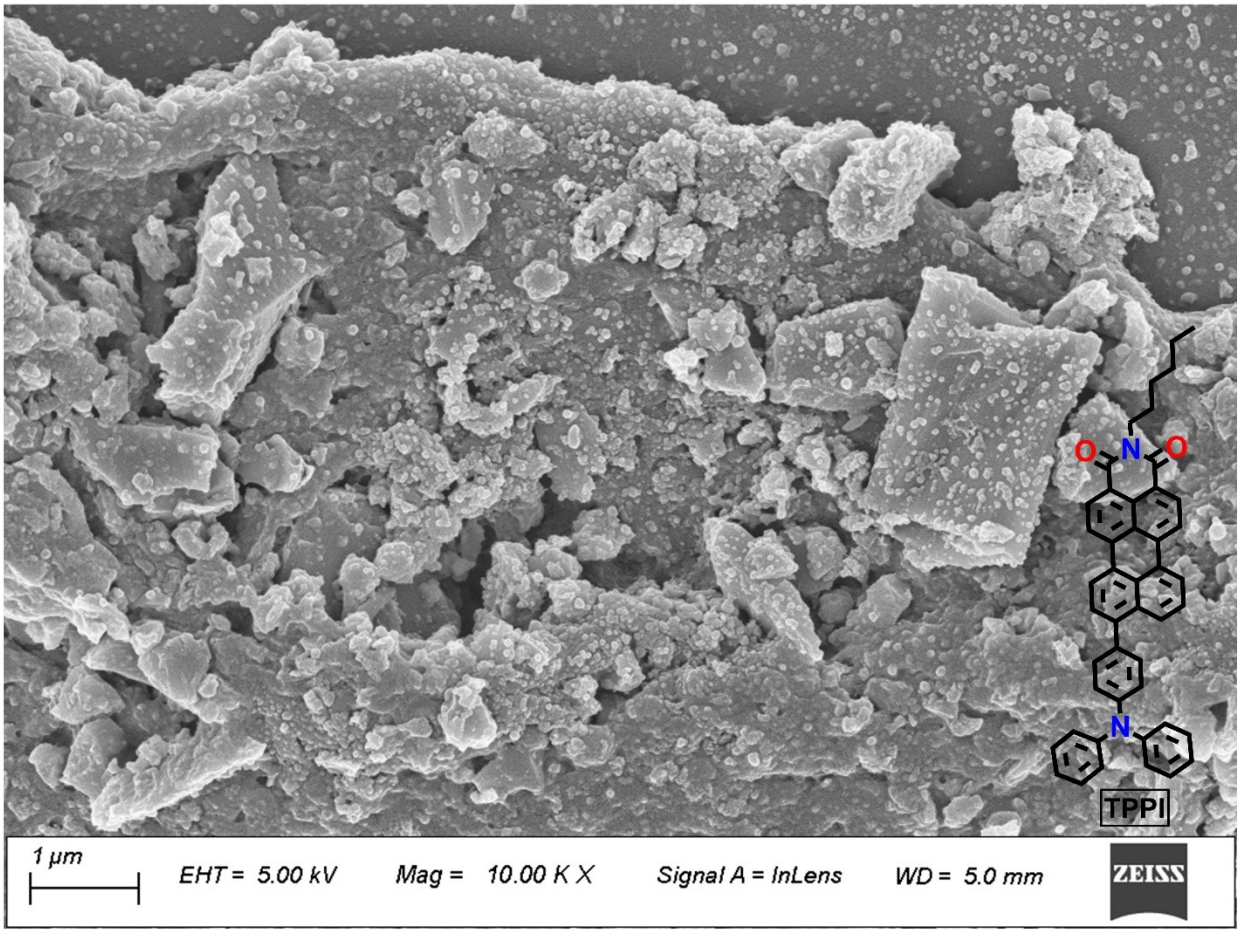

Fig. S33. FESEM images of **TPPI** aggregate after photoirradiation drop casted on the glass slide.

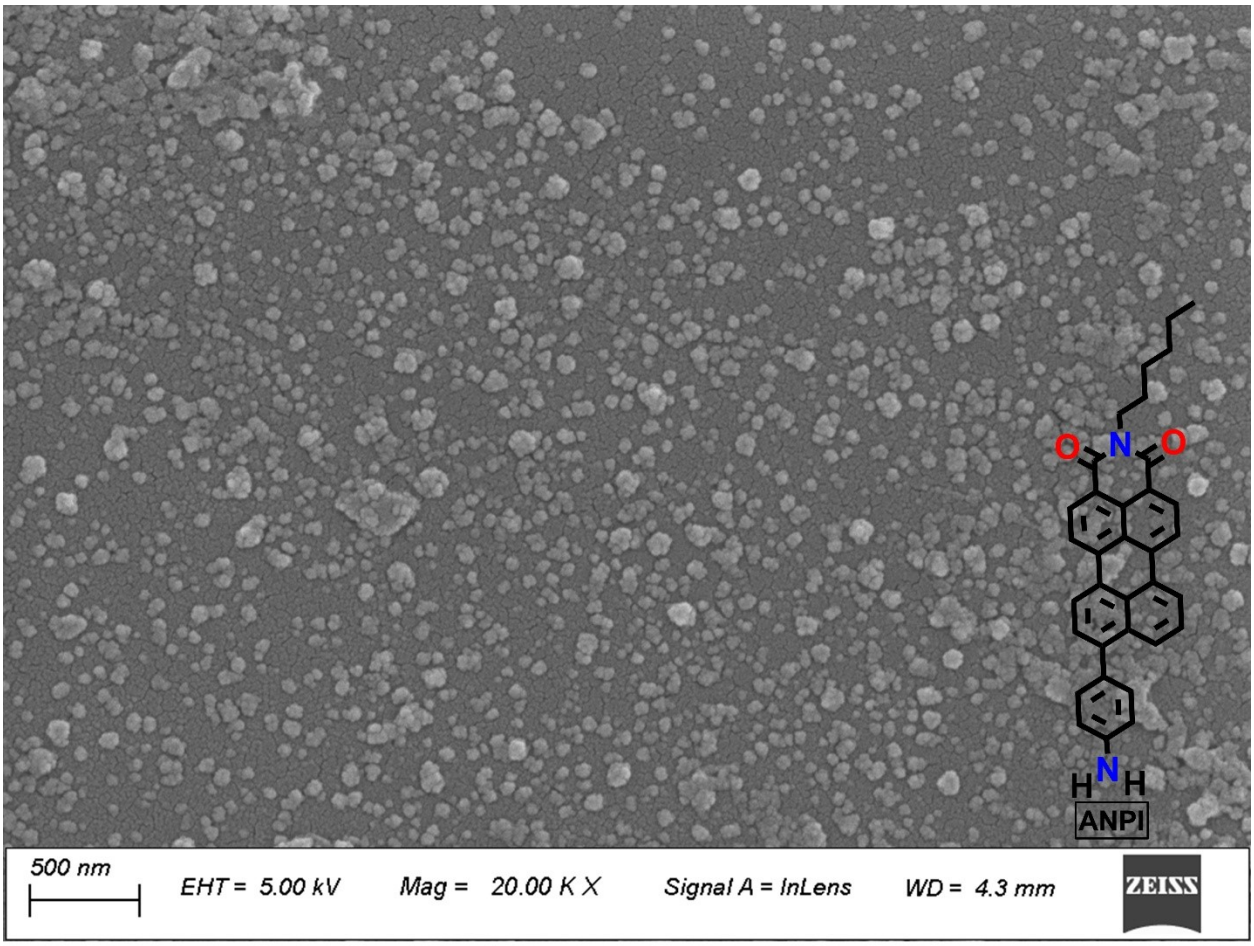

Fig. S34. FESEM images of **ANPI** aggregate before photoirradiation drop casted on the glass slide.

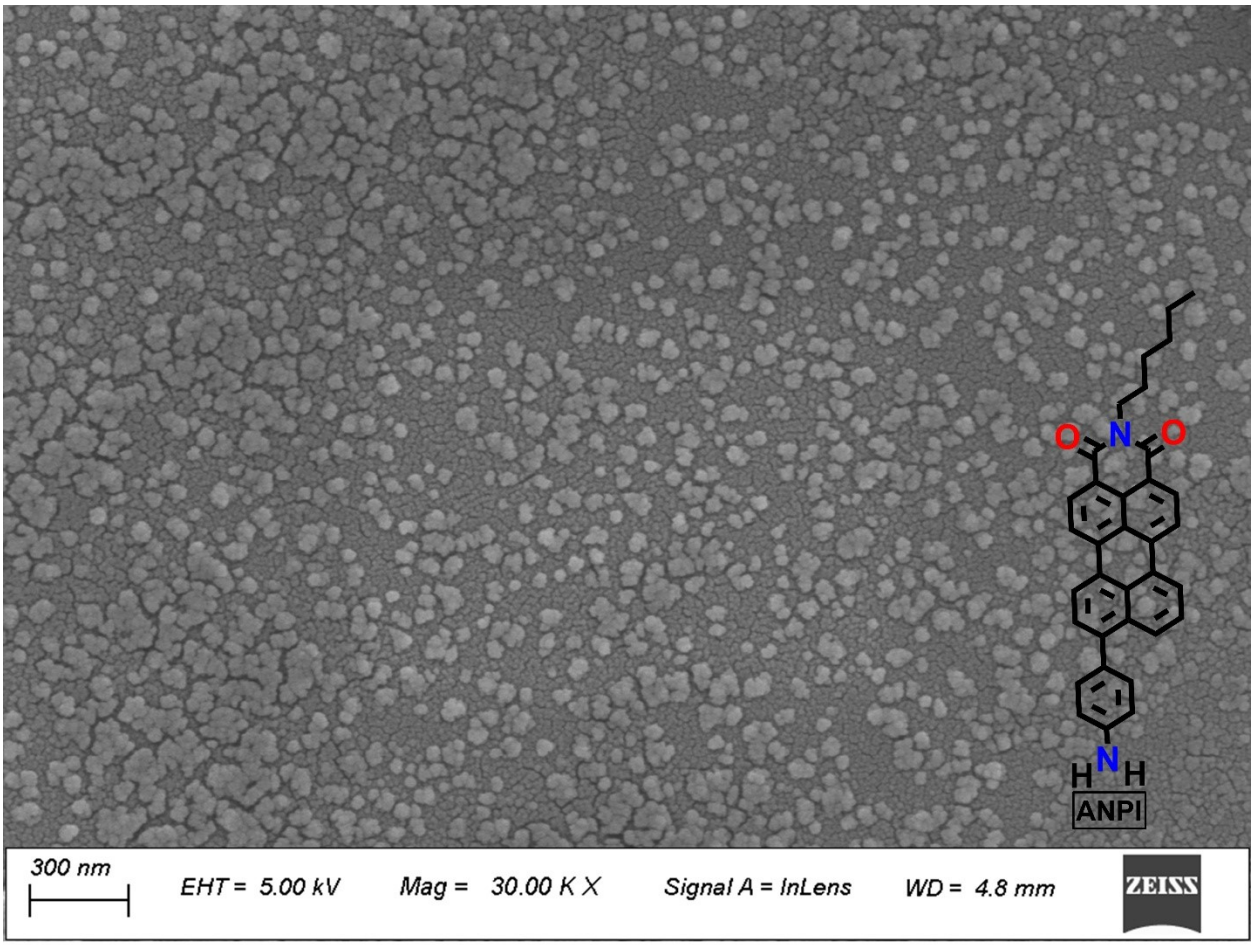

Fig. S35. FESEM images of **ANPI** aggregate after photoirradiation drop casted on the glass slide.

1.14. Fenton reaction

The Fenton reaction was initiated by adding 7.5 μL of 10 mM $FeCl_3$ (or $FeCl_2$), 7.5 μL of 10 *m*M Na_2EDTA, and 4 μL of 30% H_2O_2 to 940 μL of bicarbonate buffer (pH 7.40; 25 *m*M NaCl, 6.25 *m*M $NaHCO_3$). **TPPI** (100 μM) was then added, and the mixture was irradiated for 30 min. For the control (no light treatment), similar samples were prepared and kept in the dark. After pre-incubation for 10 min at room temperature, 41 μL of 3 *m*M salicylic acid was introduced. The reaction was allowed to proceed for an additional 2 min and was quenched by adding 200 μL of 4% phosphoric acid. Immediately after quenching, a 100 μL aliquot was collected for liquid chromatography- mass spectroscopy (LC-MS) analysis (See reference 50 in manuscript).

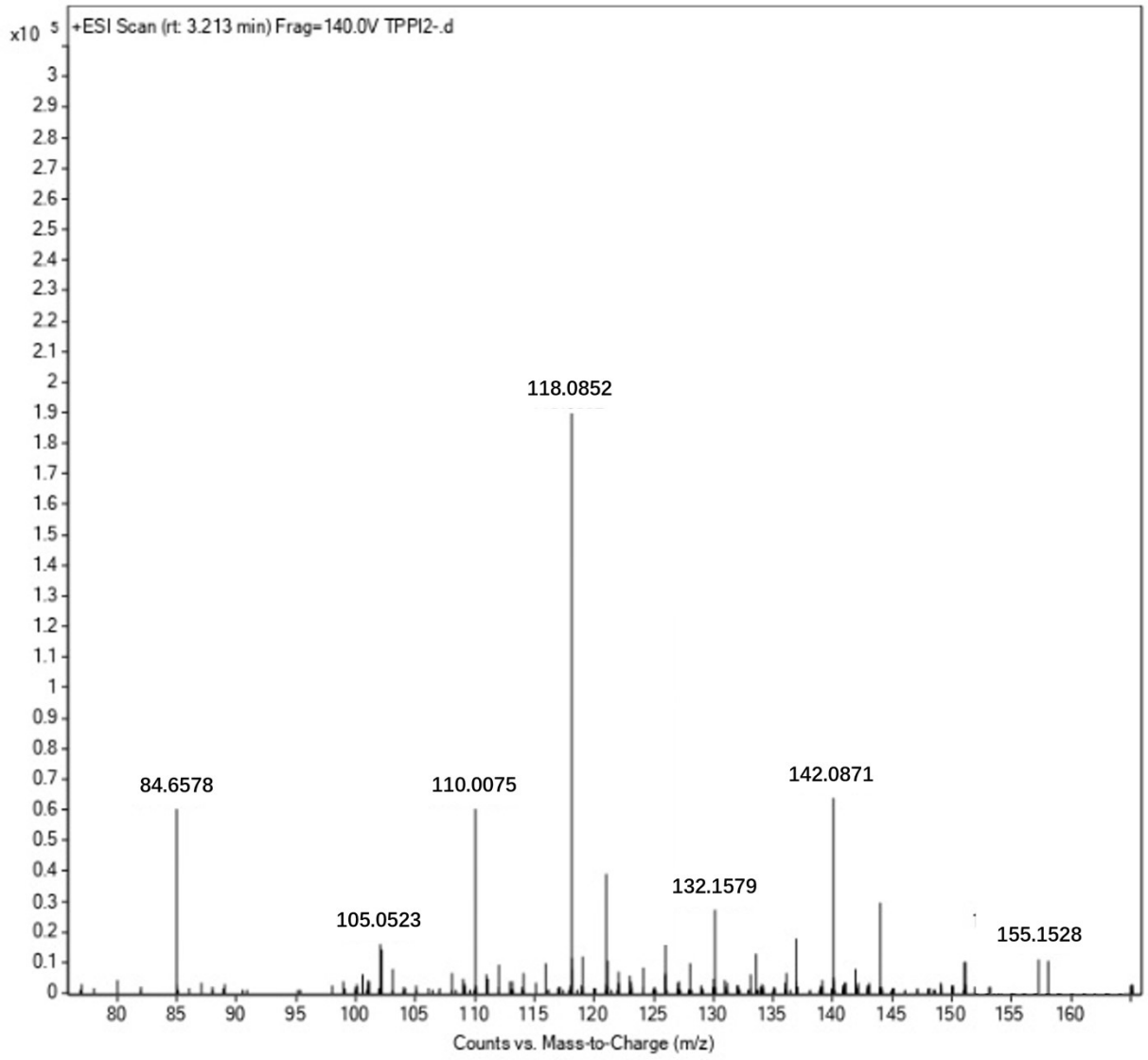

Fig. S36. LC-Mass of **TPPI** during Fenton reaction before light irradiation. [**TPPI**] =100 μM.

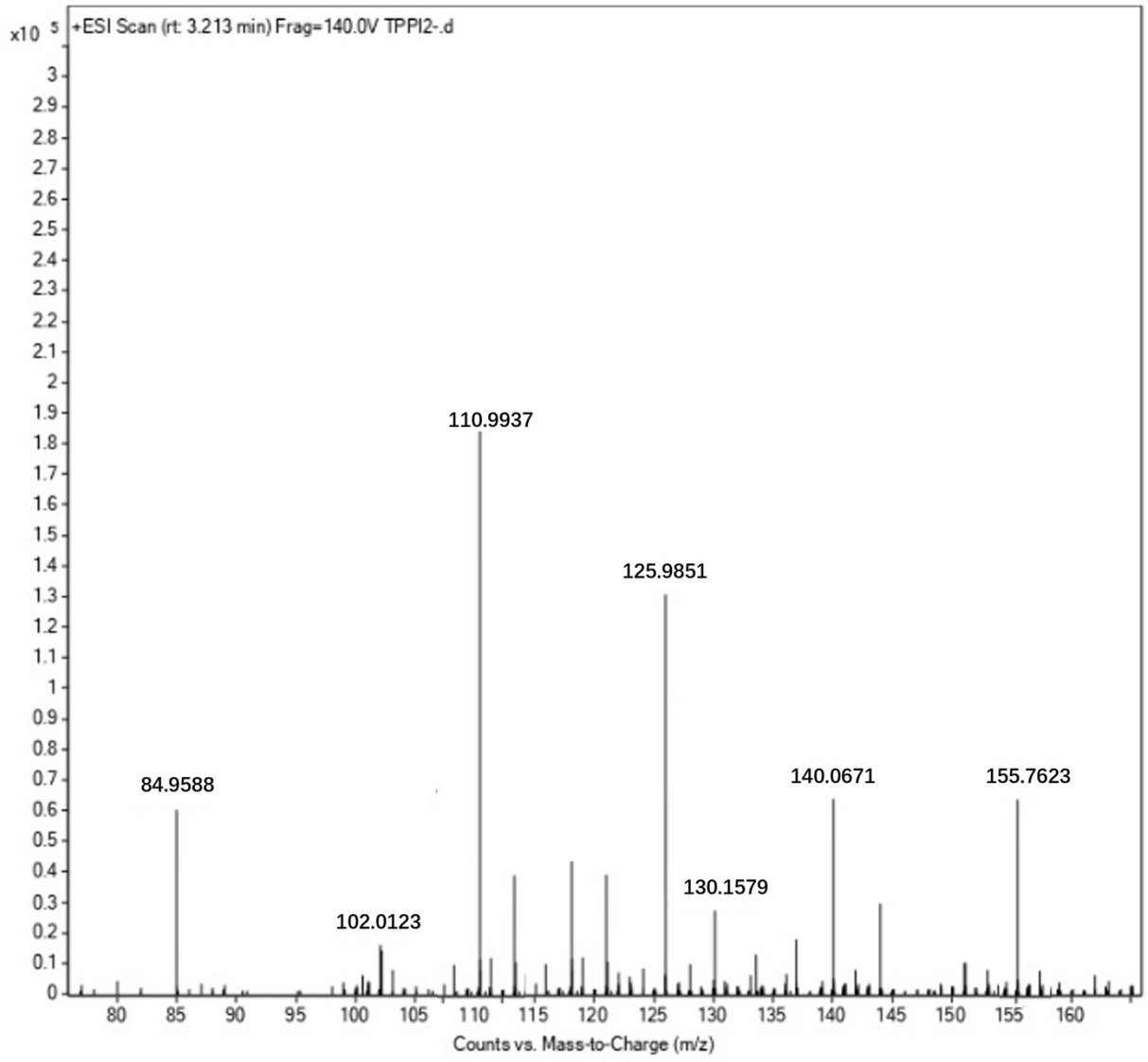

Fig. S37. LC-Mass of **TPPI** during Fenton reaction after 30 min light irradiation. [**TPPI**] =100 μM.

2. Supporting figures

^{1}H NMR spectra

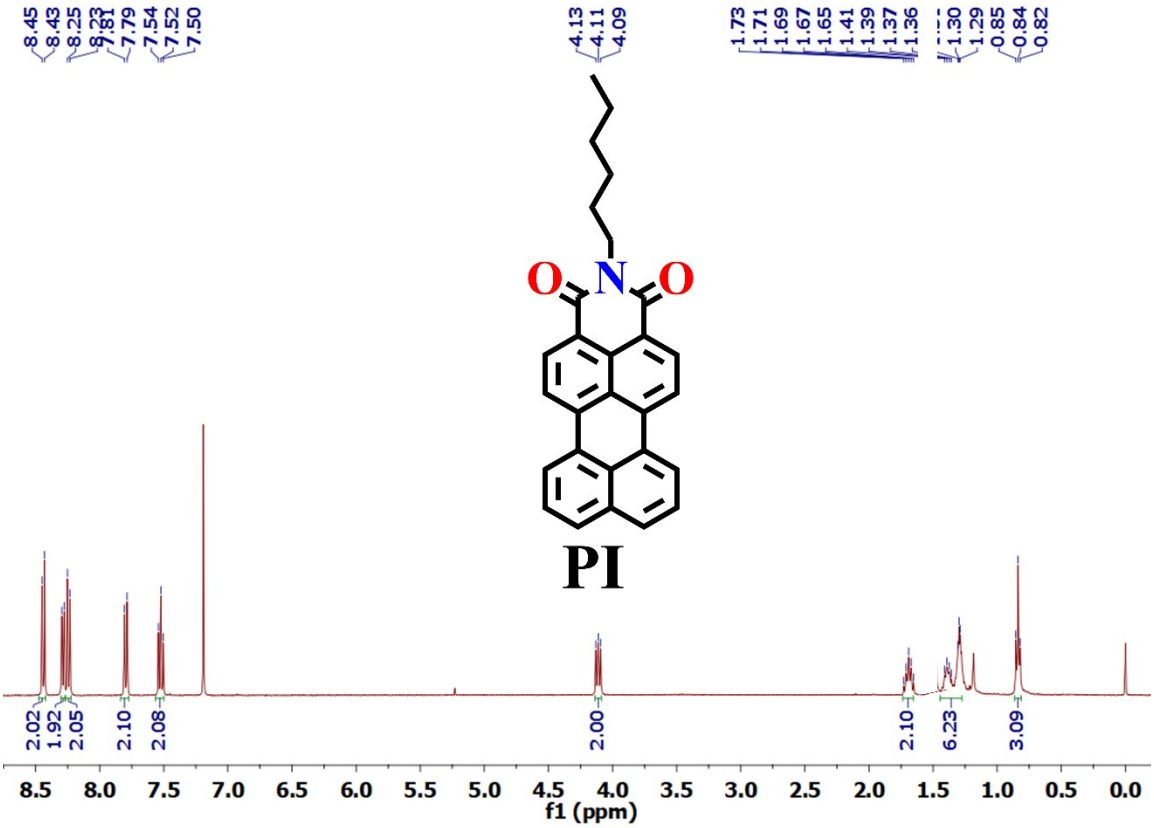

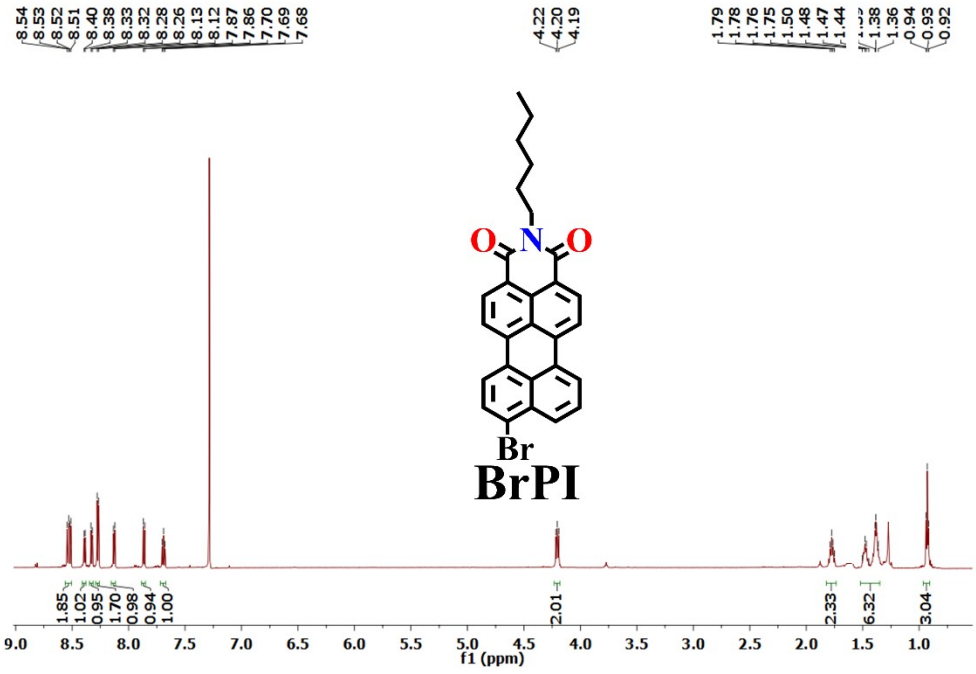

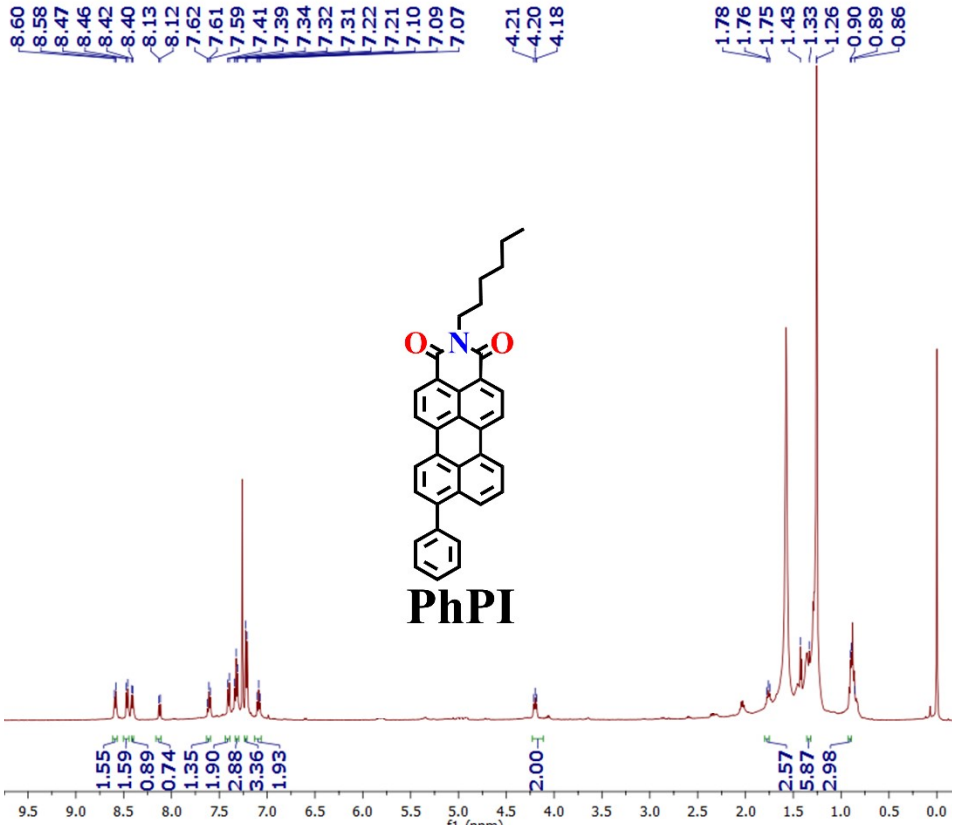
8.60
8.58
8.47
8.46
8.42
8.40
8.13
8.12
7.62
7.61
7.59
7.41
7.39
7.34
7.32
7.31
7.22
7.21
7.10
7.09
7.07
4.21
4.20
4.18
1.78
1.76
1.75
1.43
1.33
1.26
0.90
0.89
0.86
O
N
O
PhPI
1.55
1.59
0.89
0.74
1.35
1.90
2.88
3.36
1.93
2.00
2.57
5.87
2.98
9.5
9.0
8.5
8.0
7.5
7.0
6.5
6.0
5.5
5.0
4.5
4.0
3.5
3.0
2.5
2.0
1.5
1.0
0.5
0.0

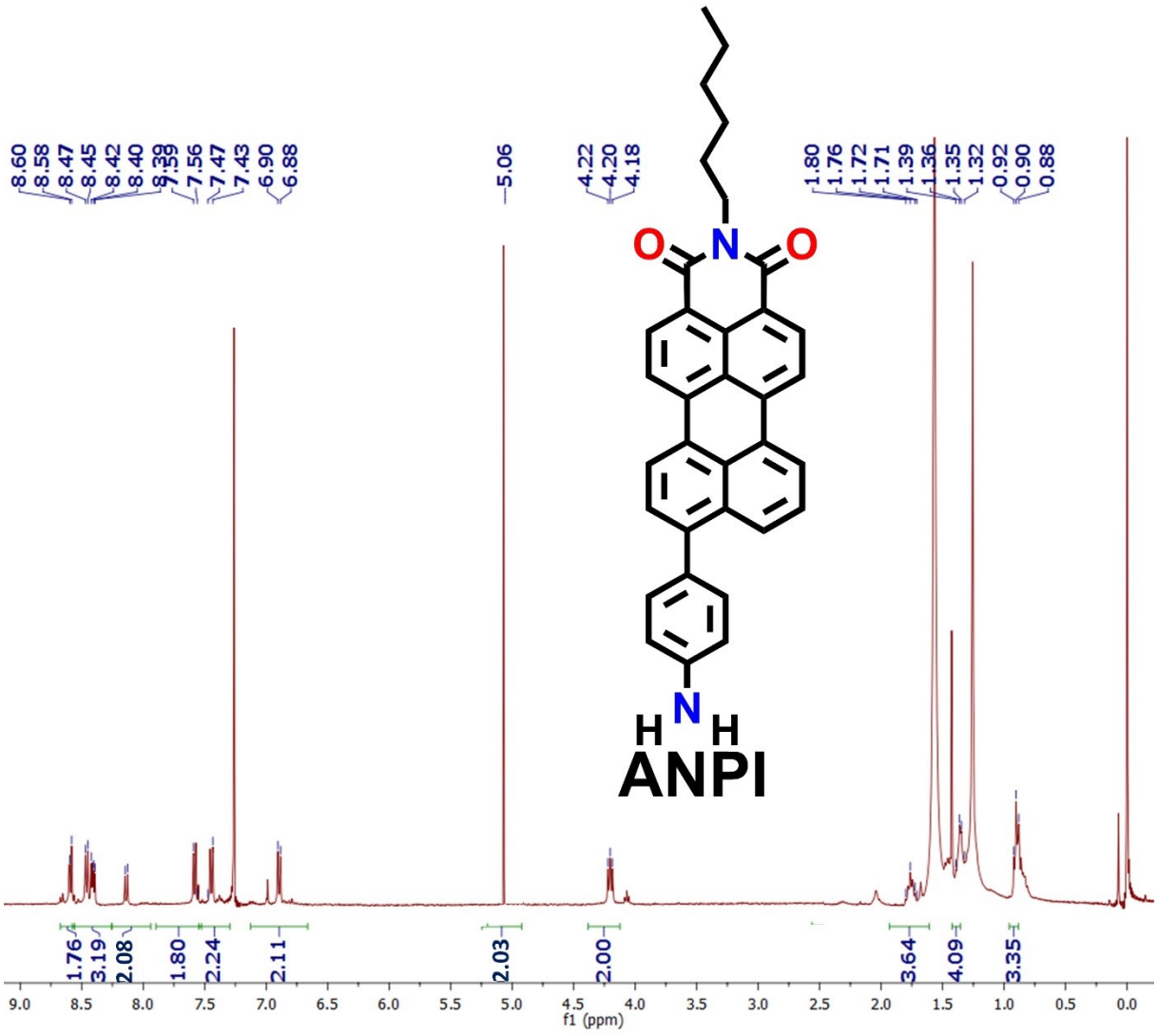
8.60
8.58
8.47
8.45
8.42
8.40
8.39
7.59
7.56
7.47
7.43
6.90
6.88
5.06
4.22
4.20
4.18
1.80
1.76
1.72
1.71
1.39
1.36
1.35
1.32
0.92
0.90
0.88
O
N
O
H
N
H
ANPI
1.76
3.19
2.08
1.80
2.24
2.11
2.03
2.00
3.64
4.09
3.35
9.0
8.5
8.0
7.5
7.0
6.5
6.0
5.5
5.0
4.5
4.0
3.5
3.0
2.5
2.0
1.5
1.0
0.5
0.0
f1 (ppm)

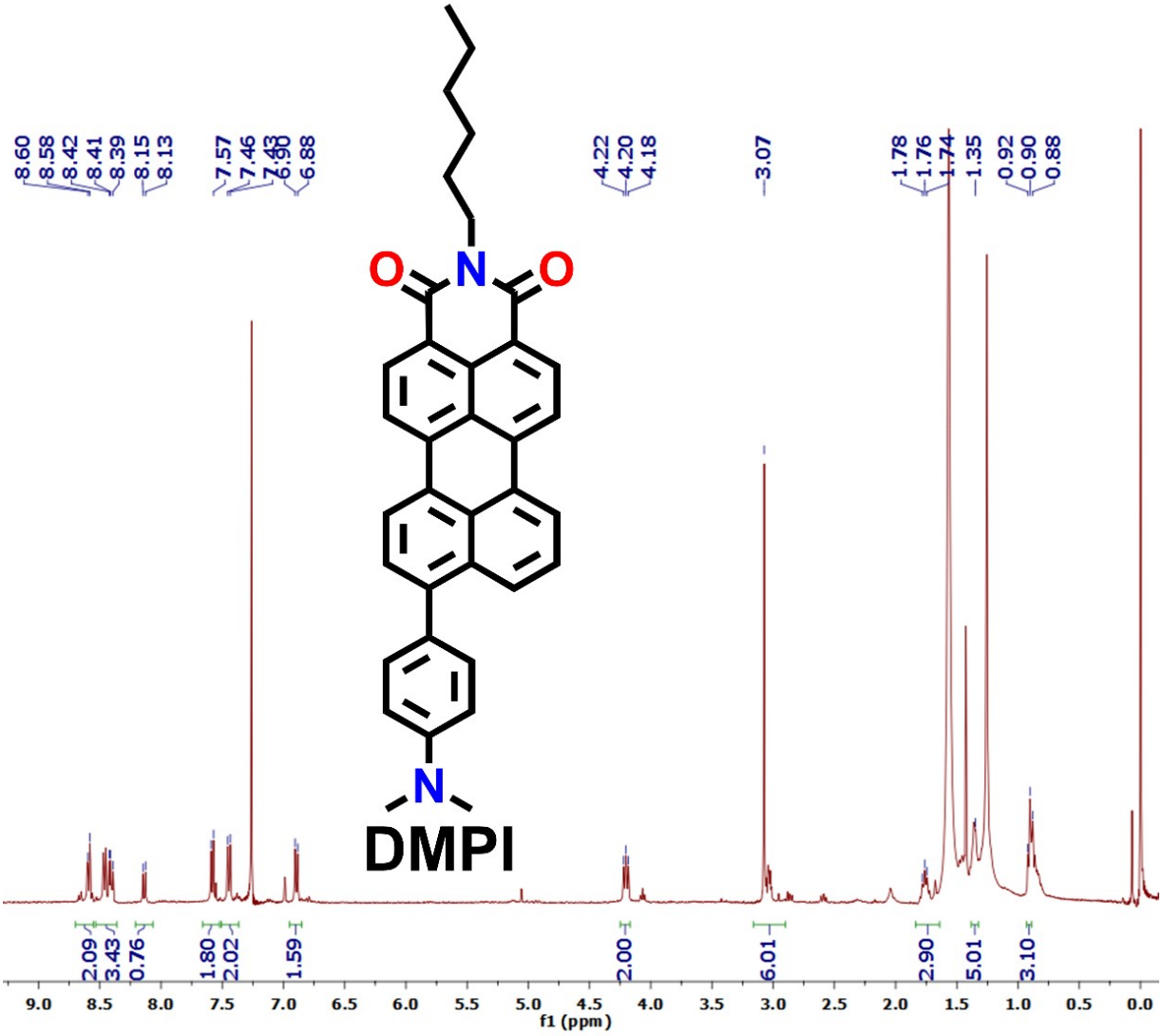
8.60
8.58
8.42
8.41
8.39
8.15
8.13
7.57
7.46
7.43
7.40
6.88
4.22
4.20
4.18
3.07
1.78
1.76
1.74
1.35
0.92
0.90
0.88
O
N
O
N
DMPI
2.09
3.43
0.76
1.80
2.02
1.59
2.00
6.01
2.90
5.01
3.10
9.0
8.5
8.0
7.5
7.0
6.5
6.0
5.5
5.0
4.5
4.0
3.5
3.0
2.5
2.0
1.5
1.0
0.5
0.0
f1 (ppm)

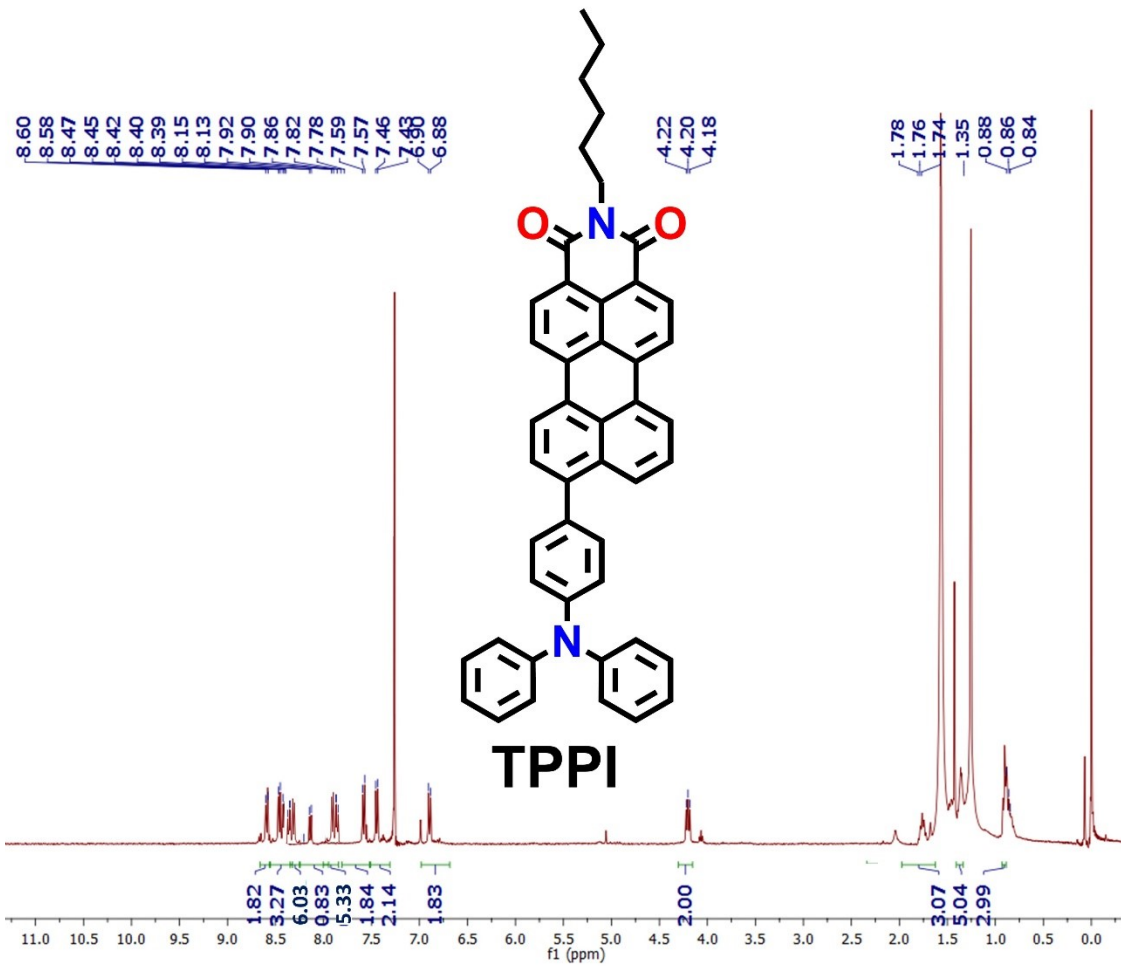
8.60
8.58
8.47
8.45
8.42
8.40
8.39
8.15
8.13
7.92
7.90
7.86
7.82
7.78
7.59
7.57
7.46
7.43
7.40
6.88
4.22
4.20
4.18
1.78
1.76
1.74
1.35
0.88
0.86
0.84
O
N
O
N
TPPI
1.82
3.27
6.03
0.83
5.33
1.84
2.14
1.83
2.00
3.07
5.04
2.99
11.0 10.5 10.0 9.5 9.0 8.5 8.0 7.5 7.0 6.5 6.0 5.5 5.0 4.5 4.0 3.5 3.0 2.5 2.0 1.5 1.0 0.5 0.0
f1 (ppm)

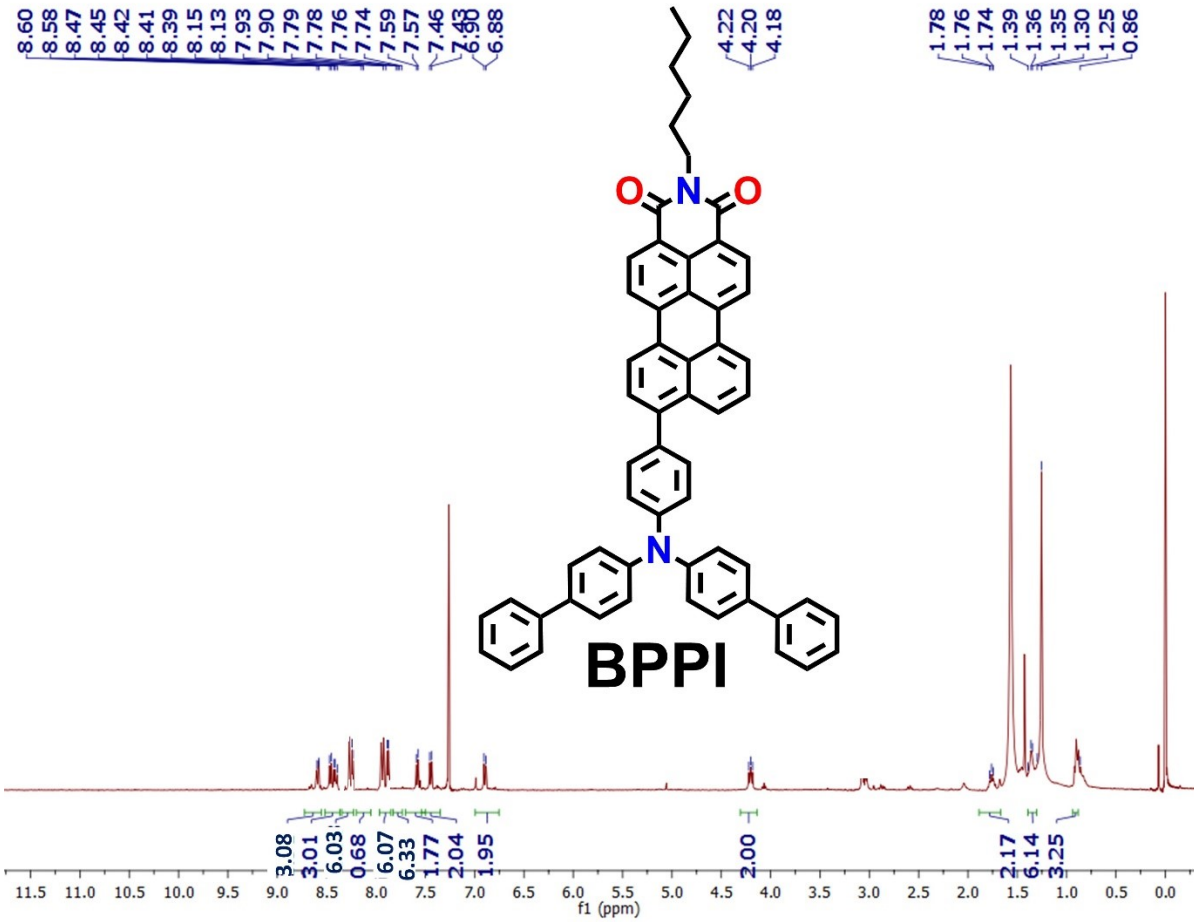
8.60
8.58
8.47
8.45
8.42
8.41
8.39
8.15
8.13
7.93
7.90
7.79
7.78
7.76
7.74
7.59
7.57
7.46
7.43
6.90
6.88
4.22
4.20
4.18
1.78
1.76
1.74
1.39
1.36
1.35
1.30
1.25
0.86
O
N
O
N
BPPI
3.08
3.01
6.03
0.68
6.07
6.33
1.77
2.04
1.95
2.00
2.17
6.14
3.25
11.5 11.0 10.5 10.0 9.5 9.0 8.5 8.0 7.5 7.0 6.5 6.0 5.5 5.0 4.5 4.0 3.5 3.0 2.5 2.0 1.5 1.0 0.5 0.0
f1 (ppm)

^{13}C NMR spectra

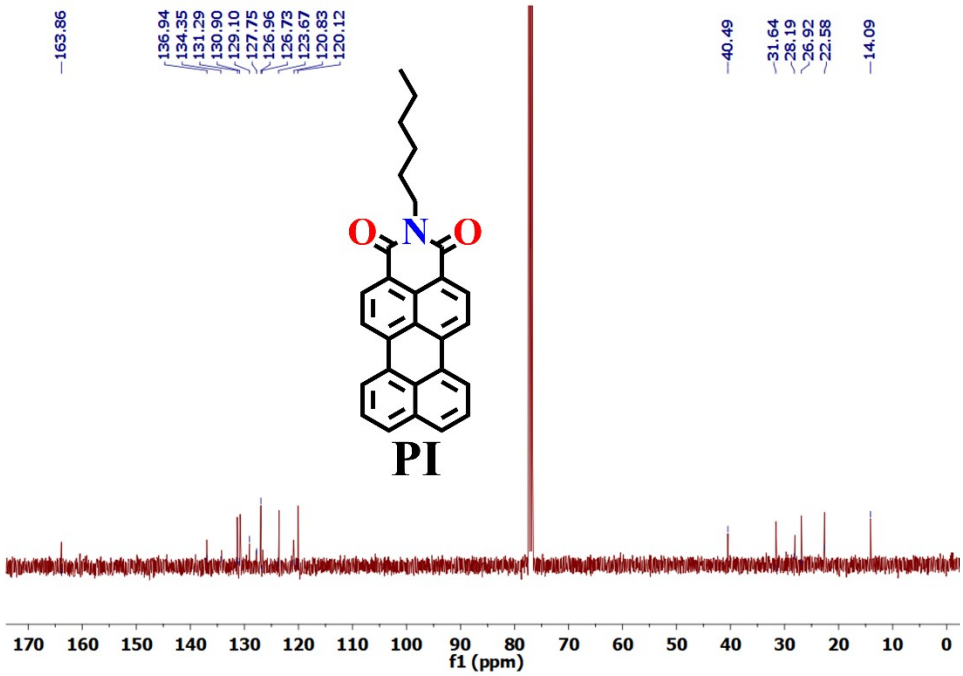

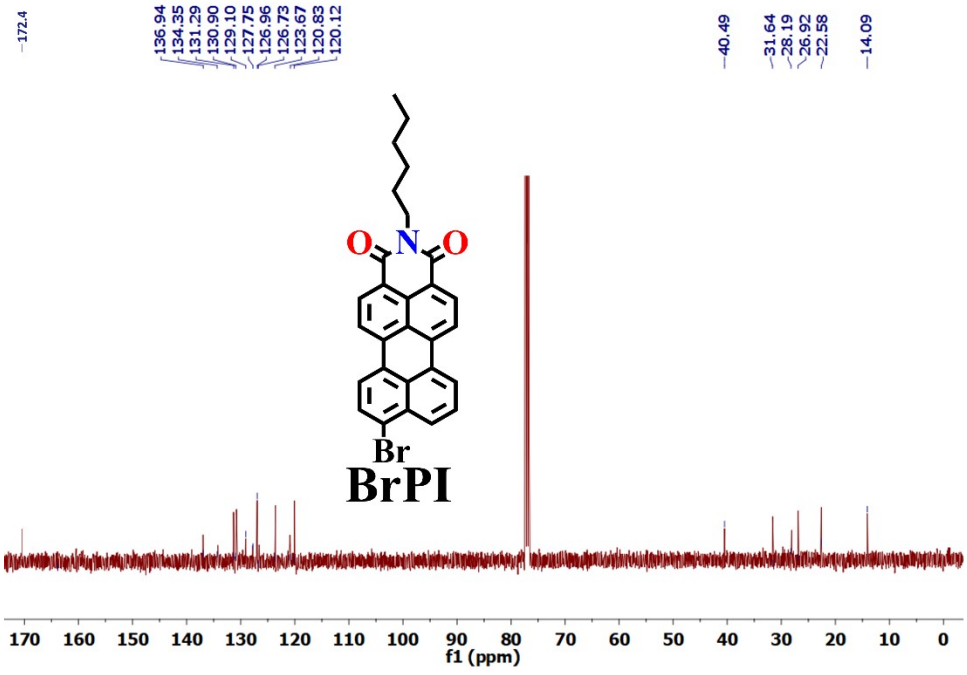

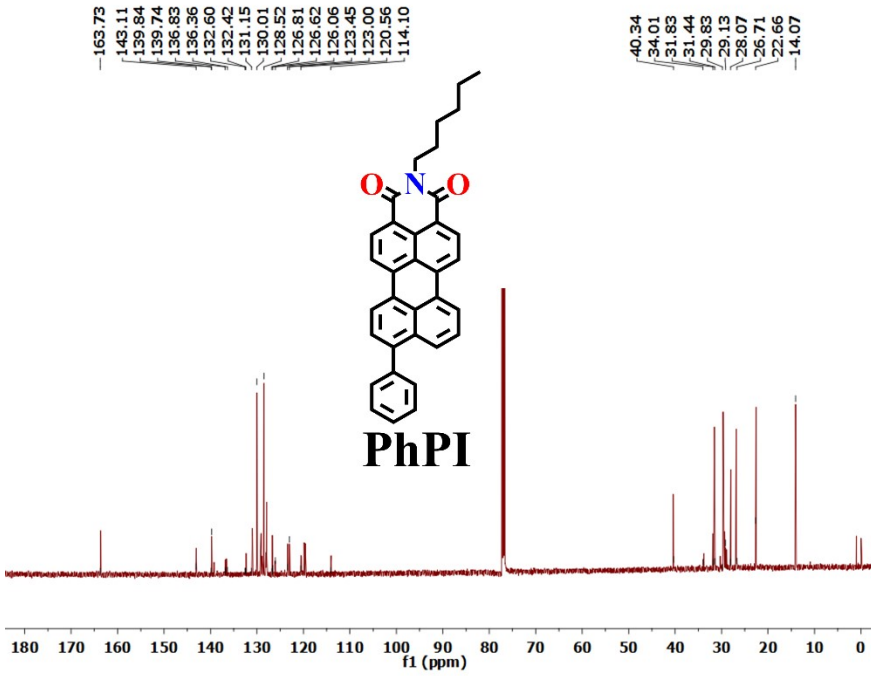
163.73
143.11
139.84
139.74
136.83
136.36
132.60
132.42
131.15
130.01
128.52
126.81
126.62
126.06
123.45
123.00
120.56
114.10
40.34
34.01
31.83
31.44
29.83
29.13
28.07
26.71
22.66
14.07
O
N
O
PhPI
180 170 160 150 140 130 120 110 100 90 80 70 60 50 40 30 20 10 0
f1 (ppm)

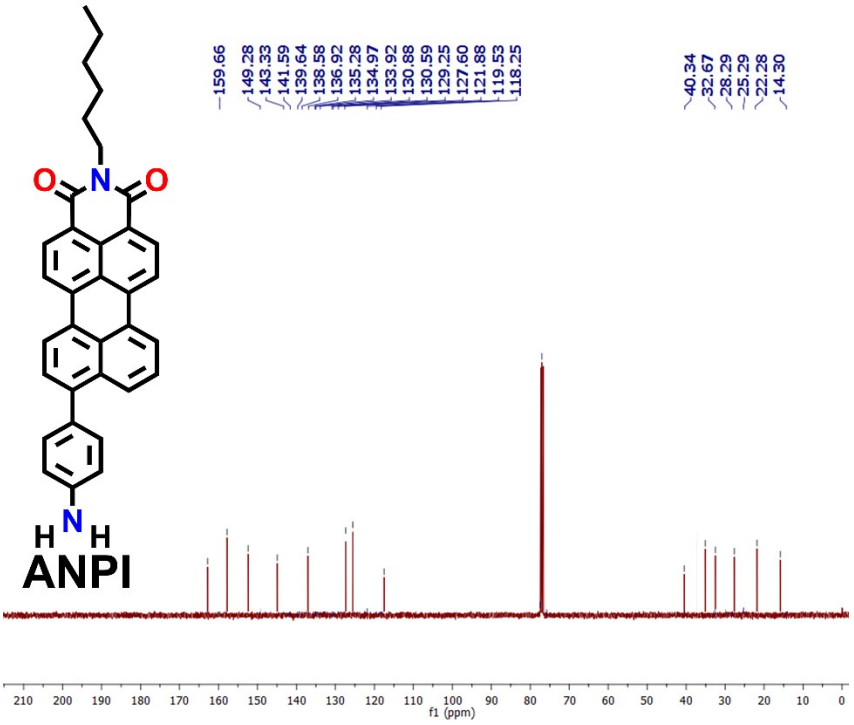
159.66
149.28
143.33
141.59
139.64
138.58
136.92
135.28
134.97
133.92
130.88
130.59
129.25
127.60
121.88
119.53
118.25
40.34
32.67
28.29
25.29
22.28
14.30
O
N
O
H N H
ANPI
210 200 190 180 170 160 150 140 130 120 110 100 90 80 70 60 50 40 30 20 10 0
f1 (ppm)

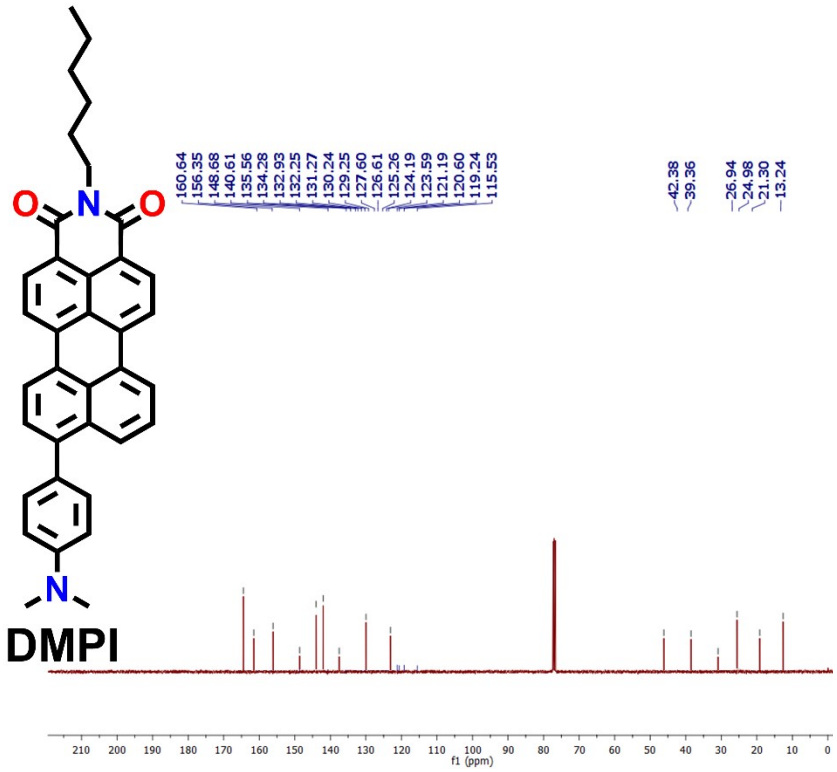
160.64
156.35
148.68
140.61
135.56
134.28
132.93
132.25
131.27
130.24
129.25
127.60
126.61
125.26
124.19
123.59
121.19
120.60
119.24
115.53
42.38
39.36
26.94
24.98
21.30
13.24
O
N
O
N
DMPI
210 200 190 180 170 160 150 140 130 120 110 100 90 80 70 60 50 40 30 20 10 0
f1 (ppm)

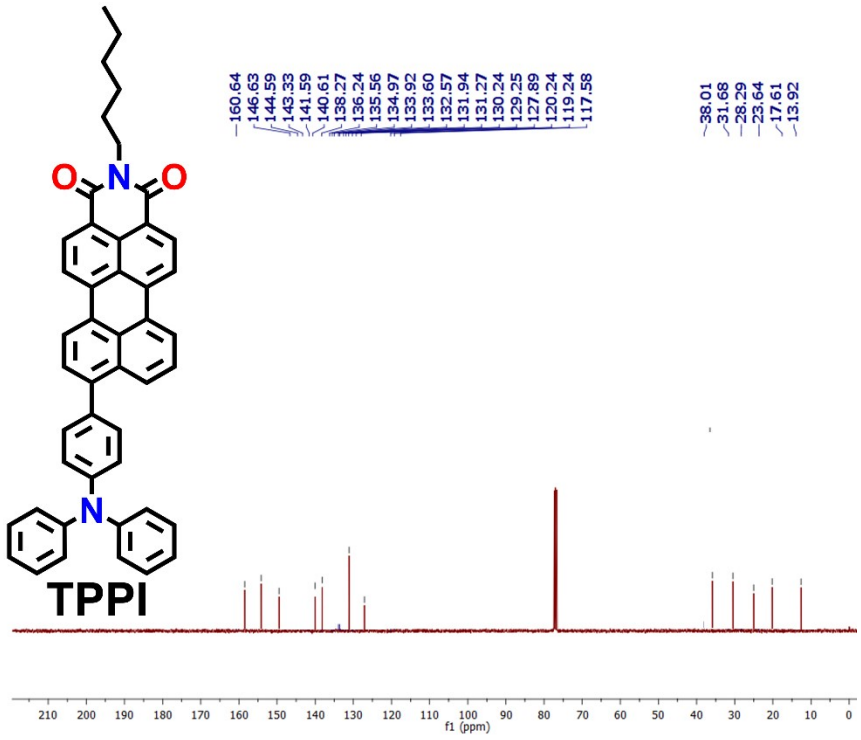

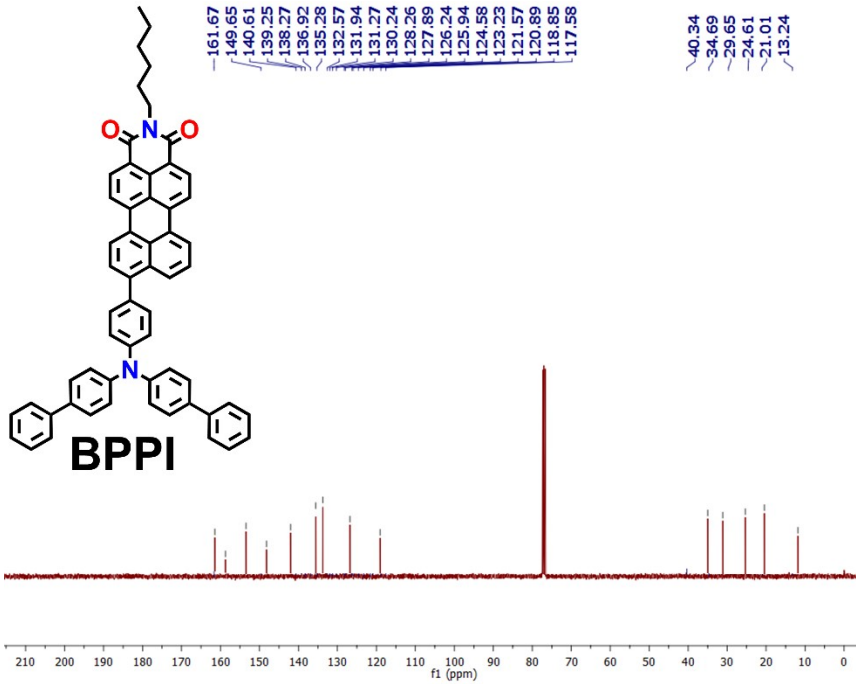

MALDI-TOF spectra

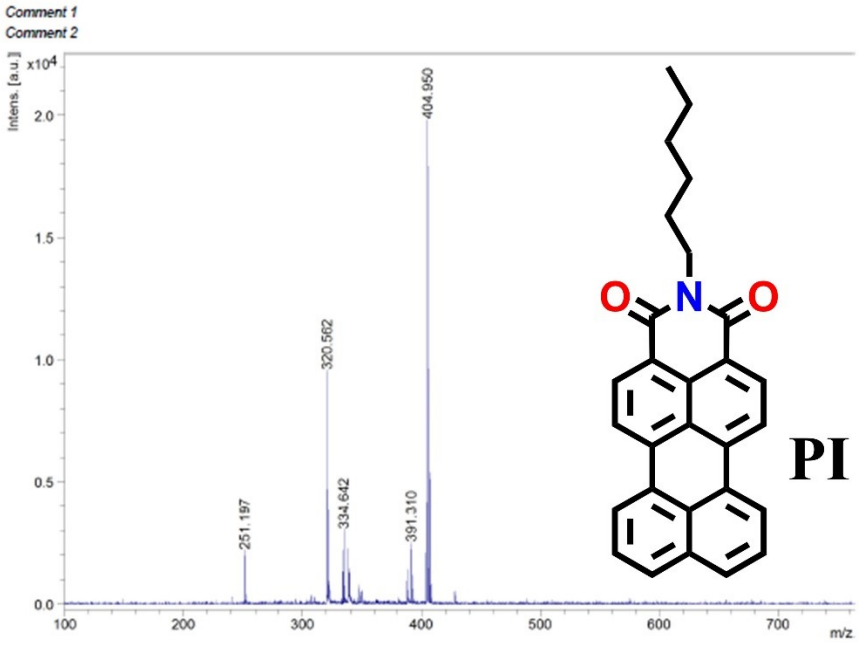

m/z	S/N	Quality Fac.	Res.	Intens.	Area
251.197	106		3340	2172	185
320.562	298		3062	9515	1277
334.642	92		3009	3013	408
387.886	44		3542	1422	227
391.310	77		2760	2486	391
404.950	629		3931	19790	2350

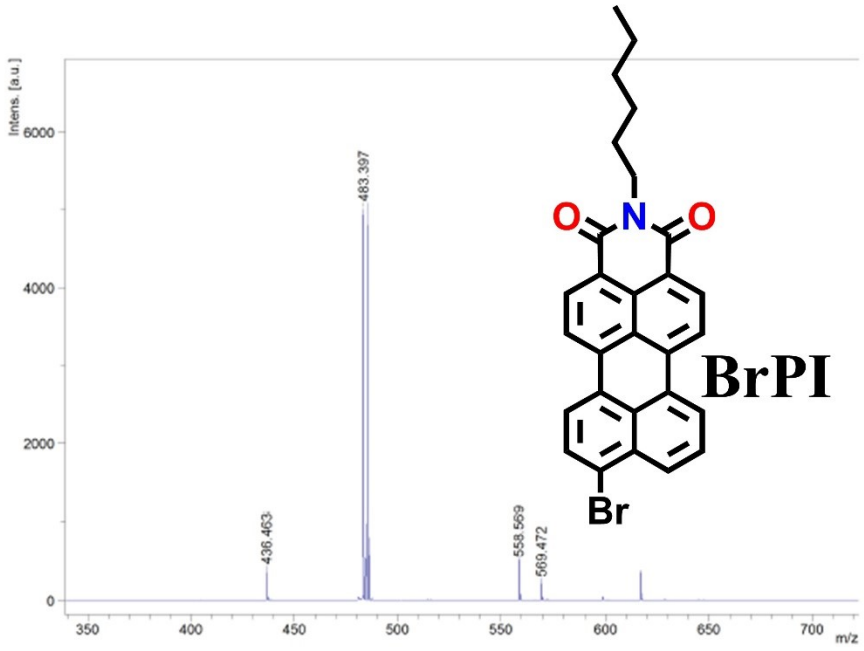

m/z	S/N	Quality Fac.	Res.	Intens.	Area
436.463	12		5242	440	80.6
483.397				4994	
484.408	30		225	984	2069
558.569	20		6983	528	94.5
569.472				276	

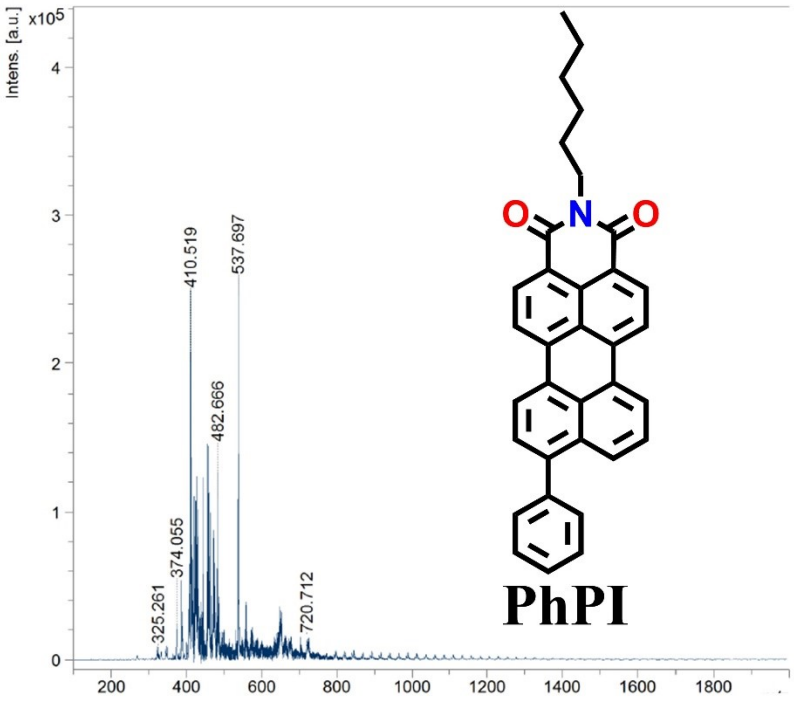

m/z	S/N	Quality Fac.	Res.	Intens.	Area
323.310	7	576	355	6710	8945
325.261	7	2199	719	7441	5168
374.055	12	4835	263	23171	4658 6
386.690	22	7108	857	4963 3	3498 6
388.308	12	4972	819	2637 9	1863 0
406.347	11	250	596	3309 5	3012 5
407.416	16	2637	516	4954 2	5936 7
408.516	13	765	1442	4070 3	1544 2
409.484	11	242	932	3430 0	2037 3
410.519	66	1139 8	1157	2005 21	1004 44
411.465	60	2351 3	980	1826 88	1207 32
412.478	28	9683	1196	8479 3	4236 5
413.477	16	8623	760	4867 5	4149 8
414.567	13	1632	1166	4080 9	2021 7
415.522	18	1381 3	829	5423 8	4242 2
416.512	16	1302 1	1064	5098 0	3152 0
417.569	8	1788	1427	2463 9	9718
418.559	7	358	1288	2377 2	1037 4
419.544	10	332	1227	3297 4	1514 0
420.	31	2094	1088	1005	6211

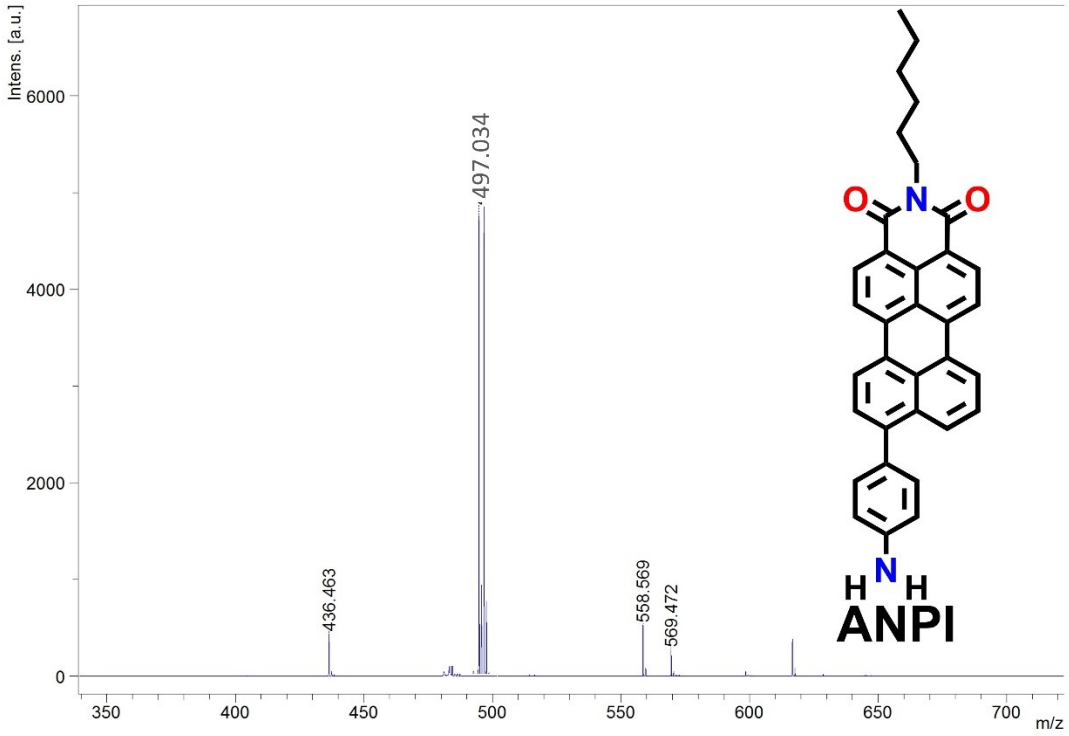

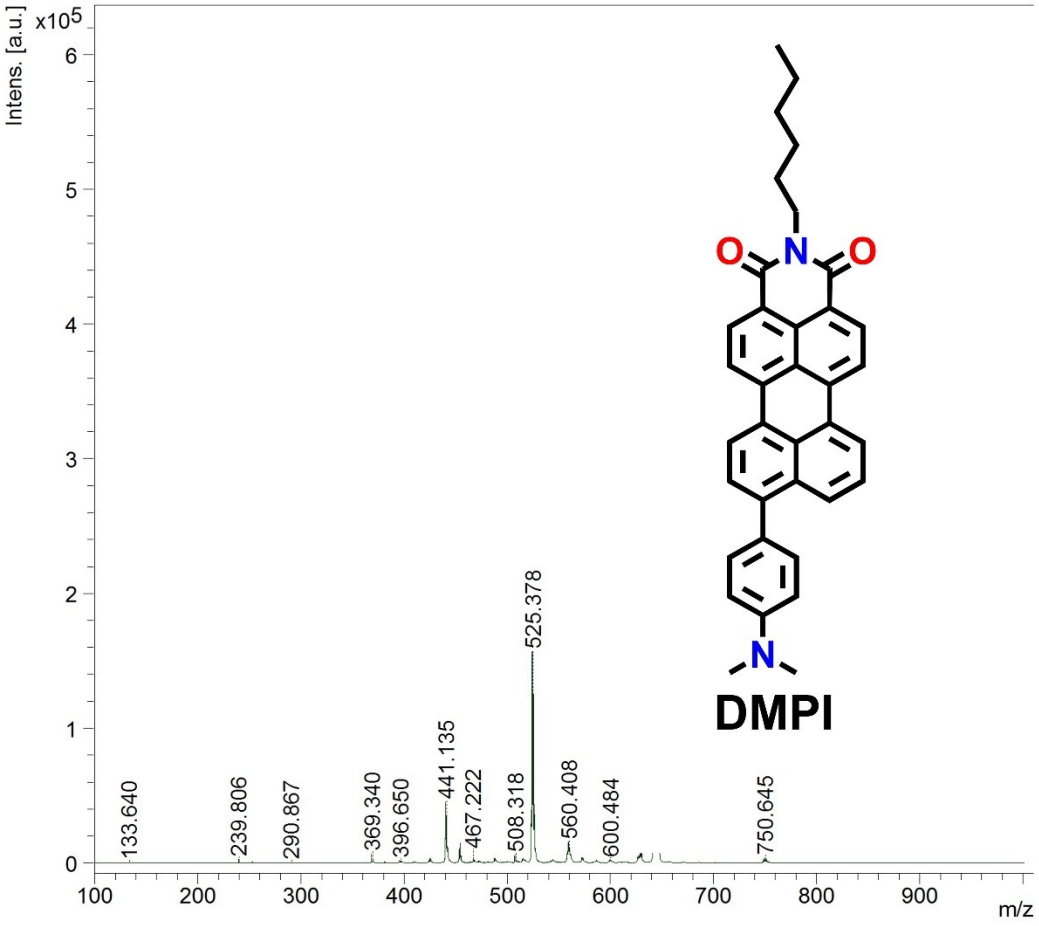
Intens. [a.u.]
x10^5
6
5
4
3
2
1
0
100
200
300
400
500
600
700
800
900
m/z
133.640
239.806
290.867
369.340
396.650
441.135
467.222
508.318
525.378
560.408
600.484
750.645
O
N
O
N
DMPI

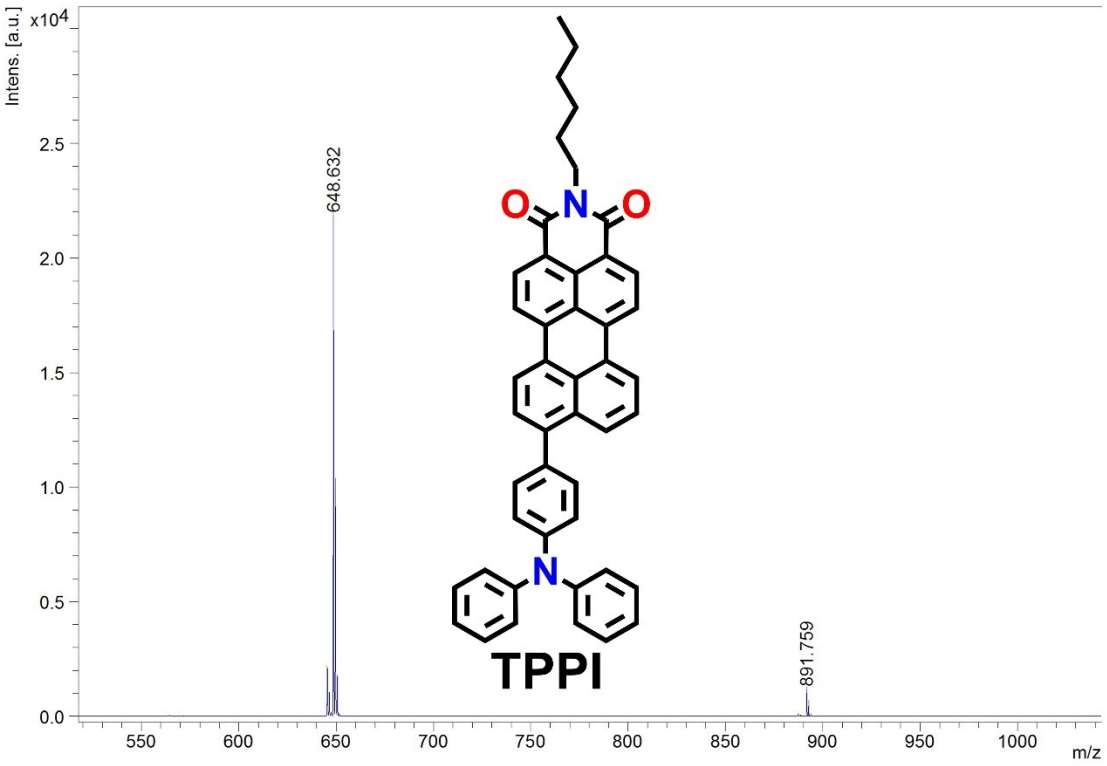
Intens. [a.u.]
x10^4
2.5
2.0
1.5
1.0
0.5
0.0
648.632
891.759
550
600
650
700
750
800
850
900
950
1000
m/z
O
N
O
N
TPPI

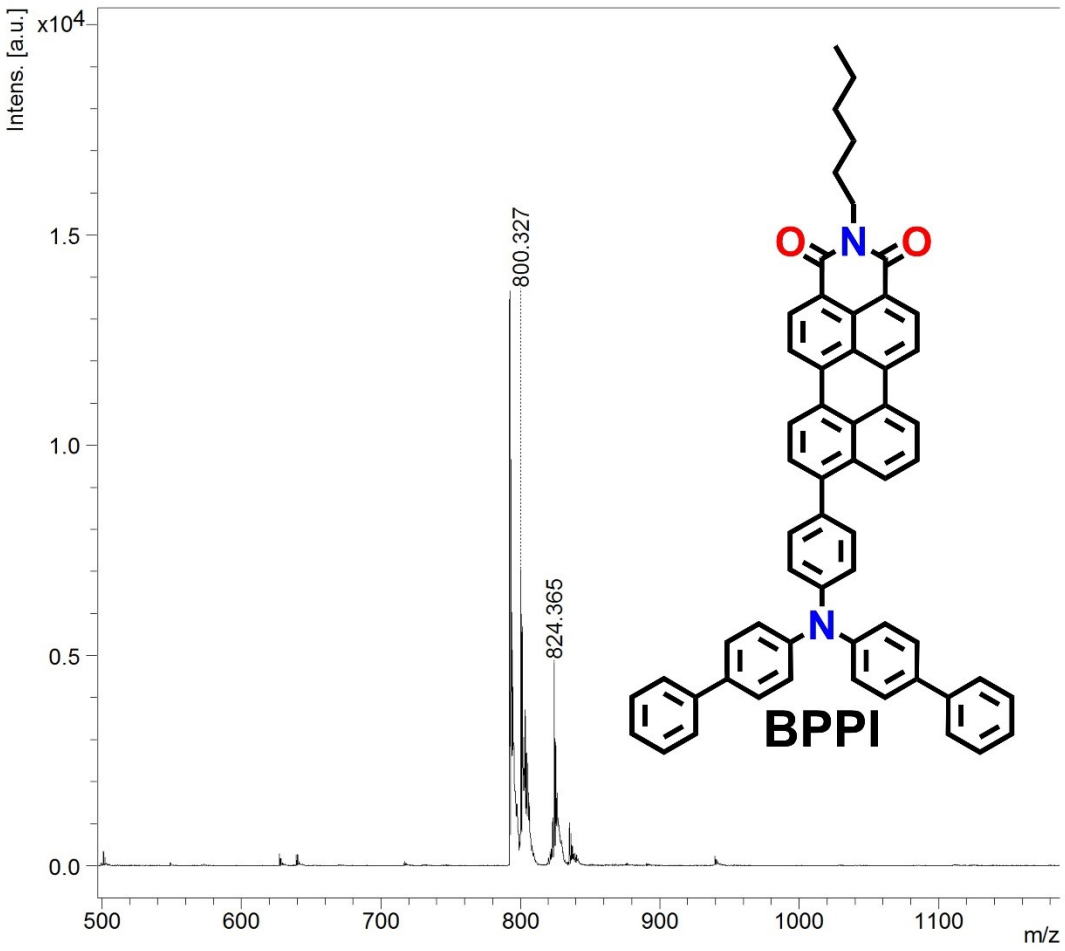

3. References

1. A. D. Becke, *J. Chem. Phys.*, 1993, **98**, 5648-5652.
2. M. J. Frisch, G. W. Trucks, H. B. Schlegel, G. E. Scuseria, M. A. Robb, J. R. Cheeseman, G. Scalmani, V. Barone, B. Mennucci, G. A. Petersson, H. Nakatsuji, M. Caricato, X. Li, H. P. Hratchian, A. F. Izmaylov, J. Bloino, G. Zheng, J. L. Sonnenberg, M. Hada, M. Ehara, K. Toyota, R. Fukuda, J. Hasegawa, M. Ishida, T. Nakajima, Y. Honda, O. Kitao, H. Nakai, T. Vreven, J. A. Montgomery, J. E. Peralta, F. Ogliaro, M. Bearpark, J. J. Heyd, E. Brothers, K. N. Kudin, V. N. Staroverov, R. Kobayashi, J. Normand, K. Raghavachari, A. Rende ll, J. C. Burant, S. S. Iyengar, J. Tomasi, M. Cossi, N. Rega, J. M. Millam, M. Klene, J. E. Knox, J. B. Cross, V. Bakken, C. Adamo, J. Jaramillo, R. Gomperts, R. E. Stratmann, O. Yazyev, A. J. Austin, R. Cammi, C. Pomelli, J. W. Ochterski, R. L. Martin, K. Morokuma, V. G. Zakrzewski, G. A. Voth, P. Salvador, J. J. Dannenberg, S. Dapprich, A. D. Daniels, O. Farkas, J. B. Foresman, J. V. Ortiz, J. Cioslowski, D. J. Fox.Gaussian 09, Revision A.02, Gaussian, Inc. *Wallingford CT*, 2009.
3. F. Neese, *WIREs Comput Mol. Sci.*, 2018, **8**, 1327.
4. F. Neese, *Comput. Mol. Sci.*, 2012, **2**, 7373-78

5. D. Wang, M. M. Lee, G. Shan, R. T. Kwok, J. W. Lam, H. Su, Y. Cai and B. Z. Tang, *Adv. Mater.*, 2018, **30**, 1802105.
6. W. Wu, D. Mao, S. Xu, M. Panahandeh-Fard, Y. Duan, F. Hu, D. Kong and B. Liu, *Adv. Funct. Mater.,* 2019, **29**, 1901791.
7. X. Shi, S. H. Sung, J. H. Chau, Y. Li, Z. Liu, R. T. Kwok, J. Liu, P. Xiao, J. Zhang and B. Liu, *Small Methods*, 2020, **4**, 2000046.
8. Y. Li, R. Tang, X. Liu, J. Gong, Z. Zhao, Z. Sheng, J. Zhang, X. Li, G. Niu and R. T. Kwok, *ACS nano*, 2020, **14**, 16840-16853.
9. M. C. DeRosa and R. J. Crutchley, *Coord. Chem. Rev.*, 2002, **233**, 351-371.
10. X. Cui, G. Lu, S. Dong, S. Li, Y. Xiao, J. Zhang, Y. Liu, X. Meng, F. Li and C.-S. Lee, *Mater. Horiz.,* 2021, **8**, 571-576.
11. Y.-L. Chen, S.-W. Li, Y. Chi, Y.-M. Cheng, S.-C. Pu, Y.-S. Yeh and P.-T. Chou, *ChemPhysChem*, 2005, **6**, 2012-2017.
12. S. Xu, Y. Yuan, X. Cai, C.-J. Zhang, F. Hu, J. Liang, G. Zhang, D. Zhang and B. Liu, *Chem. Sci.*, 2015, **6**, 5824-5830.